The homeodomain of the *Drosophila* Ceramide Synthase Schlank confers nuclear import information and DNA binding capabilities

Dissertation
zur
Erlangung des Doktorgrades (Dr. rer. nat.)
der
Mathematisch-Naturwissenschaftlichen Fakultät
der
Rheinischen Friedrich-Wilhelms-Universität Bonn

vorgelegt von

André Völzmann

aus

Berlin

Bonn 2013

Angefertigt mit Genehmigung der Mathematisch-Naturwissenschaftlichen Fakultät der Rheinischen Friedrich-Wilhelms-Universität Bonn

1. Gutachter

Prof. Dr. rer. nat. Michael Hoch

2. Gutachter

PD Dr. rer. nat. Reinhard Bauer

Tag der Promotion: 21.03.2014

Erscheinungsjahr: 2014

Erklärung

Teile dieser Arbeit wurden bereits in folgenden Publikationen veröffentlich:

2011 Voelzmann A, Bauer R (2011) Embryonic expression of *Drosophila* Ceramide Synthase Schlank in developing gut, CNS and PNS. Gene Expr Patterns 11: 501-510.

2010 Voelzmann A, Bauer R (2010) Ceramide Synthases in mammalians, worms, and insects: emerging schemes. BioMol Concepts 1: 411–422

2009 Bauer R, Voelzmann A, Breiden B, Schepers U, Farwanah H, Hahn I, Eckardt F, Sandhoff K & Hoch M (2009) Schlank, a member of the Ceramide Synthase family controls growth and body fat in *Drosophila*. EMBO J 28: 3706–3716

08/2009 **Patent:** Hoch MK, Bauer R, Schultze J, Völzmann A "New nucleic acid molecules and polypeptides involved in lipid metabolism" EP2292742 A1 (Int Cl.: C12N9/10)

That is the exploration that awaits you—not mapping stars and studying nebulae, but charting the unknown possibilities of existence.

Q, Star Trek – The Next Generation,

All Good Things...

Table of Contents

1 Introduction

1.1 Sphingolipids are major membrane and signaling lipids involved in development and disease

Sphingolipids were originally found in brains and nerve cells, where they are highly enriched. They remained enigmatic for quite a while and have thus been named after the riddle asking sphinx in Greek mythology (Thudichum, 1874). This class of lipids is a major structural component of cellular membranes, where they do not only play a role in determining overall membrane properties but also alter cellular signaling events and have themselves been implicated as bioactive lipids. Some of them even bind to their own class of receptors, directly activating intracellular signaling cascades. Sphingolipids are of major interest because they were found to be involved or altered in a great number of various human diseases states, including neuronal disorders like neurodegeneration (Arboleda et al, 2009), Alzheimer's Disease (Farooqui et al, 2010; van Echten-Deckert & Walter, 2012), Nieman-Pick disease (Vincent et al, 2003; Huang et al, 2005; Schweitzer et al, 2009; Schulze & Sandhoff, 2011), Gaucher disease (Fuller, 2010) and many more but also cell fate decisions (apoptosis and differentiation; Geilen et al, 1997; Bieberich et al, 2001; Bieberich, 2011), metabolic disorders (insulin resistance, metabolic syndrome; Holland et al, 2007b; Holland & Summers, 2008) and progression as well as occurrence of cancer (Ogretmen & Hannun, 2004; Oskouian & Saba, 2010; Ryland et al, 2011). Thus sphingolipids and their metabolizing enzymes are currently in focus of research because they seem to be promising therapeutic targets (Ryland et al, 2011; Billich & Baumruker, 2008; Delgado et al, 2012) for a great number of bodily failings and diseases whose probability of occurrence is strongly increasing with age in long-lived human populations, especially in industrialized countries (Mattson, 2003).

The molecular mechanisms by which sphingolipids act within a cell have only been partly understood – they range from changes in membrane fluidity due to their biophysical properties (Cheng et al, 2006; Guan et al, 2009; Silva et al, 2012) over the generation of micro-channels within mitochondrial membranes (Siskind et al, 2002; Colombini, 2010) and disturbance of lysosomal functions due to their accumulation (Schulze & Sandhoff, 2013) to transcriptional regulations as part of protein activity modifying interaction partners (Hait et al, 2009).

1.2 Sphingolipid distribution in subcellular compartments

Sphingolipids are a highly variable class of lipids with distinct variants numbering into the ten-thousands. They all have a sphingoid base in common. The sphingoid base can be acylated by Ceramide Synthases yielding (dihydro)ceramide which in turn can be subsequently modified by addition of sugar moieties. The carbon-chain-length of the sphingoid base and the acyl-chain added, desaturation of fatty acids as well as the different sugars branches and phosphorylations allow for a huge number of variations (Hannich et al, 2011) including sphingosines, sphinganines, ceramides, cerebrosides, sphingomyelins and many more. Sphingolipids vary in their distribution within subcellular compartments.

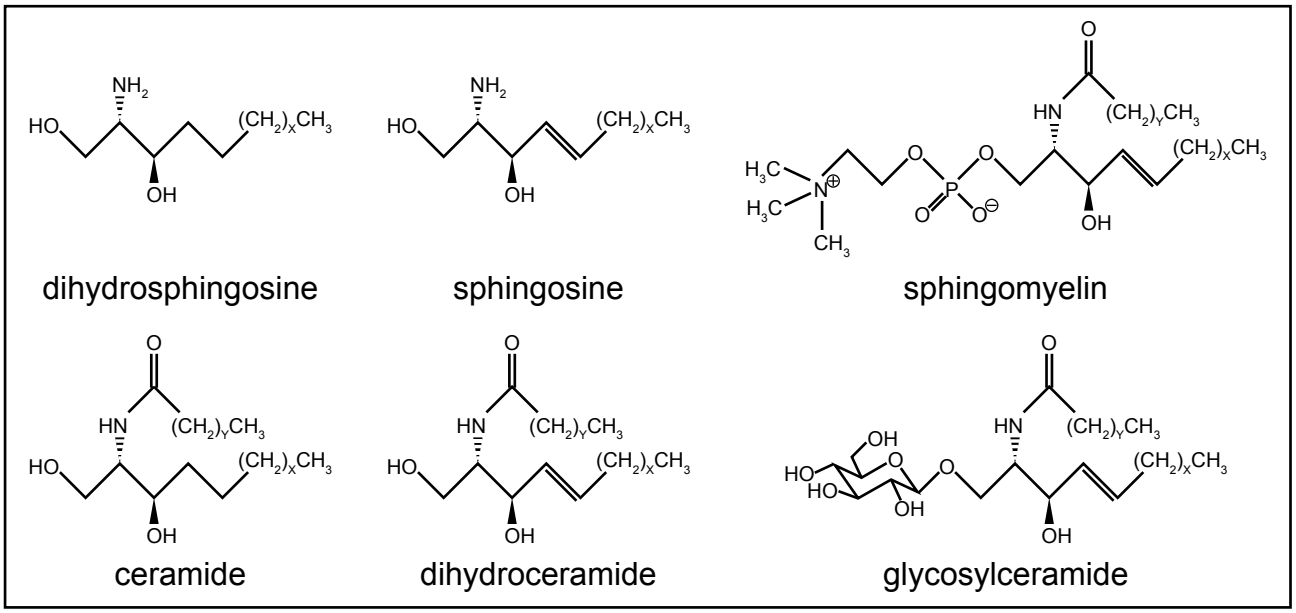

Figure 1.1 Structures of various sphingolipid classes. X and Y designate variability of carbon chain lengths in both sphingoid base and added acyl chains.

Basic sphingolipids are synthesized in the endoplasmic reticulum and then transferred to the Golgi apparatus, where they are usually modified by addition of sugars (giving cerebrosides) or conversion to sphingomyelin (SM). Ceramides can be directly transferred in a non-vesicular mechanism via the lipid-binding Ceramide Transporter (CERT, Hanada et al, 2003; Kok et al, 1998). Higher order sphingolipids are then usually transported to the plasma membrane. Thus there seems to be an ordered gradient from ER over Golgi to the plasma membrane from simple to complex sphingolipids. While still controversial, it has also been implicated that there could be a phase separation between different lipids within any given membrane, leading to distinct nano-scale lipid environments with differing compositions that would lead to enrichment of different proteins ('lipid rafts-hypothesis', Fox et al, 2007; Ernst & Brügger, 2013) in part dependent on

interaction with cortical actin structures (Kraft, 2013). In addition, it was shown that the sphingolipid composition of membranes, especially the chain length, can have a tremendous impact on membrane fluidity and in consequence on endo- and exocytotic processes (Roccamo et al, 1999; Marks & Pagano, 2002; Silva et al, 2012) as well as linked receptor signaling (Pepperl et al, 2013). Moreover it was shown that sphingosine and its phosphorylated version sphingosine-1-phosphate (S1P) can act as signaling lipid themselves, with their own receptor cascades (Rosen et al, 2009; Granado et al, 2009).

1.3 Protein structure and implicated functions of Ceramide Synthases (CerS)

Ceramide Synthases are right at the center of sphingolipid metabolism, synthesizing two of the major sphingolipid classes, dihydroceramides and ceramides, from precursors sphingosine and sphinganine, derived from both *de novo* synthesis and recycling pathways (Mullen et al, 2012). Structurally, CerS are membrane bound by multiple transmembrane domains and have one conserved defining Lag1 motif that seems to be essential for the synthesis reaction itself (Spassieva et al, 2006). The enzymes have been described to be localized to the endoplasmic reticulum (ER) where the ceramide synthesis reaction takes place at the cytosolic leaflet of the ER membrane (van Meer & Lisman, 2002).

Although CerS have been characterized quite well in recent years, due to the availability of animal knock out models (Guillas et al, 2001; Bauer et al, 2009; Imgrund et al, 2009; Tedesco et al, 2008; Jennemann et al, 2012), various aspects are currently still not addressed and highly controversial.

During evolution, the following two CerS classes emerged (usually with both variants within the same species): One class is only characterized by the transmembrane domains and the Lag1 motif (class I in this thesis). The other class in addition incorporated a homeodomain into its protein structure (class II in this thesis), a domain that has so far only been found in nuclear proteins for which it mediates direct DNA and RNA interaction (Gehring et al, 1994; Dubnau & Struhl, 1996). This led to speculations about a DNA binding affinity (Venkataraman & Futerman, 2002) that were stifled rather fast based on amino acid sequence considerations (Mesika et al, 2007; Levy & Futerman, 2010).

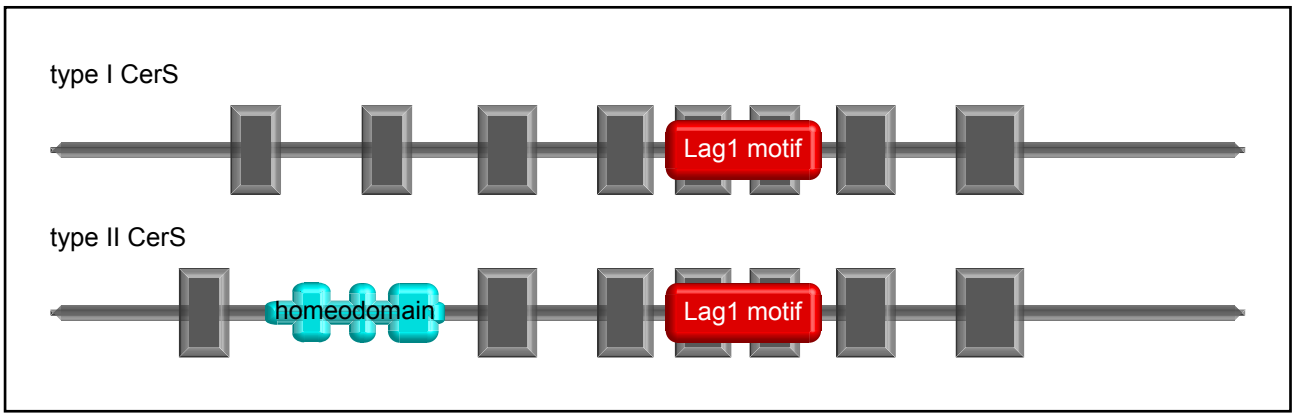

Figure 1.2 Ceramide Synthases can be grouped into two classes: type I that is only characterized by transmembrane domains and the Lag1 motif and type II which in addition contains a homeodomain. A, Illustration of the overall structure of type I and type II Ceramide Synthases (CerS). The overall protein backbone is depicted as grey line; predicted transmembrane domains are shown as grey boxes, the Lag1 motif is marked in red and the homeodomain in blue.

1.4 Mutants for the only *Drosophila* CerS gene, *schlank*, show developmental delay and transcriptional regulation of enzymes involved in fat storage

The Schlank gene encodes the only *Drosophila* Ceramide Synthase variant (André Völzmann, 2007). Ceramide Synthase assays and metabolic labeling verified that Schlank is a *bona fide* Ceramide Synthase (Bauer et al. 2009).

We previously showed that Schlank mutants are developmentally delayed (André Völzmann, 2007; Bauer et al, 2009). Various phenotypes were observed, including the inability to deflate wings after hatching from the pupal cage and defects during eye development that are partly consistent with the role of CerS and ceramides in apoptosis (Geilen et al, 1997; Pepperl et al, 2013) as well as differentiation events (Bieberich, 2011). Schlank mutant allele G0061 showed excess pigment cells at the end of pupal development (Fig. AP1.1.1-AP1.1.2) but a clear mapping into the apoptosis cascade was not possible (Fig. AP1.1.3). After eye development finished, misdifferentiation of photoreceptor cells was visible in sections of adult eyes (Fig. AP1.2). The most prominent phenotype, however, was a less opaque fat body in the third larval stage and a strongly reduced triacylglycerol content (André Völzmann, 2007; Bauer et al, 2009). This phenotype goes hand in hand with a transcriptional upregulation of lipase *brummer* and *lipase 3* (*lip3*) as well as the *adipokinetic hormone* (*akh*) in mutants and a downregulation upon overexpression, respectively (André Völzmann, 2007; Bauer et al, 2009)

Lipase 3 has been predicted to be a triacylglycerol lipase and was shown to be regulated in starvation situations (Zinke et al, 2002). Brummer lipase was shown to be an adipose triglyceride

lipase (ATGL) whose mutation leads to strong fat accumulation (Grönke et al, 2005). Akh is a hormone produced in a subset of cells in the ring gland, which is attached to the insect brain. Akh, which is thought to be the insect glucagon analog (Bharucha et al, 2008), was shown to be released into the hemolymph from where it is distributed throughout the body. It binds the G-protein coupled Akh-receptors in target tissues and activates a signaling cascade which leads to the dissociation of lipid droplet-associated protein (Lsdp1) from intracellular lipid droplets (Patel et al, 2005; Patel et al, 2006, Arrese et al, 2006). This in turn allows lipases to access and metabolise triglycerides stored in the lipid droplets (Arrese et al, 2008). Thus, Akh determines the activity of lipases by allowing them access to their substrate.

By regulating several aspects of lipolysis, the amount of lipases as well as the modulation of the signaling pathway that determines lipase activation, Schlank seems to have tight control over the general fat stores in the animal.

Moreover, Schlank seems to primarily determine the transcription of those three genes. Due to the fact that Schlank is a class II CerS, it is quite tempting to speculate, whether or not the homeodomain might be involved in the observed transcriptional regulations and if they would be a result of nuclear protein activity. This might also call for a subcellular redistribution of the protein to the nucleus.

There is supporting evidence that sphingolipid metabolism might also take place in the nucleus, since sphingolipids as well as sphingolipid metabolizing enzymes have been found in this compartment as well.

1.5 Nuclear sphingolipids and sphingolipid metabolizing enzymes

Various sphinoglipids were directly isolated from nuclear extracts, like sphingosine, S1P as well as GM1 (Wu et al, 1995). In addition, nuclear extracts also show enzyme activity for several sphingolipid-metabolising enzymes, including Sphingomyelin Synthase (Albi & Magni, 1999), Neutral Sphingomyelinase, Ceramidase (Tsugane et al, 1999) and Sphingosine-Kinases 1 & 2 (SphK1 & 2, Igarashi et al, 2003; Hait et al, 2009). It is not yet clear which sphingolipids are directly transferred to nuclear membranes by lipid transporters or membrane fusion events but it has been suggested that there should be local lipid synthesis within nuclear membranes (Lucki & Sewer, 2012) as well.

This local synthesis necessitates the nuclear import of sphingolipid synthesizing and metabolizing enzymes. Thus it might not be surprising that various enzymes involved in

sphingolipid synthesis have been isolated from nuclear extracts (e.g. Sphingosine Kinases, Ceramidases, Sphingomyelin Synthases) or have been found to shuttle between cytoplasm and nucleus.

1.6 Nuclear import mechanisms for proteins

Classical nuclear import of proteins is based on a number of transporters (Importin-ß-family) that recognize their target proteins either directly or in a complex with a α-Importin. Recognition of cargo proteins targeted for nuclear import relies on the binding of nuclear localization sequences (NLSs) within the cargo proteins. Those NLSs are usually rich in positively charged amino acids (lysine, K; arginine, R; histidine, H) following only partly understood sequence patterns ranging from four amino acids to bipartite sequences covering dozens of amino acids (Kosugi et al, 2009a). Upon binding, Importin-ß transports them to the nuclear envelope, where, after interaction with the nuclear pore complex (NPC), binding of RanGTP on Importin-ß and a CAS / RanGTP-complex on Importin-α results in a conformational change in importins leading to the release of the cargo (Fig. 1.3). Both importins are then exported from nucleoplasm to cytoplasm via RanGTP (complexes), where, after GTP hydrolysis, the importins are released. RanGDP is subsequently imported to the nucleus in an importin-ß-independent mechanism (Ribbeck, 1998).

This process is well understood for cytosolic proteins but has only recently investigated for membrane-bound proteins. It was shown that the mammalian membrane-bound epidermal growth factor (EGF) receptor is endocytosed and then recognized by Importin-ß and Sec61ß. Passing through Golgi and endoplasmic reticulum (ER) the EGF receptor is then transported through the nuclear pore complex in its membrane-bound state and thus shuttle to the inner nuclear membrane.

Thus it would be conceivable that membrane-bound Ceramide Synthases could be imported to the nucleus in a similar fashion. Experimental evidence validating or dismissing the nuclear translocation and DNA binding capacity of Ceramide Synthases is still not available. If the assumption that CerS might have a nuclear function would turn out to be true, this would give a new layer of complexity to sphingolipid metabolism and the enzymatic networks involved, especially in light of the fact that already one central spingolipid, Sphingosine-1-phosphate, and its synthesizing enzyme Sph2K were shown to be involved in chromatin modifications and transcriptional regulation (Hait et al, 2009). Whether or not CerS would act complementary or independently in this context would have to be addressed in more detail, then.

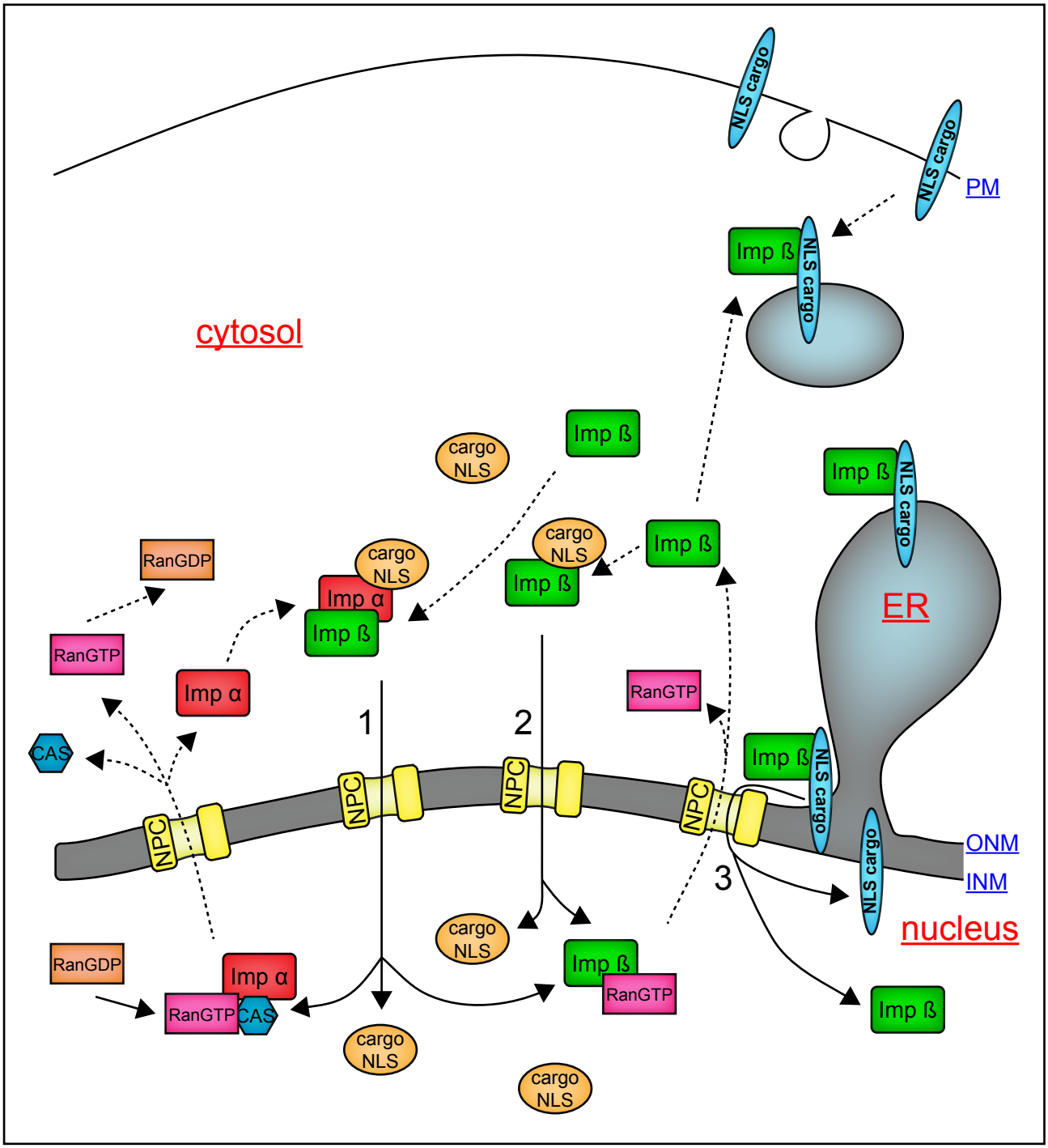

Figure 1.3 Nuclear protein import mechanisms. Cartoon modified from (Ganten & Ruckpaul, 2006). Cargo proteins with NLS can be bound in an α-ß (1) or ß (2)-dependent manner. Membrane bound cargo was shown to be bound and imported by ß-Importin (3). RanGTP releases the cargo and exports the ß-Importins from the nucleus. Export of α – Importin needs CAS as cofactor. PM, plasma membrane; ER, endoplasmic reticulum; INM, inner nuclear membrane; ONM, outer nuclear membrane; NPC, nuclear pore complex; Imp, Importin; NLS, nuclear localization sequence; GTP, guanosine triphosphate; GDP, guanosine diphosphate.

1.7 Rationale of the thesis

Ceramide Synthases are right at the heart of the sphingolipid synthesis pathway. Most research is focused on the properties and effects of the various metabolites generated by the CerS enzyme family in part neglecting the properties and functions of the enzymes themselves. Previous experiments showed that Schlank is the only *Drosophila melanogaste*r CerS and mutant phenotypes could not be entirely explained by its enzymatic activity. Expression patterns and localization studies in combination with structure function analysis of the homeodomain should be employed to explore a potential homeodomain function that might explain the Lag1 motif-independent regulation of overall fat stores.

2 Materials and Methods

2.1 Cloning and expression of GST-SchlankCT and GST-Schlank aa65-138

The cDNA region coding for homeodomain and C-terminus of Schlank were amplified via PCR and ligated into pGEX4T3 via EcoRI / BamHI. Following primers were used:

construct	vector	primer	sequence	comment
GST-Schlank aa65-138	pGEX4T3	forward primer	cagGATCCATATCGCCCGTAGGC	stop is in vector
		reverse primer	accaGAATTCCTCGCAGAACTTCACCAG	BamHI + EcoRI
GST-SchlankCT	pGEX4T3	forward primer	accaGGATCCCTCAAGATTGTTGTCGACTC	stop is in vector
		reverse primer	accaGAATTCCTCCTCTCTCCGTTCC	BamHI + EcoRI

BL21 or DH5α were freshly transformed with the vector for the corresponding GST constructs. Several colonies were combined and grown as overnight culture at 37°C in a 100ml ampicillin containing LB broth. The next morning, cultures were filled up to 800-1000ml with ampicillin containing LB broth.

After 2 hours at 37 °C, cultures were induced with 0.5 to 1 mM IPTG and grown for another 2 hours. Cultures were than induced with 0.5 mM IPTG and grown for an additional hour. Afterwards, cells were pelleted at 5000 g for 15 min and resuspended in 1 / 20 culture volume of PBS containing protease inhibitor. Due to the fact that addition of lysozyme led to the precipitation of the GST-Schlank aa65-138 protein, cells were disrupted with a sonifier at 70 % power, 100 % duty cycle for 1 min 30 sec. DTT was added to a concentration of 2 - 5 mM and the lysate was cleared from insoluble protein by centrifugation at 10000 g for 15 min. GST-proteins were bound overnight to PBS-prewashed glutathione-beads under constant rocking motion at 4°C. Beads were then centrifuged at 500 g for 3 min and the supernatant kept for later use. Beads were washed 4 - 5 times in 50ml 1 % PBT and an additional 4 times with 1x PBS. The beads were then transferred to a Pierce disposable column and washed with 2 column volumes of PBS. GST-proteins were subsequently eluted with 50 mM Tris, pH 8 and 15 mM reduced free glutathion in 500-1000 µL fractions (usually 6-8). 10 µL of the collected fractions were cooked for 5 min with 1x SDS sample buffer and run on a 12 % SDS polyacrylamide. Proteins were stained with coomassie.

2.2 Generation of schlank C-terminal antibodies

Purified GST-tagged C- terminal Schlank protein fragments were tested for their stability for 3 day at -20 °C, 4 °C and 37 °C. Proteins were stable and send to Pineda antibody service, Berlin, Germany for injection into suitable host animals. After a standard 60 day immunization scheme, antisera were tested for their immune response to purified SchlankCT protein and larval lysate containing either eGFP-tagged schlank full length or HA-tagged Schlank full length protein via western blot. Final immune sera from guinea pigs were collected at day 105, serum from sheep at day 225.

2.3 Preparation of CNBr-SchlankCT-affinity columns

GST-SchlankCT was bound to glutathione-beads as described above but not eluted. GST-SchlankCT-beads (on-column) were incubated overnight (~16 hours, room temperature) with 0.5 - 1 unit thrombin in 20 µL PBS per 20 µL bead volume (giving a 50 % slurry).

The GST-column supernatant (thrombin digest) is loaded onto a capped benzamidine column (pre-washed once with water and 3 – 4 times with PBS) to clear out thrombin. Remaining SchlankCT-thrombin digest is wash from the GST-column and added to the benzamidine column with 1 column-volume PBS. The supernatant is incubate rotating at room temperature for 30min (benzamidine column cleanup: wash column in PBS + 0.85 M NaCl; elute thrombin with either 0.05 M glycine pH 3.0 or 10 mM HCl + 0.5 M NaCl, pH 2.0 ; store in 0.05 M acetate buffer, pH 4.0 containing 20 % ethanol). The flowthrough from the benzamidine column (which contains SchlankCT cleaved off from GST, verified by Western Blot analysis) was collected and concentrated by centrifugation on a 3 kD Amicon column at 4000 g for 25 – 30 minutes. The concentrated SchankCT protein was dissolved in 2 – 3 ml 0.1 M $NaHCO_3$, pH 8.3 + 0.5 M NaCl and loaded on a cyanobromide column (prewashed with 40 - 70 ml 1 mM HCl; 0.5 g CNBr powder per column).

After incubation while rotating for 1 – 2 hours at room temperature, the column was washed with 5 column volumes of coupling buffer (0.1 M $NaHCO_3$, pH 8.3 + 0.5 M NaCl). Remaining reactive groups on the CNBr column were blocked by incubation with 0.1 M Tris-HCl buffer, pH 8.0 for 2 hours at room temperature while rotating. Afterwards, the column is washed with more than 3 alternating cycles of 0.1 M acetate buffer, pH 4.0 containing 0.5 M NaCl, followed by a wash with 0.1 M Tris-HCl, pH 8 containing 0.5 M NaCl. SchlankCT-affinity-columns were stored in PBS + 0.01 % NaAzide at 4 °C.

2.4 Affinity purification of schlankCT (sCT) antibodies

To affinity purify schlankCT antibodies, guinea pig or sheep sera were loaded onto separate CNBr-SchlankCT columns and incubated for 2 hours at room temperature with constant rotation. The column was then washed 5 - 7 times with 1 x PBS and the antibodies eluted in 500 µL fractions of 0.1 M glycine-HCl (pH 2.7) and immediately neutralized with 0.2 volumes 1M Tris-HCl (pH 8.8).

Antibodies (guinea pig, sCTgp; sheep, sCTs) were dialyzed to PBS using Slide-A-Lyzer Dialysis cassettes (20000 MWCO; Thermo Scientific) and aliquots were then frozen with or without 30% glycerol at -80°C.

2.5 Cloning of *schlank* promoter fragments

Various fragments of the 5' region before the schlank transcriptional start were amplified via PCR and inserted to the pCaSPeR-AUG-Gal4-X vector (gift from C. Melcher) via EcoRI and NotI restriction sites. The vectors generated should express Gal4 protein under control of schlank regulatory elements. Following primers were used for the PCRs:

construct	vector	primer	sequence
0-794	pCaSPeR-AUG-Gal4-X	forward primer	TTTGAATTCCAACTGCTCGGCAATCTG
region -2000 to -1206		reverse primer	ATGCAGCGGCCGCAGCAGTAGCAATAGCAGCA
775-1092	pCaSPeR-AUG-Gal4-X	forward primer	TTTGAATTCCTGCTGCTATTGCTACTG
region -1225 to -908		reverse primer	ATGCAGCGGCCGCCAAGAGACTCAAGAAACTG
1042-1626	pCaSPeR-AUG-Gal4-X	forward primer	TTTGAATTCTCTTCTTCGCTACTATCGG
region -958 to -364		reverse primer	ATGCAGCGGCCGCTCCAATTGTTGTCAGCAC
3-2049	pCaSPeR-AUG-Gal4-X	forward primer	CCGGAATTCACTGCTCGGCAATCTGCT
region -2000 to +49		reverse primer	ATAAGAATGCGGCCGCAACAACAATACAGTGTGCCCA
775-2049	pCaSPeR-AUG-Gal4-X	forward primer	TTTGAATTCCTGCTGCTATTGCTACTG
region -1225 to +49		reverse primer	ATAAGAATGCGGCCGCAACAACAATACAGTGTGCCCA
1552-2636	pCaSPeR-AUG-Gal4-X	forward primer	TTTGAATTCCATTGCAGAACTACAGTGGATCCT
region -448 to +636		reverse primer	ATGCAGCGGCCGCGTTGCTGCTTCAGTTGCC
3-2049	pCaSpeR-hs43-lacZ	forward primer	CCGGAATTCACTGCTCGGCAATCTGCT
region -2000 to +49		reverse primer	ATAAGAATGCGGCCGCAACAACAATACAGTGTGCCCA

To map down expression patterns to specific regions of the promoter, fragments were chosen to be partially overlapping.

To generate transgenic fly lines, pCaSPeR-AUG-Gal4-X and pCaSPeR-hs43-LacZ constructs and Δ2,3-vector DNA were precipitated using sodium acetate and isopropanol, washed in 70 % ethanol and resuspended in 15 µL injection buffer (5 mM KCl + 0.1 mM sodium phosphate buffer, pH 7.8). The constructs were then injection into w- embryos and transgenic flies back crossed to w- males or females for 2 generations. Fly lines were made homozygous if applicable or otherwise crossed over a fitting balancer chromosome.

2.6 Generation of N-terminally eGFP-tagged Schlank fragments and Schlank NLS mutations

eGFP was cloned into a pUAST vector via EcoRI / NotI restriction sites (pUAST-NeGFP). Schlank coding regions were amplified by PCR and cloned into pUAST-NeGFP via NotI / XbaI restrictions sites. The following primers were used for amplification of the coding regions:

construct	vector	primer	sequence	comment
NeGFP	pUAST	forward primer	accaGAATTCATGGTGAGCAAGGGCGAG	stop is in vector
		reverse primer	accaGCGGCCGCCTTGTACAGCTCGTCCATG	EcoRI + NotI
NeGFP-schlank-aa1-63	pUAST-NeGFP	forward primer	ttcaGCGGCCGCtATGGACATATTGAATG	stop is in vector
		reverse primer	accaTCTAGACGAAACGCTCCAG	NotI + XbaI
NeGFP-schlank-aa1-138	pUAST-NeGFP	forward primer	ttcaGCGGCCGCtATGGACATATTGAATG	stop is in vector
		reverse primer	accaTCTAGACTCGCAGAACTTCACCAG	NotI + XbaI
NeGFP-schlank-aa64-138	pUAST-NeGFP	forward primer	ttcaGCGGCCGCtTGGATATCGCCCGTAGG	stop is in vector
		reverse primer	accaTCTAGACTCGCAGAACTTCACCAG	NotI + XbaI
NeGFP-schlank-aa73-133	pUAST-NeGFP	forward primer	ttcaGCGGCCGCtTGGCATACGTAGTTCTAG	stop is in vector
		reverse primer	accaTCTAGACGTTGACGGTTTATCCTG	NotI + XbaI
NeGFP-schlank-aa1-158	pUAST-NeGFP	forward primer	ttcaGCGGCCGCtATGGACATATTGAATG	stop is in vector
		reverse primer	accaTCTAGACCACAGCACGATCAC	NotI + XbaI
NeGFP-schlank-aa64-158	pUAST-NeGFP	forward primer	ttcaGCGGCCGCtTGGATATCGCCCGTAGG	stop is in vector
		reverse primer	accaTCTAGACCACAGCACGATCAC	NotI + XbaI

NeGFP-schlank-aa139-158	pUAST-NeGFP	forward primer	ttcaGCGGCCGCtAACACGTGGCGTTGC	stop is in vector NotI + XbaI
		reverse primer	accaTCTAGACCACAGCACGATCAC	
NeGFP-schlank-aa64-138ΔRPKK	pUAST-NeGFP	forward primer	ttcaGCGGCCGCtTGGATATCGCCCGTAGGCAAATCACTTGG CATACGTAGTTCTGCGGCAAATGTTCCT	stop is in vector NotI + XbaI
		reverse primer	accaTCTAGACTCGCAGAACTTCACCAG	
NeGFP-schlank-aa64-138Δhelix1	pUAST-NeGFP	forward primer	ttcaGCGGCCGCtTGGATATCGCCCGTAGGCAAATCACTTGG CATACGTAGTTCTAGGCCTAAGAAATCGACGCGATTGGAC	stop is in vector NotI + XbaI
		reverse primer	accaTCTAGACTCGCAGAACTTCACCAG	
NeGFP-schlank-aa64-138Δ117-123	pUAST-NeGFP	forward primer	ttcaGCGGCCGCtTGGATATCGCCCGTAGGCAAATCACTTGG CATACGTAGTTCTGCGGCAAATGTTCCT	stop is in vector NotI + XbaI
		reverse primer	accaTCTAGACTCGCAGAACTTCACCAGCGTTGACGGTTTAT CCTGGGCCCTGCGTTCGCGCTCGCTCATATC	
NeGFP-schlank-aa64-138 R6A R54A	pUAST-NeGFP	forward primer	ttcaGCGGCCGCtTGGATATCGCCCGTAGG	stop is in vector SOE-PCR
		reverse primer	accaTCTAGACTCGCAGAACTTCACCAG	
		SOE-1	GCCGCTTTCTTAGGTGCAGAACTACGTATGC	
		SOE-2	GCATACGTAGTTCTGCACCTAAGAAAGCGGC	
		SOE-3	TTATCCTGGGCCCTTGCTAGACGCCACCAGC	
		SOE-4	GCTGGTGGCGTCTAGCAAGGGCCCAGGATAA	

Restriction sites are underlined; bases added to stay in-frame are marked in red.

2.7 Cell culture and transfections

Schneider cells (S2) were grown in PAN Schneider's medium supplemented with 10 % FCS at 25 °C. Cells were transfected following the $CaPO_4$ transfection method described in the Invitrogen S2 cell manual. For expression, pUAST-constructs were co-transfected with pAc-GAL4 vectors at a ratio of 5:1.

2.8 Fly lines

Different chromosomes are separated by semicolons, different alleles of the same chromosome are separated by slash, plus signs indicate wildtypic chromosomes, and commas are used as separators for different constructs on the same chromosome. If not mentioned otherwise, flies were present in the laboratory.

[Oregon R]; [w^{1118}]; [*schlank*^{G0349} / FM7 *kr*-GAL4, UAS-GFP]; [*schlank*^{G0061} / FM7 *kr*-GAL4, UAS-GFP]; [*schlank*^{G0349} / FM7 *DfdGMR*_YFP]; [*schlank*^{G0061} / FM7 *DfdGMR*_YFP]; [UAS-*schlankRNAi*^{33896}] (VDRC #33896, Vienna, Austria); [UAS-*schlankH215D*] (Reinhard Bauer); [UAS-*schlankNTHA*]; [UAS-*schlank-eGFP*]; [*da*-GAL4]; [*en*-GAL4]; [ketel-GFP / CyO] (gift János Szabad, Szeged University, Hungary); [*ketelRNAi*^{27567}] (Bloomington Stock Center #27567, Indiana, USA); [*hs*FLP y^1 w*; +/+; *act5c* promoter FRT CD2stop FRT GAL4, UAS-GFP / TM6B, Tb^1]; [*hs*FLP y^1 w*; UAS-Dcr2; *act5c* promoter FRT CD2stop FRT GAL4, UAS-GFP / TM6B, Tb^1]; [UAS-NeGFP-Schlank-aa1-138] (germline transformed in this thesis); [tGS-GAL4; [UAS-GFP.nls] (gift Nina Moderau, University of Bonn, Germany); [*GMR*hid] (Bloomington Stock Center #5253, Indiana, USA); [*GMR*rpr] (Bloomington Stock Center #5773, Indiana, USA); [*GMR*grim] (Bloomington Stock Center #9923, Indiana, USA); *ey*-FLP; *eya*-GAL4; [y^1 w* FRT19A]; [y^1 w* *schlank*^{G0349} FRT19A]; [0-794 GAL4] (germline transformed in this thesis); [775-1092 GAL4] (germline transformed in this thesis); [1042-1626 GAL4] (germline transformed in this thesis); [1552-2636 GAL4] (germline transformed in this thesis); [3-2049 GAL4] (germline transformed in this thesis); [775-2049 GAL4] (germline transformed in this thesis); [3-2049 LacZ] (germline transformed in this thesis); [y* w* P{GawB}schlank^{NP7130} / FM7c] (Bloomington Stock Center # 105376; Indiana, USA); [UAS -myc-tau -GFP]; [UAS-Pex19RNAi] (VDRC #22064, Vienna, Austria); [*act*-GAL4]; [*nrv2*-GAL4] (gift Nina Moderau, University of Bonn, Germany); [*P101*-LacZ]; [*M84*-LacZ]; [*Svp*-LacZ]; [cyc-HA] (gift Michael Rosbash, Brandeis University, Waltham, USA); [UAS-KDEL-GFP]; [UAS-Serca-YFP] (gift Anthony Dornan, University of Glasgow, UK)

2.9 Larval length and width measurement

Larvae were transferred to PBS and heated to 60 °C for 10 minutes. Images were taken with a Olympus SZX binocular and larval length and width measure via Cell^F software.

2.10 Oil red O staining

Oil red O staining of larval epidermis was done following the protocol described in (Gutierrez et al, 2007).

2.11 LacZ stainings

larvae were prepped in ice-cold PBS / embryos dechorionated and fixed in 0.2% glutaraldehyde in PBS. After a wash step with PBS tissues were permeabilized for 10 minutes in 0.1% PBT (PBS + 0.1 % TX-100). Samples were equilibrated with ß-Gal staining solution (5 mM $K_3Fe(CN)_6$, 5 mM $K_4Fe(CN)_6$, 2 mM $MgCl_2$) for 30 minutes at 37 °C. The staining solution was exchanged and 1 mg / ml X-ß-Gal was added. After incubation at 37 °C for 4 hours to overnight, samples were washed rinsed PBS imaged.

2.12 Heat fixation embryos

Embryos were collected, rinsed in tap water and dechorionated with hypochloric solution for 3 minutes and thoroughly washed in water. Embryos were transferred to preheated NaCl-Triton solution (150 mM NaCl, 0,05 % v / v TX-100 ad H2O; 95°C) in a 50 ml falcon in a 95°C bain-marie for 5 – 10 seconds. Embryos were immediately cooled with ice-cold NaCl-Triton solution and cooled on ice for 10 minutes. NaCl-Triton solution is removed and replaced with 5 ml n-heptane. Methanol was added to a 1 : 1 ratio and embryos were shaken vigorously for 90 seconds. Embryos were transferred to an Eppendorf tube and the solution exchanges several times for ethanol. Embryos were store in ethanol at -20 °C.

2.13 Flat preparation of live embryos

Embryos were raised to stage 15 and 16 and then transferred to double-sided adhesive tape. The embryos were then dechorionated by hand with a dissection needle and transferred to apple juice agar. After orientation with the nervous system upwards, they were transferred to double-sided sticky tape on a new slide (Thermo Fisher, Menzel-Gläser). The area containing the sticky tape was encircled by liquid blocker pap pen and filled with PBS. Vitellin membrane and dorsal side of the embryos were opened with a sharpened tungsten wire and the embryo attached to the slide with the ventral side down. Embryos were flattened with the tungsten needle and any tissue covering the nervous system removed. After fixation in 4 % formaldehyde, samples were processed for antibody staining directly on the slide.

2.14 Antibody stainings of larval tissues and pupal eyes

Larva were prepped inside-out or pupal eyes prepped free in ice-cold PBS, fixed in 4 % methanol-free formaldehyde in PBS, washed once in PBS and 3 – 4 times in 0.2 – 0.3 % PBT. Samples were incubated with primary antibodies in 0.2 % PBT at 4 °C overnight. Primary antibody was removed, samples washed 3 – 4 times in 0.2 – 0.3 % PBT and incubated with secondary antibodies in 0.2 % PBT on a rocker at room temperature in the dark. After 3 – 4 wash steps with 0.2 % PBT, tissues were transferred to a slide, prepped clean and mounted in Fluoromount (with or without DAPI).

Primary antibodies used: α-SchlankCT guinea pig pep (sCTpep; 1:50; peptide antibody); α-SchlankCT guinea pig (sCTgp; 1:50; immunized and purified during the thesis work); α-SchlankCT sheep (sCTs; 1:50; immunized and purified during the thesis work); α-Schlank Hox rabbit (1:50); α-Lamin Dm0 84.12 mouse (1:100; DSHB); α-Bocksbeutel guinea pig (Bocks, 1 : 300; Georg Krohne, University of Würzburg, Germany); α-Otefin guinea pig (Ote, 1:300; Georg Krohne, University of Würzburg, Germany); α-GFP ab290 rabbit (1:500; Abcam); α-GFP ab6556 rabbit (1:1000-1:5000; Abcam); α-HRP 647 (1:500); α-SP2637 (1:1000; Benjamin Altenhein, University of Mainz, Germany); α-Nazgul rabbit (Naz, 1:1000; Benjamin Altenhein, University of Mainz, Germany); α-Discs large (Dlg, 1:10; DSHB); α-Prospero (Pros, 1:10; DSHB); α-hemagglutinin-tag rat (HA, 1:500; Roche); α-ß-Galactosidase (ß-Gal, 1:8000; Molecular Probes); α-Wrapper mouse (Wrap, 1:200; DSHB); α-Neprilysin 4 rabbit (1:500, tissue equilibration needed: 5 min, 0,04% SDS in PBS; Heiko Meyer, University of Osnabrück, Germany); α-Reversed polarity mouse (Repo, 1:50; DSHB); α-Fasciclin II (Fas II, 1:10; DSHB); α-BP104 (1:10; DSHB); α-HRP goat (1:200); α-Embryonic lethal abnormal vision 7E8A10 rat (Elav, 1:100; DSHB).

Secondary antibodies were acquired from Dianova and Jackson Laboratories: α-mouse Alexa 488; α-rabbit Alexa 488; α-rat Alexa 488; α-goat Alexa 488 ;α-guinea pig Cy3; α-sheep Cy3; α-rabbit Cy3; α-mouse Cy3; α-rat Cy3; α-mouse Dylight 647; α-rabbit Alexa 633; α-rat Alexa 633. All Alexa 488, 633 and Dylight 647 antibodies were used 1:100 – 1:200, Cy3 antibodies were used 1:200.

2.15 Adult eye sections and stainings

Flies were decapitated, heads transferred to a slide, cut in half (medial sagittal) and prefixed for 20 minutes in 25 % glutaraldehyde in phosphate buffer eyes were fixed in 0.1 M sodium phosphate, pH 7.2. Samples were washed once in phosphate buffer and fixed in 2 % glutaraldehyde/1 % OsO4

in phosphate buffer on ice for 30 minutes. After a phosphate buffer washing step, samples were post-fixed in 2 % OsO4 for 1 hour on ice. After sequential dehydration to 100% ethanol, samples were washed twice for 10 minutes in 100% acetone. The eyes were equilibrated in acetone-araldite solution (1:1) at 4 °C overnight. The solution was exchanged for araldite and eyes incubated for more than four hours at room temperature and then placed in molds and incubated at 60 °C overnight. Eyes were sectioned tangentially (1 µm), placed on slides and stained with toluidine blue. Samples were rinsed in water and mounted in DEPE for imaging.

2.16 Imaging of antibody stainings and image analysis

Antibody stainings were imaged with the Zeiss LSM710 system. Where indicated, imaging stacks were recorded. Orthogonal sections were created in FIJI (Fiji is just ImageJ; Schindelin et al, 2012) and exported as tiff-files. Where needed, colors of imaging channels were adjusted either by Fiji or Adobe Photoshop. Mean staining intensities were calculated for defined regions of interest in Fiji. Image panels were assembled in Adobe Illustrator.

2.17 Phylogenetic analysis

Sequences were aligned with ClustalW (Larkin et al, 2007) with following paramteres: Gonnet matrix, gap open penalty 25, gap extension penalty 0.5, gap distance penalty 5, end gaps allowed, 3 iterations for the calculations with the neighbor joining algorithm and nexus file output format.

Due to the large number of species and the need to resume calculations upon interruptions, phylogenic relations of CerS proteins were calculate with MrBayes (Huelsenbeck et al, 2001; Ronquist & Huelsenbeck, 2003; Altekar et al, 2004) in four independent runs with a heated and a cold chain each. A multi-processor environment running Scientific Linux using the MPI-framework and beagle extensions for SSE support was employed. Following settings were used in MrBayes: fixed Jones amino acid substitution model (test runs showed fastest convergence with this model); 4 runs with 2 chains each, sampling, print, check and diagnostic frequencies of 40000 generations; random start tree; activated saving of branch lengths; checkpoint saves for resume functionality. The Bayesian Markov Chain Monte Carlo calculations were run for 1.28252 billion generations. For quality control, convergence of the runs were tested on a regular basis with MrBayes sump function as well as ‘Are we there yet?’s run compare and cumulative split plot functions and Tracer’s (Rambaut A & Drummond AJ, 2007) LnL plot. Calculation time was ~12 months.

2.18 Statistical analysis

Two-sided T-tests were calculate in Microsoft Excel, Mann-Whitney-U-tests were calculate with eutest (Leon Avery, Virginia Commonwealth University, USA; http://elegans.som.vcu.edu/~leon/stats/utest.html)

2.19 TM predictions

Schlank sequences were analyzed by Phobius (Käll et al, 2004; Käll et al, 2007), TMHMM v2 (Krogh et al, 2001; Sonnhammer et al, 1998), HMMTOP (Tusnády & Simon, 1998; Tusnády & Simon, 2001), TMpred (Stoffel & Hofmann, 1993) and PHDhtm (Rost et al, 1996). The annotated domains and protein annotations were modeled according to scale in Adobe Illustrator.

2.20 Structure and tree depictions

3D structures of following homeodomains were downloaded from the protein database (PDB) in .ASN1 format: *Drosophila melanogaster* Ultrabithorax (Ubx; PDB #1B8I; X-ray), *Mesocricetus auratus* Pancreatic And Duodenal Homeobox 1 (Pdx1; PDB #2H1K; X-ray), *Mus musculus* CerS5 (PDB #2CQX; solution NMR) and *Mus musculus* Cers6 (PDB #1X2M; solution NMR). The Schlank homeodomain was model after *Drosophila melanogaster* Bicoid (Bcd) and *Mus musculus* CerS6 via the SWISS-MODEL workspace (Arnold et al, 2006). The model was then uploaded to VAST search (Gibrat et al, 1996) to convert it to the ASN1 file format. All 3D structure models were visualized, highlighted and exported with Cn3D (Wang et al, 2000).

2.21 Transcription factor binding site predictions

Potential promoter regions (1kb range 5’ of the transcription start) were analyzed via the JASPAR transcription factor binding site database (Mathelier et al, 2013) with a matrix score of ≥ 85 % for the Schlank consensus (MA0193.1).

2.22 General DNA binding assay

Purified GST protein solutions were dialyzed to PBS + 3 mM $MgCl_2$ Overnight at 4 °C under constant stirring. After precipitation of insoluble protein by centrifugation at 20000 g for 20 minutes, protein was biotinylated by EZlink Sulfo-NH3-LC-Biotin in 4-fold excess at room temperature for one hour biotinylated GST-proteins were dialyzed to PBS + 3 mM $MgCl_2$. Biotinylation of the proteins was verified by dot blot analysis with α-Biotin-FITC antibody. 100 µg protein were loaded on 500 µL Streptavidin-coated Dynabeads in PBS (+ 1 mg / ml BSA) for 30 minutes. After 3 wash steps in PBS, protein-coated beads solution was filled up to 1.5 mL and stored at 4 °C.

For the DNA binding assays, D3 DNA library (randomized DNA sequence flanked by primer sequences; GCTGTGTGACTCCTGCAA$[N]_{43}$GCAGCTGTATCTTGTCTCC) was amplified by PCR and 5 µL (10 µM) dsDNA was labeled with $\gamma^{32}P^{-}$ATP via T4-poly-nucleotide-kinase (PNK) at 37 °C. Labeled dsDNA was purified via G25 columns and filled up to 100 µL with water. 10 µL of radioactively labeled D3 library were incubated with 80 µL protein beads in PBS + 3 mM MgCl2 for 30 minutes at room temperature. The beads were washed up to 8 times in PBS-$MgCl_2$ buffer. DNA was eluted from the beads by incubation at 80 °C for 3 minutes. If DNA stayed on the beads, 65 µL H2O were added and heated to 100 °C for 2 minutes. For competition experiments, beads were incubated with the indicated amounts of heparin of salmon sperm DNA prior to the addition of labeled D3 library.

2.23 Next generation RNA sequencing

RNAs were isolated from larvae following the miRNeasy Kit instructions. Quality of the RNAs was checked on an RNAse-free 1 % agarose gel and prepared for RNA sequencing on an Illumina next-gen-sequencing platform (Michael Kraut, Marc Beyer, Joachim Schultze). Data were analyzed with Partek Genomics Suite 6.5 (Marc Beyer).

2.24 Electromobility Shift Assays (EMSA)

2.24.1 Non-radioactive EMSAs

0.5 – 2 µg purified GST or GST-Schlank aa65-138 fusion protein was incubate with 1 µg poly dI-dC, 8% glycerol, 50 µg BSA in 1x EMSA buffer (20 mM Hepes pH 8.0, 50 mM KCl, 5 mM DTT, 10 mM MgCl2, 5 % glycerol; Aimee's buffer) with or without up to 100 pmole unlabeled probe for 10 minutes. 100 fmole to 10 pmole Biotin-labeled probes (added on the forward strand during synthesis; annealed complementary oligos) were added and the reaction incubate at room temperature for 30 minutes.

Samples were run in a 6 % TBE-polyacrylamide gel (0.5 % TBE buffer) at 60 - 120 V, the gel itself was pre-run. After a suitable separation length, gels were wet-blotted to a positively charged nitrocellulose membrane at 60 - 90 V for 20 - 30 minutes in 0.5 % TBE.
The blot was then shortly dried and the DNA crosslinked to the membrane via UV irradiation with 1200 mJ / cm². The blot was blocked, washed and incubated with streptavidin-HRP and developed using the Pierce Lightshift Chemiluminescent EMSA Kit and x-ray films.

2.24.2 Radioactive EMSA

Oligos were designed with AG-overhangs at the termini after annealing forward and reverse strand. α-^{32}P-dCTP and unlabeled dTTP were attached via Klenow polymerase at 30° C for 2 hours. Oligos were purified by QuantiProbe G50 columns. 0.2 - 0.6 µg GST-purified protein were incubated with Aimee's binding buffer, supplemented with 1 µg poly dI-dC, and if needed with unlabeled oligos (10 minutes). Labeled oligos (25000 counts per minute) were added and the mix inubated for 20-30 minutes at room temperature. Where indicated, GST-antibody (1 µL) was added and incubated for another 10 minutes. Loading buffer was added to the samples and they were run in a 5 % TBE gel for 2.5 hours at 200 V. The gel was dried under vacuum and used to expose an X-ray film.

2.25 TF-ChIP protocol

Solutions used: Hypotonic buffer: 10 mM HEPES pH 7.9, 1.5 mM MgCl2, 10 mM KCl, 0.5 mM Dithiothreitol, add fresh: protease inhibitor; Lysis buffer I: 50 mM Hepes-KOH pH7.5, 140 mM NaCl, 1 mM EDTA, 10 % glycerol, 0.5 % NP-40, 0.25 % TX-100, fresh: protease inhibitor; Lysis buffer II: 200 mM NaCl, 1 mM EDTA, 0.5 mM EGTA, 10 mM Tris pH 7.5 + complete inhibitor; Lysis buffer III: 1 mM EDTA, 0.5 mM EGTA, 10 mM Tris pH 7.5, 100 mM NaCl, 0.1 % Na-Deoxycholate, 0.5 % N-lauroyl sarcosine + complete inhibitor; IP buffer: 2 mM EDTA, 150 mM NaCl, 20 mM Tris-HCl pH

8.1, 0.1 % TX-100, fresh protease inhibitor; Wash buffer I: 2 mM EDTA, 20 mM Tris-HCl pH 8.1, 0.1 % SDS, 1 % TX-100, 150 mM NaCl; Wash buffer II: 2 mM EDTA, 20 mM Tris-HCl pH 8.1, 0.1 % SDS, 1 % TX-100, 500 mM NaCl; Washing buffer III: 1 mM EDTA, 10 mM Tris-HCl pH 8.1, 250 mM LiCl, 1 % Deoxycholate, 1 % NP-40; Wash buffer IV: 1 mM EDTA, 10 mM Tris-HCl pH 8.1; Wash buffer V: 1 mM EDTA, 10 mM Tris-HCl pH 8.1, + 50 mM NaCl; Elution buffer: 50 mM Tris pH 8, 1 mM EDTA, 1 % SDS

150 larvae stage 3 were ground in liquid nitrogen using a mortar and pistil. The powdered tissue was transferred to a 15 mL falcon and resuspended in 2 mL hypotonic buffer. The solution was dounced (10 strokes) via a loose douncer on ice. Formaldehyde was added to the solution to a final concentration of 1 % and incubated at room temperature for 25 min on a rocker. The crosslinking was stopped by adding glycine to a final concentration of 0.125 M and incubation for 10 minutes on ice.

Cells were spun down at 2500 g for 10 min at 4 °C and the pellet resuspended in 1 mL lysis buffer I. After douncing the cells with a tight douncer for 20 strokes on ice, the solution was filtered through 2 layers of miracloth and incubated on a rocker on ice for 10 min. Cells and nuclei were spun down at 2500 g for 3 min at 4 °C and the pellet was resuspended in 1 mL lysis buffer II. After incubation at 4 °C for 5 min the nuclei were spun down at 2500 g for 3 min at 4 °C. The pellet was resuspended in 300 µL lysis buffer III and incubated for 20 min on ice. The lysate was sonicated with varying duty and power cycles (30 - 100 % duty, 50 - 100 % power) for 3 x 30 – 60 seconds on ice with 60 seconds pause in between cycles.

After the addition of Triton X-100 to a final concentration of 1 % the lysate was centrifuged at 16000 g for 10 min at 4 °C. 150 µL supernatant (nuclear extract) was diluted with 250 µL IP buffer. To precipitate unspecific DNA-protein complexes, 5 µg sonicated salmon sperm DNA and 40 µL pre-washed 50 % protein A / G-Sepharose slurry were added and the mixture incubated at 4 °C on a rocker for 3 - 4 hours. Unspecific complexes were pelleted by centrifugation at 800 g for 1 min at 4 °C. The supernatant was diluted with 100 µL IP buffer and incubated with 2 µg of the respective ChIP-grade antibody, 2 µg of sonicated salmon sperm DNA and 80 µL of pre-washed 50 % protein A / G-Sepharose slurry overnight at 4 °C on a rocker. The beads containing the tagged IPed protein / DNA complexes were pelleted via centrifugation at 800 g for 1 min at 4°C. Afterwards, the beads were washed once in 300 µL wash buffer I to III, twice in wash buffer IV and once in wash buffer V. Each wash was followed by centrifugation at 800 g for 1 min at 4 °C. Protein-DNA complexes were eluted by incubation of the beads in 200 µL elution buffer at 65 °C for 15 min with brief vortexing every 2 minutes. After centrifugation at 16000 g for 1 min, the

supernatant was de-crosslinked by overnight incubation at 65 °C. Samples were treated with RNAse A (0.2 µg / µL) at 37 °C for 1 hours and proteinase K (0.2 µg / µL) at 55 °C for 1 hours.

Samples were then extracted with sequential purifications with phenol, phenol : chloroform : isoamylacohol and chloroform : isoamylacohol. DNA was precipitated via NaOAc-ethanol, washed twice in 70 % ethanol and resuspended in 10 mM Tris, pH 8.

2.25.1 Ligation-mediated PCR

60 µL immunoprecipitated DNAs were incubated with T4-buffer, 0.5 µL BSA, 0.1 mM dNTPs, 0.5 units T4-DNA-polymerase in 50 µL volume at 12°C for 20 minutes. DNAs were spiked with 12 µL 3 M NaOAc, 20 µg glycogen and 120 µL phenol : chloroform : isoamylacohol. After vortexing, samples were centrifuged at 14000 g at 4 °C for 3 minutes. The upper phase was collected and incubated with 300 µL pre-chilled 100 % ethanol at –20 °C for 20 minutes. DNAs were precipitated by centrifugation at 14000 g at 4 °C for 30 minutes and washed in 70 % ethanol. Dried DNAs were resuspended in 50 µL dH_2O.

25 µL of the purified DNAs were incubated with annealed oJW102 / 103 or annealed L1 / L2 linkers and T4-DNA-ligase (1 µL) in ligation reaction mix at 12 °C overnight. Afterwards, the samples were precipitated by NaOAc-ethanol and washed in 70 % ethanol. The DNAs were resuspended in GoTaq reaction mix and amplified with oJW102 or L1 primers (100 µL reaction volume). After 15 initial amplification steps, 2 µL reaction product were amplified for additional 40 cycles. As a proof of principle, a nested PCR on samples from Cycle-HA pulldown for E-Box binding regions of the genes timeless and period were added.

Following linkers were used:

linker	Sequence	linker	sequence
oJW102	GCGGTGACCCGGGAGATCTGAATTC	L1	AGAAGCTTGAATTCGAGCAGTCAG
oJW103	GAATTCAGATC	L2	CTGCTCGAATTCAAGCTTCT

Following primers were used:

gene region	forward primer	reverse primer	comment
tim1	TATTGCTGTTGTTCCCAGAC	GAATGCGATCTGAGTTACGG	E-BOX region
per1	GACACTCACCCGAAATCAC	CTTTATGCCTTATCAGCCGT	E-BOX region
per3	GCCTACGTGAAGTGAACTC	TGGATAACAGTCGCATAACC	E-BOX region

2.26 Realtime qRT-PCR analysis

RNAs were isolated with the Macherey & Nagel RNA extract II kit followed by reverse transcription with Qiagen Quantitect Reverse Transcription kit (both according to manufacturer's instructions). Realtime qRT-PCRs were run with SYBR green supermix (BioRad) in a BioRad iQ5 cycler. Ribosomal protein 49 (rp49), actin (act) and mitochondrial elongation factor Tu (EFTuM) were simultaneously used as reference genes. Following primers were used:

gene	forward primer	reverse primer
4ebp	CATGCAGCAACTGCCAAATC	CCGAGAGAACAAACAAGGTGG
ACC	GTGCAACTGTTGGCAGATCAGT	TTTCTGATGACGACGCTGGAT
ACS	AAATCCCATGGACCGATGAC	TGTAGAGCATGAACAATGGATCCT
akh	GGTCCTGGAACCTTTTTCGAG	TTGCACGAAGCGGAAGATC
Ance-5	TGAATCGTTGGGCTTAATGG	ATACCTGCGACTTGCACTC
bmm	ACGCACAGCAGCGACATGTAT	CTTTTCGCTTTGCTACGAGCC
bnb	GACCAAGACCATCGAAGCC	CTCCACGCTGTTGATCTCC
CG13360	AAGCTGGGCAAGTTCCAC	AATCGCTCGTTGGTTCTG
CG16771	AAGGAGACGGTGGAAATAGG	AACCACGGATATGAGGAAGAG
CG30002	ACAAGTGGATTCTTCACGAGG	AGGCATATGGGTCGTATGTG
CG31683	ATGAGCTGGTGAAACTTGGA	GAGATCGATGAAGAACTGTTGG
CG4259	GCGTTTCTCACGACACTG	AATGTCGCTCTGGGATTACTG
CG6910	GACTGTGGATTTCGTCAAGGG	ACCAAATCGTTCAGCTTCTC
CG7763	TTTGGTACTCCCGTTGTGTC	AGACACCGTAGCAATATGCAG
CG8193	GCCATTCACCAAGGATTTGTC	TGATTCAATCATGTTGCCGAG
CG8908	ACCATCCATACAGCACTGTC	CCTTCAAGTTCTCCATGTACTC
Damm	GCCTTACCAGGGACTTTCAG	GAAGTTGTGCGACTCCTCAG
dilp2	CTGAGTATGGTGTGCGAGGA	GCGGTTCCGATATCGAGTTA
EFTuM	CATGTCCTTCATCCAACTGCA	AATGAGCTTGGTGTCTTCGCC
FAS	CCCCAGGAGGTGAACTCTATCA	GACTTGACCGATCCGATCAAC
FCS	CATCGCCCAGCGTAGCATA	CGAGCCGAATGGATGATAGC

InR	AACAGTGGCGGATTCGGTT	TACTCGGAGCATTGGAGGCAT
Pxn	CGCTAGATTTGCGTTTCAATCAC	GTAAGCCAGCTCGTTGTC
rp49	GCTAAGCTGTCGCACAAATG	GTTCGATCCGTAACCGATGT
Snmp-2	GTCTCTGATTGTCAGTGCCC	TCTTGTATAACAACGCTCTGCT
Sr-CI	CCATGTGGAATAGGTTCAGAG	CTTGCATCTCGTCAATGCTG
SREBP	CGCAGTTTGTCGCCTGATG	CAGACTCCTGTCCAAGAGCTGTT
ssSPT	ACCCTCTACGAACTGAACAC	CGGCACAAAGGCAAAGGA
tig	GCAGAAATTCAACGTCCTCTC	TCAGAACTCAATTGGTCCAG
vkg	CTTCTGGGCGTCGTTTATCTG	CCCTTGATTCCTTTGCAGTC

Following vectors were created in the course of this thesis:

CHAB-SchlankProm-3-2049 (LacZ), pCaSPeR-AUG-Gal4-SchlankProm-0-2636, pCaSPeR-AUG-Gal4-SchlankProm-0-794, pCaSPeR-AUG-Gal4-SchlankProm-1042-1626, pCaSPeR-AUG-Gal4-SchlankProm-1552-2636, pCaSPeR-AUG-Gal4-Schlank-Prom-3-1042, pCaSPeR-AUG-Gal4-SchlankProm-3-1664, pCaSPeR-AUG-Gal4-SchlankProm-3-2049, pCaSPeR-AUG-Gal4-SchlankProm-775-1092, pCaSPeR-AUG-Gal4-SchlankProm-775-1664, pCaSPeR-AUG-Gal4-Schlank-Prom-775-2049, pCaSPeR-AUG-Gal4-SchlankProm-Intron1-part1, pCS2-SchlankΔLLMLL, pGEX4T3-Df31, pGEX4T3-Schlank FL, pGEX4T3-SchlankCT, pGEX4T3-SchlankHOM, pGEX4T3-SchlankHOX, pGEX4T3-SchlankNT, pMTV5-myc-lip3, pMTVB-myc-SchlankΔLLMLL-HA, pTriEx4.0 - doubleHIS-schlank-HOM, pUAST-attB-Schlank-fl-internal GFP, pUAST-attB-Schlank-fl-KKKtoEEE internal GFP, pUAST-attB-Schlank-NTtoHOM RPKK->QPQQ | KKK->EEE | RLRR->QLQQ internal GFP, pUAST-BiPleaderNeGFP-SchlankHOM, pUAST-myc-Schlank llmll->llmaa, pUAST-myc-Schlank ΔLYSFIFGVIV-HA, pUAST-myc-Schlank-R122A-HA, pUAST-myc-SchlankΔ119-125-HA, pUAST-NeGFP, pUAST-NeGFP-mRFP, pUAST-NeGFP-Schlank-fl, pUAST-NeGFP-SchlankHOM, pUAST-NeGFP-SchlankHOM-R124A, pUAST-NeGFP-SchlankHOM-R78A-R124A, pUAST-NeGFP-SchlankHOMΔ119-125, pUAST-NeGFP-SchlankHOMΔHelix1, pUAST-NeGFP-SchlankHOMΔHelix2, pUAST-NeGFP-SchlankHOMΔHelix3, pUAST-NeGFP-SchlankHOMΔRPKK, pUAST-NeGFP-slak-aa1-138, pUAST-NeGFP-slak-aa1-158, pUAST-NeGFP-slak-aa138-158, pUAST-NeGFP-slak-aa1-63, pUAST-NeGFP-slak-aa64-158, pUAST-Schlank-eGFP (c-terminal), pUAST-Schlank-fl-RPKK->QPQQ | KKK->EEE | RLRR->QLQQ internal GFP, pUAST-Schlank-LLMAA, pUAST-Schlank-NTtoHOM internal GFP, pUAST-SchlankΔllmll, pUAST-SchlankΔLYSFIFGVIV, pWIZ-lagRNAi-18-2, pWIZ-lagRNAi-18-7, Topo NheI-Gal4SV40pA-BglII, Topo T7-eGFP dsRNA B2-1-T7, Topo T7-ketel dsRNA 30677 A1-T7, Topo T7-LacZ dsRNA C2-2-T7, Topo T7-Sec61ß dsRNA 31249-C1-T7, Topo T7-Sec61ß dsRNA 31250 D1-T7, Topo-lip3FL-1, Topo-myc-Schlank-LLMAA-HA, Topo-myc-Schlank-R122A-HA, Topo-Schlank-LLMAA, Topo-SchlankΔ119-125, Topo-T7-EGFP-T7, Topo-T7-schlank-SP6, Topo-T7-Sec15-dsRNA-T7

3 Results

3.1 Changes in *schlank* expression affect lipid storage by regulating key enzymes of lipolysis and lipogenesis independently of altered ceramide levels

Previous analyses had revealed that *schlank* mutant larvae are delayed in development (André Völzmann, 2007; Bauer et al, 2009) and in addition show a reduction in the larval length / width ratio as well as a more transparent appearance of *schlank* mutant fat bodies (Fig. 3.1 A, B). Earlier analyses via an enzymatic triacylglycerol (TAG) assay (André Völzmann, 2007) as well as a refined TAG content determination in collaboration with Reinhard Bauer and Bernadette Breiden via thin layer chromatography (Bauer et al, 2009) showed that the visual impression is caused by a strong loss of substantial amounts of storage fat that is usually deposited in the larval fat body (loss of 30-60% depending on the strength of the allele; (Bauer et al, 2009). To exclude that the changes were due to differences in feeding, various hallmarks of feeding and starvation were checked.

Feeding red-colored yeast showed that the food can pass the entire gastro-intestinal tract and that there is no blockage (Fig. 3.1.1 A). Also there was no difference in the take-up of radioactively labeled food supplements (Bernadette Breiden, Reinhard Bauer personal communication).

Another hallmark of starvation is decreased activity of the Insulin-signaling pathway: In a starvation situation, the pathway activity is reduced, which leads to enhanced translocation of the transcription factor 'Forkhead box, sub-group O' (Foxo) from cytoplasm to the nucleus. Thus, nuclear Foxo activity leads to transcriptional upregulation of e.g. *elongation factor 4 binding protein* (*4ebp*) and the *insulin receptor* (*InR*). Transcription of these target genes is not differentially regulated between wildtype and *schlank* mutant animals, indicating that the animals do not starve. Also, there was no obvious change in *drosophila insulin like peptide 2* (*dilp2*) transcription. Dilp2 protein is thought to regulate insulin signaling activity (Fig. 3.1.1 C).

As an additional indicator of the feeding status of the larvae, the hepatocyte-like oencytes in the body wall of larval segments are known to accumulate neutral fats upon a starvation situation (Gutierrez et al, 2007). There is no increase in Oil red O staining in well fed $schlank^{G0061}$ mutant compared to wildtypic oenocytes. Starvation can still be induced in *schlank* mutants by food deprivation. The starvation response is still intact, shown by the accumulation of lipids in oenocytes visualized by Oil red O staining.

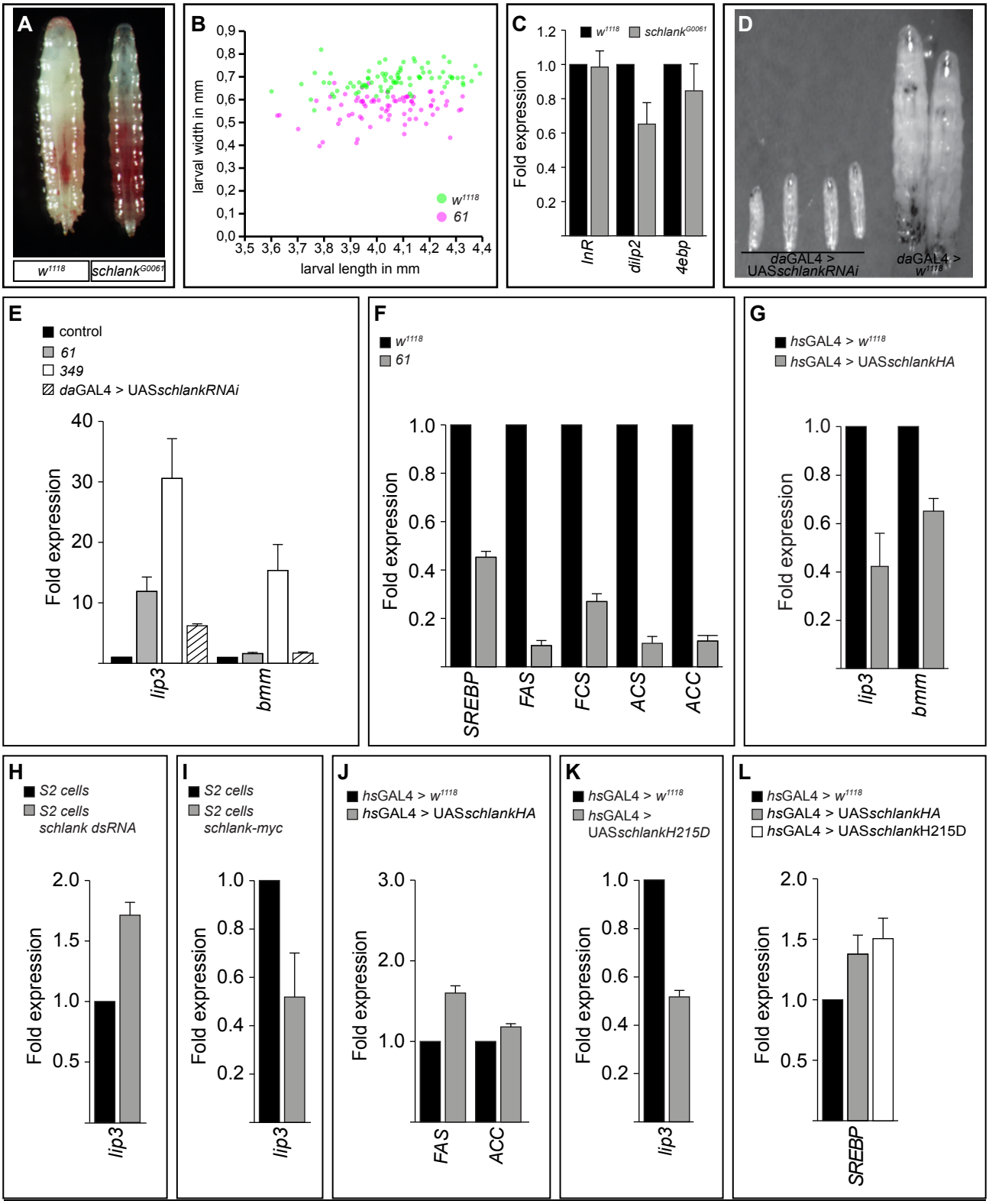

Figure 3.1.1 Modification of *schlank* expression levels lead to a disturbance of overall fat storage by changing the expression of key enzymes in lipolysis and lipogenesis in an insulin- and feeding-independent mechanism that is not mediated by ceramide synthesis activity. A, Picture of wildtypic and *schlank*^{G0061} mutant larvae at stage 3. Note that mutants seem to be thinner than wildtypes when reaching the same size and the fat body is less pronounced in opaqueness and filling. Larvae were fed red-colored yeast to exclude differences in food uptake or blocked food passage as cause. **B**, Comparative quantification of larval length and width: length-width values of wildtypic larvae are depicted in magenta, values for *schlank*^{G0061} mutant larvae are in green. At any given larval length, the *schlank*^{G0061}

mutant population is thinner than wildtypic one. **C**, Expression of Insulin-signaling regulated Forkhead box, subgroup O (FOXO) target genes was determined by realtime-qRT-PCR. There are no obvious differences in the expression of the *insulin-receptor* (*InR*), *insulin-like peptide 2* (*dilp2*) or *elongation factor 4 binding protein* (*4ebp*) genes. **D**, Ubiquitous expression of UAS-*schlankRNAi*^{33896} via the *daughterless* (*da*)-GAL4 driver line leads to developmental retardation and death, similar to phenotypes observed in *schlank*^{G0349} and *schlank*^{G0061} mutants. **E-L**, Quantification of the transcript expression of key regulators involved in lipolysis and lipogenesis upon modification of schlank expression levels via realtime-qRT-PCR. **E**, Downregulation of the expression of schlank either by mutation (*schlank*^{G0061}, *61*; *schlank*^{G0349}, *349*) or RNAi (UAS*schlankRNAi*) leads to an increase expression of *lipase 3* (*lip3*) and the lipase *brummer* (*bmm*). **F**, Similarly, *schlank*^{G0061} mutants show decreased expression of the transcription factor *sterol element binding protein* (*SREBP*) and its target genes *fatty acid synthase* (*FAS*), *fatty acyl-CoA synthase* (*FCS*), *acetyl-CoA-synthase* (*ACS*) and *acetyl-CoA-carboxylase* (*ACC*) compared to wildtypic controls (*w*^{1118}). **G**, Upon short term overexpression of full length hemagglutinin-tagged schlank (*schlankHA*) via a heatshock (hs)-GAL4 driver line, *lip3* and *bmm* expression decreases. **H**, Downregulation of *schlank* in S2 cell culture via dsRNA treatment (*schlank dsRNA*) leads to an increase in *lip3* expression, thus further excluding feeding differences and systemic signaling as cause for *lip3* expression changes. **I**, Complementarily, overexpression via transfection of a myc-tagged full length schlank variant (*schlank-myc*) decreases *lip3* expression. **J**, Short term overexpression of schlank leads to an increase in *FAS* but only minor in *ACC* expression. **K-L**, Overexpression of a schlank version that lost Ceramide Synthase enzyme activity (*schlankH215D*) still decreases *lip3* expression (**K**) and increases SREBP expression to similar levels as when an intact full length schlank version is overexpressed (**L**). All realtime-qRT-PCR quantifications were repeated ≥ three times. Error bars indicate standard error of the mean (s.e.m.).

It is, however, noteworthy that overall Oil red O intensity in *schlank*^{G0061} mutants is decreased in well fed as well as starved conditions (Fig 3.1.2). This might be a secondary effect due to the overall reduced TAG levels.

Two processes were shown to affect storage fat levels in *Drosophila* larvae (Grönke et al, 2007): lipogenesis and lipolysis. Lipogenesis is the build-up of fatty acids and ultimately of DAGs/TAGs via a cascade of enzymatic reactions. Sterol element binding protein (SREBP) is a key transcription factor that directly activates transcription of enzymes involved in lipogenesis, like *fatty acid synthase* (FAS), *fatty acylCoA-synthase* (FCS), *acetylCoA-synthase* (ACS) and *acetylCoA-carboxylase* (ACC). Transcription of those enzymes is downregulated in *schlank*^{G0061} mutants (Fig. 3.1.1 F). We could show in addition, that overall SREBP protein levels are also reduced in *schlank*^{G0061} mutant adults (Bauer et al, 2009). Upon short term overexpression of Schlank, SREBP targets slightly increase (Fig. 3.1.1 J). Overall, the results indicate that lipogenesis is reduced in *schlank* mutants.

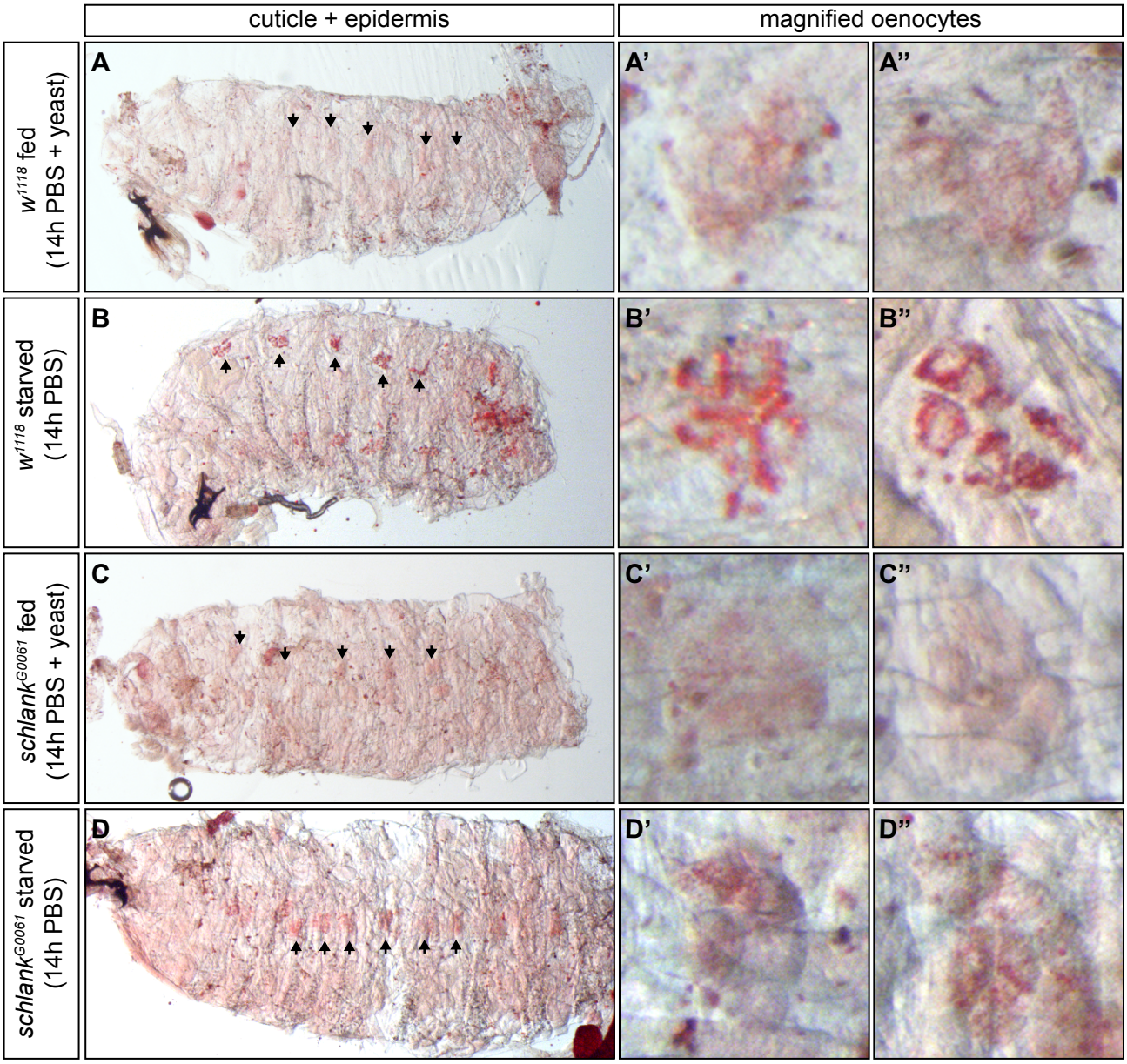

Figure 3.1.2 Schlank mutant phenotypes are not due to starvation. A-D'' Neutral lipids in epidermal oenocytes (arrows) were stained in fed (**A-A''**, **C-C''**) and starved (**B-B''**, **D-D''**) wildtypic (**A-B''**, w^{1118}) and $schlank^{G0061}$ mutant (**C-D''**) L3 larvae. **A-D** shows overview images of larval epidermises, **A'-D''** show magnifications of oenocyte clusters after Oil red O staining. While oenocytes are barely detectible by Oil red O staining in well-fed larvae (**A-A''**), upon starvation after a transfer of animals on PBS soaked filter material, there is strong accumulation of lipids which give a clear red staining via Oil red O (**B''**). Oenocytes of well-fed $schlank^{G0061}$ mutant larvae don't show enriched Oil red O staining (**C-C''**) but starved *schlank* mutants accumulate lipids in oenocytes (**D-D''**). This indicates that fed *schlank* mutants don't starve and that the normal starvation reaction as visualized by Oil red O staining in oenocytes is still intact, albeit that the overall lipid levels in the mutants are lower than in wildtypes, both under well-fed as under starvation conditions.

Fat stores are also tightly controlled by lipolysis. Upon starvation or increased energy demands, a cascade of Lipases is activated that can sequentially split fatty acids from TAGs and DAGs which are then metabolized by ß-oxidation to meet the energy requirements of the animal.

Consistent with the reduction of TAG levels, misregulations of Schlank levels lead primarily to transcriptional misregulation of enzymes important for lipolysis and lipogenesis. The transcription of *lipase 3* and *brummer lipase*, which are main enzymes in the lipolysis cascade, is upregulated in two *schlank* mutant alleles (G0349 and G0061, Fig. 3.1.1 E). When *schlankRNAi*^{33896} is ubiquitously expressed (Fig. 3.1 D), *lipase 3* is also upregulated (Fig. 3.1.1 E). This indicates that Schlank is an inhibitor of *lipase 3* expression.

Analogously, upon short term overexpression of *schlank* in wildtypic background, *lipase 3* and *brummer* transcript levels decrease (Fig. 3.1 G). The described effects could be reproduced in S2 cell culture by modifying *schlank* levels (André Völzmann, 2007; Fig. 3.1 H, I): Treatment with *schlank* dsRNA leads to an increase in *lipase 3* transcript (Fig. 3.1.1 H) and a decrease in *FAS* (data not shown). On the other hand, *schlank* overexpression decreases *lipase 3* transcription (Fig. 3.1.1 I). Interestingly, the resulting loss of storage fat in cell culture *schlank knock down* situations could be rescued by an additional downregulation of *lipase 3* transcription (Ute Schepers, unpublished data), indicating that *lipase 3* misregulation might be the main cause of the observed storage fat alterations.

To tackle the question whether *lipase* misregulation upon *schlank* overexpression is due to its Ceramide Synthase activity, a full length variant of Schlank was used that is point mutated in the catalytic Lag1 motif: H215D. Upon overexpression, Schlank H215D does not increase ceramide levels, in contrast to intact full length Schlank versions and is therefore considered catalytically inactive (Bauer et al, 2009).

However, overexpression of H215D still leads to a decrease in *lipase 3* expression (Fig. 3.1.1 K), an increase in TAG levels (Bauer et al, 2009) and an increase in *SREBP* transcription (Fig. 3.1.1 L) comparable to overexpressions of wildtypic *schlank* variants (Bauer et al, 2009), indicating that the observed effects are independent of the ceramide synthase activity of Schlank.

These findings raise major questions: could it be that the observed transcriptional changes (*lipases*, SREBP targets) and the change in TAG content upon modification of *schlank* levels are mediated by protein itself that would be independent of altered ceramide levels? And what other domain than the enzymatic core might mediate the observed transcriptional changes?

3.2 Schlank is a transmembrane protein containing a Lag1 motif and a homeodomain

Ceramide Synthases are multi-transmembrane proteins and can be subdivided into two classes. Both CerS classes have the defining Lag1 motif in common. However, while one class only codes

for the Lag1-motif (defined as class I CerS in this thesis), most metazoans express another CerS class that harbors a homeodomain-like stretch in addition (defined in this thesis as class II CerS) (Fig. 1.2 A).

prediction program	start	TM 1	TM 2	TM 3	TM4	TM 5	TM 6	TM 7
Phobius	ER lumen	43-60	143-163	183-202	209-228	234-251	263-283	303-326
TMHMM v2	ER lumen	43-60	141-158	182-204			266-288	303-325
HMMTOP	ER lumen	43-60	140-157	182-199			266-283	306-323
TMpred	ER lumen	42-61	143-164	182-202	210-232		263-282	305-321
TMpred	cytoplasm		143-164	182-202	210-232		263-282	305-321
PHDhtm	NOT DEFINED	45-62	142-159	183-200	218-235		267-289	302-326

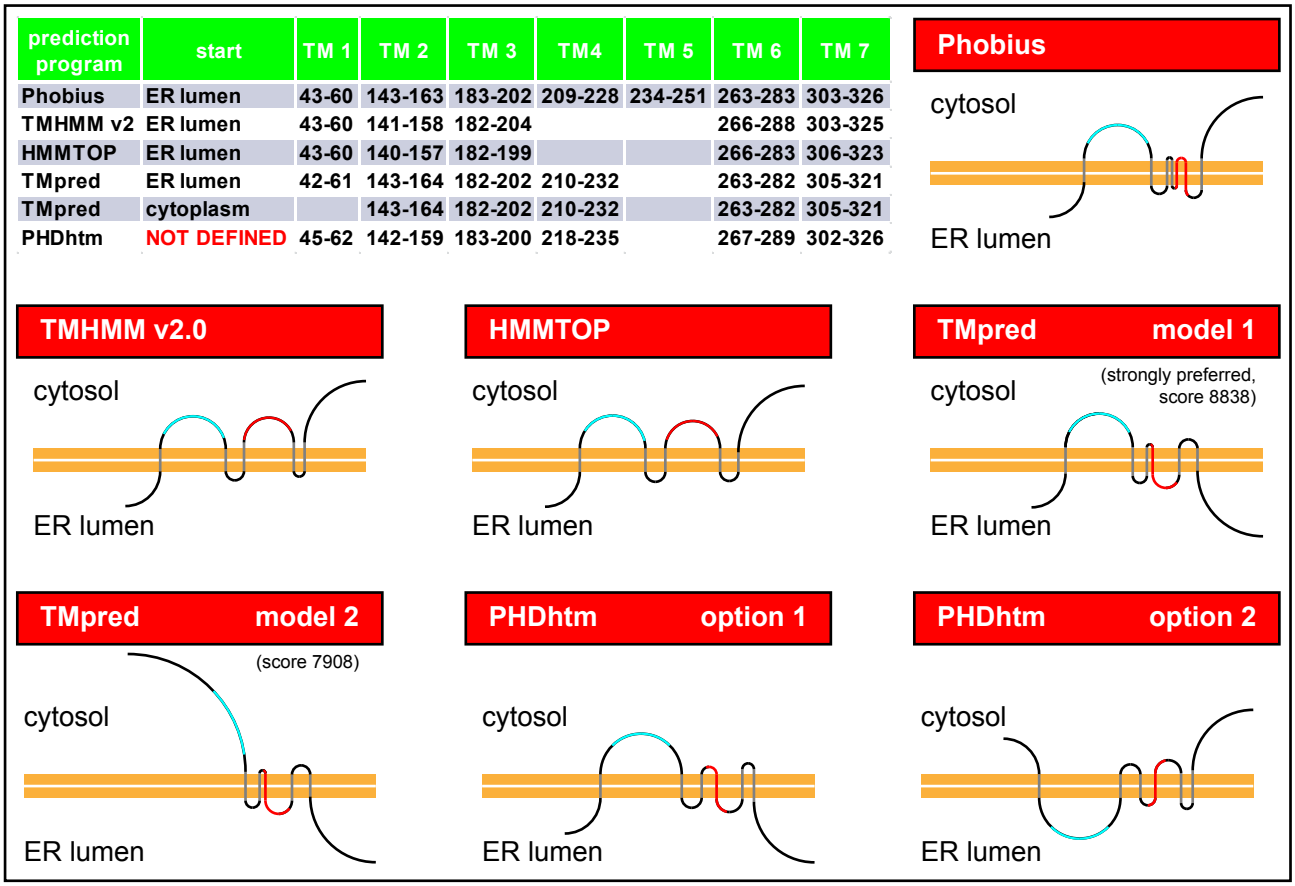

Figure 3.2 Schlank encodes a type II Ceramide Synthases with its homeodomain facing the cytosol. A, Summary table of the position (numbers) of predicted transmembrane domains (TM). Various prediction programs predict to which compartment the N-terminus of the protein would face. PHDhtm was used for consistency with previously published models of CerS topology that were based on this program. Note, however, that PHDhtm does not allow any prediction of protein orientation, it only predicts the position of potential TMs within a protein. Models and variants predicted by the prediction programs are drawn to amino acid scale. The ER membrane is depicted in light brown, protein backbone in black, homeodomain in blue, Lag1 motif in red and TMs in grey. Cytosolic and ER luminal sides are indicated. If multiples models were calculated, the score is of each model is given.

The fruit fly CerS Schlank belongs to the second class coding for both, the Lag1-motif and a homeodomain. Furthermore, for the Schlank protein various transmembrane domain prediction programs determine that the homeodomain is located between a first and second transmembrane domain (out of 5-7 TMs) and would be facing the cytosol (for programs, employing an algorithm that allows a prediction of protein orientation; Fig. 3.2 A). Homeodomains have been identified in homeobox transcription factors, where they mediate DNA-interaction. Due to the fact that the changes observed in the Schlank mutants are mostly transcriptional in nature, it seems worthwhile

to investigate the properties of CerS homeodomains and whether or not they might mediate DNA interaction and transcription factor activity.

3.3 Ceramide Synthases are conserved and the homeodomain was already present in early metazoans

Alignments and Bayesian phylogenetic analysis of 218 Lag1-motif carrying proteins in 66 species compared to the closely related 'Translocating chain-associating membrane' (TRAM) and 'Ceroid-lipofuscinosis, neuronal 8' (CLN8) proteins (Fig. AP3.3.2 for quality control via 'Are We There Yet?' [AWTY] Nylander et al, 2008) showed two things:

1. Both Ceramide Synthase classes are closely related while there is substantial phylogenetic distance to TRAM and CLN8 proteins.
2. The homeodomain was taken up rather early in metazoan development.

While basic single cell fungi only contain multiple class I CerSs without homeodomain, other single cell eukaryotic sister groups of metazoans contain either class I or class II variants (although lateral gene transfer cannot be excluded at this stage). Following the course of evolution to higher animals, both classes are found in most species, usually with one class I paralog and multiple class II paralogs (Fig. 3.3 A, Fig. AP3.3.1, for quality control see Fig. AP3.3.2). Exceptions can be found in nematodes that seem to have secondarily lost type II members or the homeodomains specifically, while insects mainly encode only one class II CerS without any other paralogs (Fig. 3.3 A).
To more easily identify conserved amino acid stretches in various homeodomains of eukaryote Ceramide Synthases, a WebLogo of 153 Ceramide Synthase homeodomains from 48 species was generated from a ClustalW alignment (Larkin et al, 2007) (Fig. 3.3 B). The logo shows

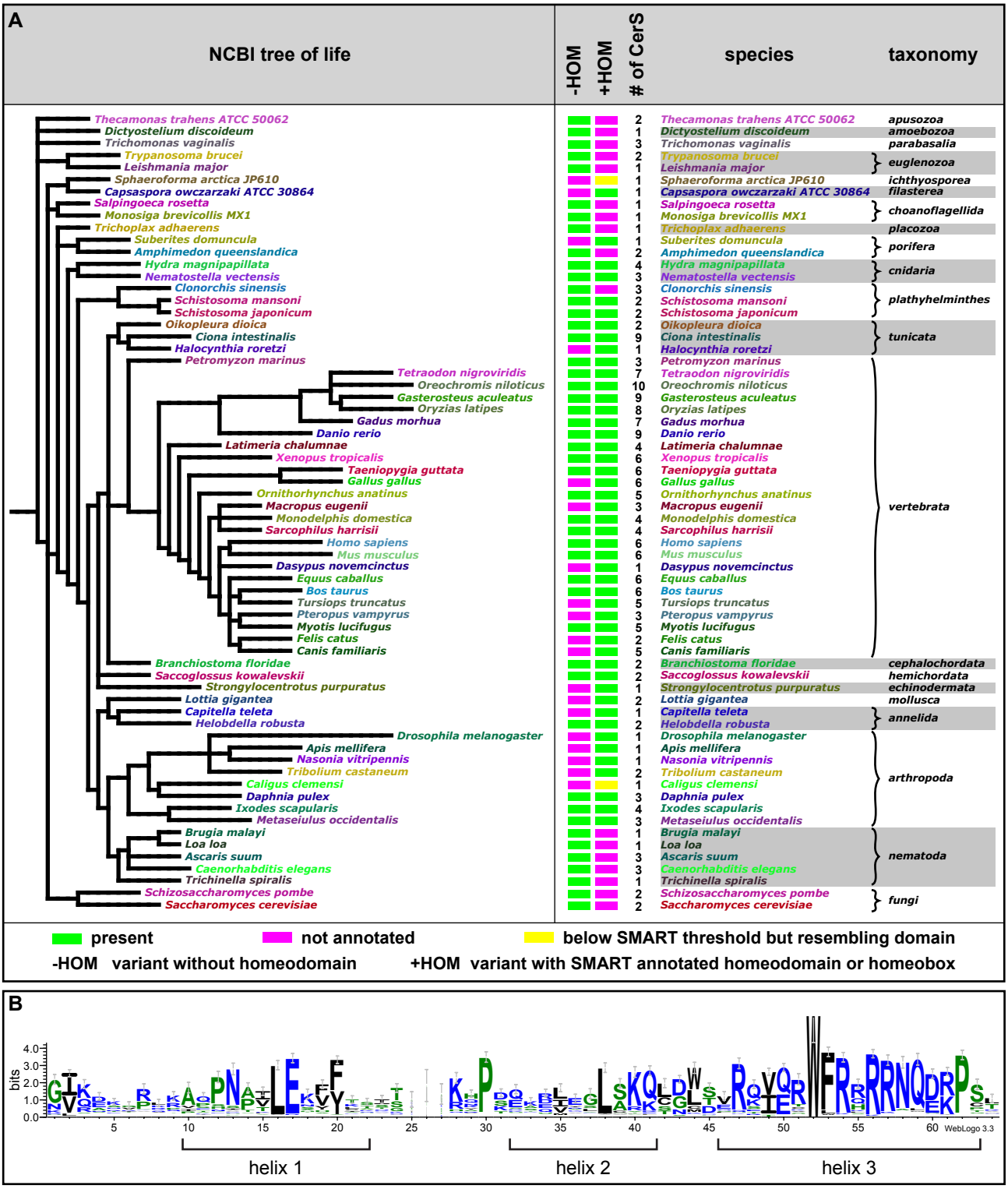

Figure 3.3 Type II (homeodomain-containing) CerS appeared already in Filasterea, latest in Cnidarians and their homeodomain conforms to a consensus motif. A, Tree of Life (NCBI database via iTOL) of identified species containing *ceramide synthase* genes. The color bars indicate the presence (green) or absence (magenta) of any given CerS type (with [+] or without [-] homeodomain [HOM]). The number of CerS (#) in any given species is indicated. Taxonomic identifiers are given, wherever possible. Originally without homeodomain, multiplication events took place and eventually a homeodomain-like stretch was incorporated in front of the Lag1 motif. The fact that Sphaeroforma and Capsaspora (for classification see Suga et al, 2013) both contain CerS versions with a homeodomain and that the homeodomains are conserved on sequence level indicates that the uptake took place even before the occurrence of

multicellularity. Additionally, there was a secondary loss in several species of either of the Ceramide Synthase versions. **B**, Consensus sequence logo of 153 Ceramide Synthase homeodomains from 48 species generated via WebLogo. Size of the letters corresponds to the number of occurrence at any given position within the alignment. Due to insertions within a low number of homeodomains, there are position gaps and shifts (amino acids 25-28 of the homeodomain), especially in the loop between helix 2 and 3.

that especially the third helix is nearly identical in all CerS homeodomains with additional substantial conservation before and in the first and second helix, as well (Fig. 3.3 B). This verifies that all CerS homeodomains are related and seem to be derived from one common precursor (for review on conserved amino acids between CerS and classical homeodomains, see Voelzmann & Bauer, 2010). Furthermore, phylogenetic analysis of the majority of human homeodomains (Holland et al, 2007a) showed that CerS homeodomains are closely related to Zhx / HOMEZ homeodomain families. Indeed, for some species, the CerS homeodomain is even predicted as HOMEZ-like (Fig. AP3.3.1, purple-colored domains)

3.4 CerS homeodomain three-dimensional structure is indistinguishable from classical homeodomains

So far there is only one study that experimentally analyzed the 3D-structure of Ceramide Synthase homeodomains: an NMR analysis of *Mus musculus* (Mm) CerS5 and 6 homeodomains (RIKEN project, PDB IDs 1x2m & 2cqx, Wada & Tanaka, 2002). 3D-models of those data show that there are three helices at angles similar to classical homeodomains from e.g. *Drosophila melanogaster* (Dm) Ultrabithorax (Ubx) or *Mesocricetus auratus* (Ma) Pancreatic And Duodenal Homeobox 1 (Pdx1) (Fig. 3.4). If only the backbone is depicted, those three as well as a SWISS-MODEL-3D model of the Schlank homeodomain are virtually identical in their orientation (Fig. 3.4 A-D).

Amino acid side chains especially in helix 3 but also in the beginning of the homeodomain (positions 2-7) were shown to be involved in DNA-homeodomain interaction (Wilson et al, 1996; Noyes et al, 2008a). The corresponding amino acids in the homeodomain models of Ubx and Pdx1 point towards either the phosphate backbone or directly to the DNA bases in the bound consensus site (Fig. 3.4 E, F). Overlays of the Pdx1-DNA to the homeodomain models of CerS6 and Schlank indicate that the corresponding amino acid side chains would also point towards phosphate backbone / DNA bases (Fig. 3.4 G, H). These data indicate that from a structural point of view, CerS homeodomains have the potential to bind DNA.

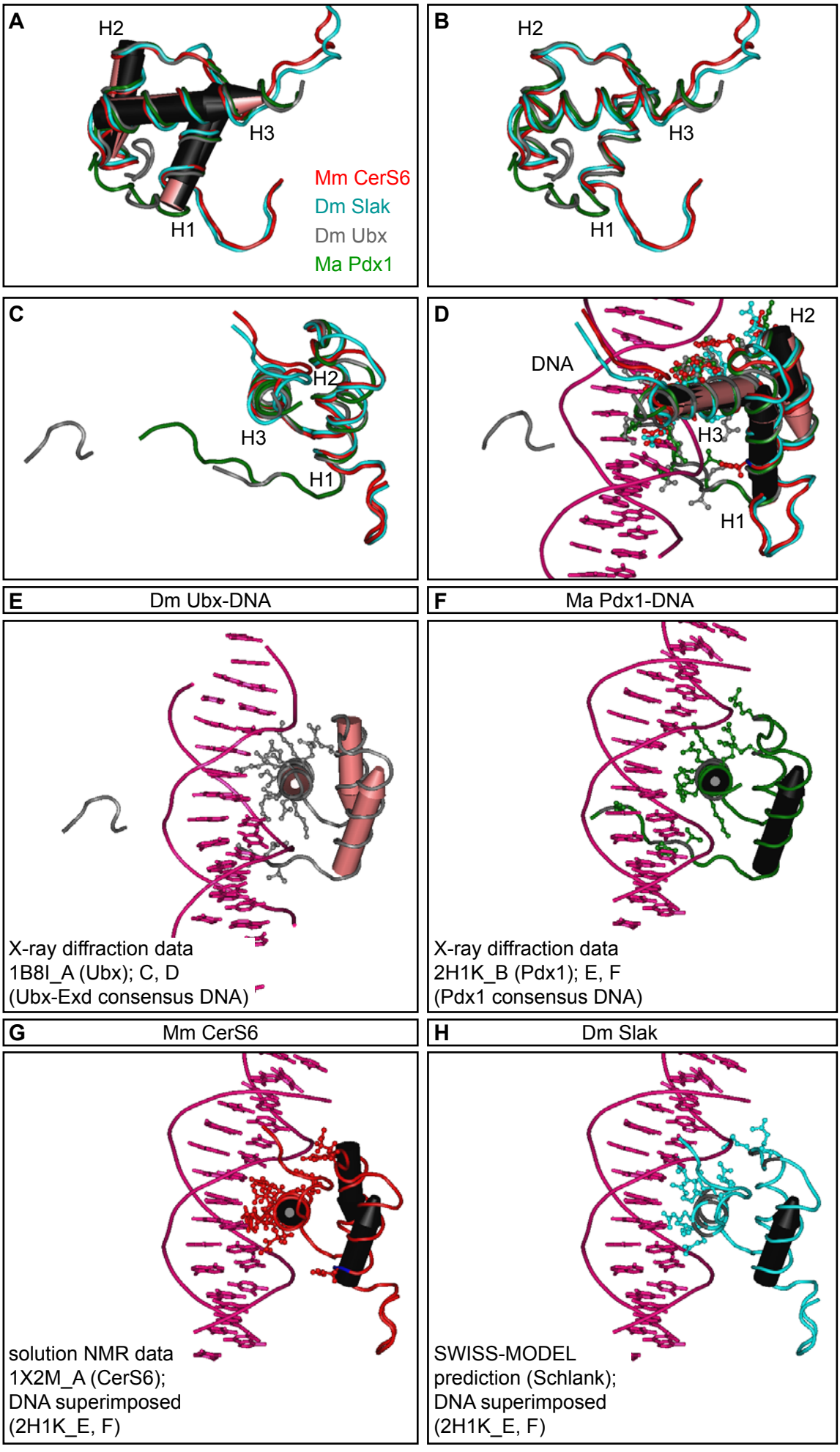
A
H2
H3
H1
Mm CerS6
Dm Slak
Dm Ubx
Ma Pdx1
B
H2
H3
H1
C
H2
H3
H1
D
DNA
H2
H3
H1
E
Dm Ubx-DNA
X-ray diffraction data
1B8I_A (Ubx); C, D
(Ubx-Exd consensus DNA)
F
Ma Pdx1-DNA
X-ray diffraction data
2H1K_B (Pdx1); E, F
(Pdx1 consensus DNA)
G
Mm CerS6
solution NMR data
1X2M_A (CerS6);
DNA superimposed
(2H1K_E, F)
H
Dm Slak
SWISS-MODEL
prediction (Schlank);
DNA superimposed
(2H1K_E, F)

Figure 3.4 NMR-based 3D models of CerS homeodomains are indistinguishable from X-ray based 3D models of classical homeodomains. 3D models of *Drosophila melanogaster* Ultrabithorax (Dm Ubx, PDB: 1B8I chain A, grey), *Mesocricetus auratus* Pancreatic and duodenal homeobox 1 (Ma Pdx1, PDB: 2H1K chain B, green), *Mus musculus* Ceramide Synthase 6 (Mm CerS6, PDB: 1X2M chain A, red) and *Drosophila melanogaster* Ceramide Synthase Schlank (Dm Slak, SWISS-MODEL prediction, blue) homeodomains illustrated by Cn3D viewer (Wang et al, 2000). The 3D backbone of CerS6 and Schlank homeodomains is indistinguishable from the backbone of classical homeodomains Ubx and Pdx1, both in helix arrow (**A**, arrows) and tube-worm representation (**B**). **B** represents a side view and **C** a frontal view of the homeodomains. **D**, DNA model from the Pdx1 model is superimposed. Amino acids side chains of helix 3 of all homeodomains point towards the DNA. **E**-**F** show the individual 3D models in frontal view of helix 3 with the corresponding bound consensus DNA, with the exception of CerS models in **G** and **H** where the DNA from the Pdx1 model is superimposed.

Another prerequisite for a potential function of the homeodomain in binding DNA, however, is a nuclear localization of the protein with the homeodomain facing the nucleoplasm.

3.5 Endogenous Schlank is localized to cytoplasm and nucleus of fat body cells

The major site of storage fat deposition and lipase activity is thought to be the larval and adult fat body. Consistent with the mutant phenotype, this is also where *schlank* is enriched at larval stages as revealed by the analysis of *schlank* promoter fragments, LacZ enhancer traps (Fig. AP 3.5.1-3.5.4) as well as antibody stainings of native protein (André Völzmann, 2007).

DNA-binding of a homeodomain usually requires its nuclear localization. Thus subcellular Schlank localization was determined by a series of newly generated affinity purified and Schlank specific antibodies (Fig. AP 3.5.5 & 3.5.6 for verification) and a Schlank-homeodomain-specific antibody. For co-labeling experiments, KDEL-GFP and Serca-YFP (Fig. 3.5) were used to mark the endoplasmic reticulum (ER; Okajima et al, 2005; Collado-Hilly et al, 2010), Lamin Dm0 antibodies recognize Lamin associated to the inner nuclear membrane (INM) and DAPI stains DNA. SchlankCT antibodies show that Schlank partly localizes to KDEL-GFP and SercaYFP-positive structures near the nucleus, confirming the CerS-typical localization at the ER (Fig. 3.5 A, A'). However, in addition to this ER-based protein pool, there is substantial enrichment of Schlank protein in the nucleus, well within the space enclosed by INM-marker Lamin Dm0 (Fig. 3.5 B). Noteworthy is a punctate to tubular Schlank pattern within the nucleus that can be easily identified in orthogonal views of confocal sections through fat body cells (Fig. 3.5 B').

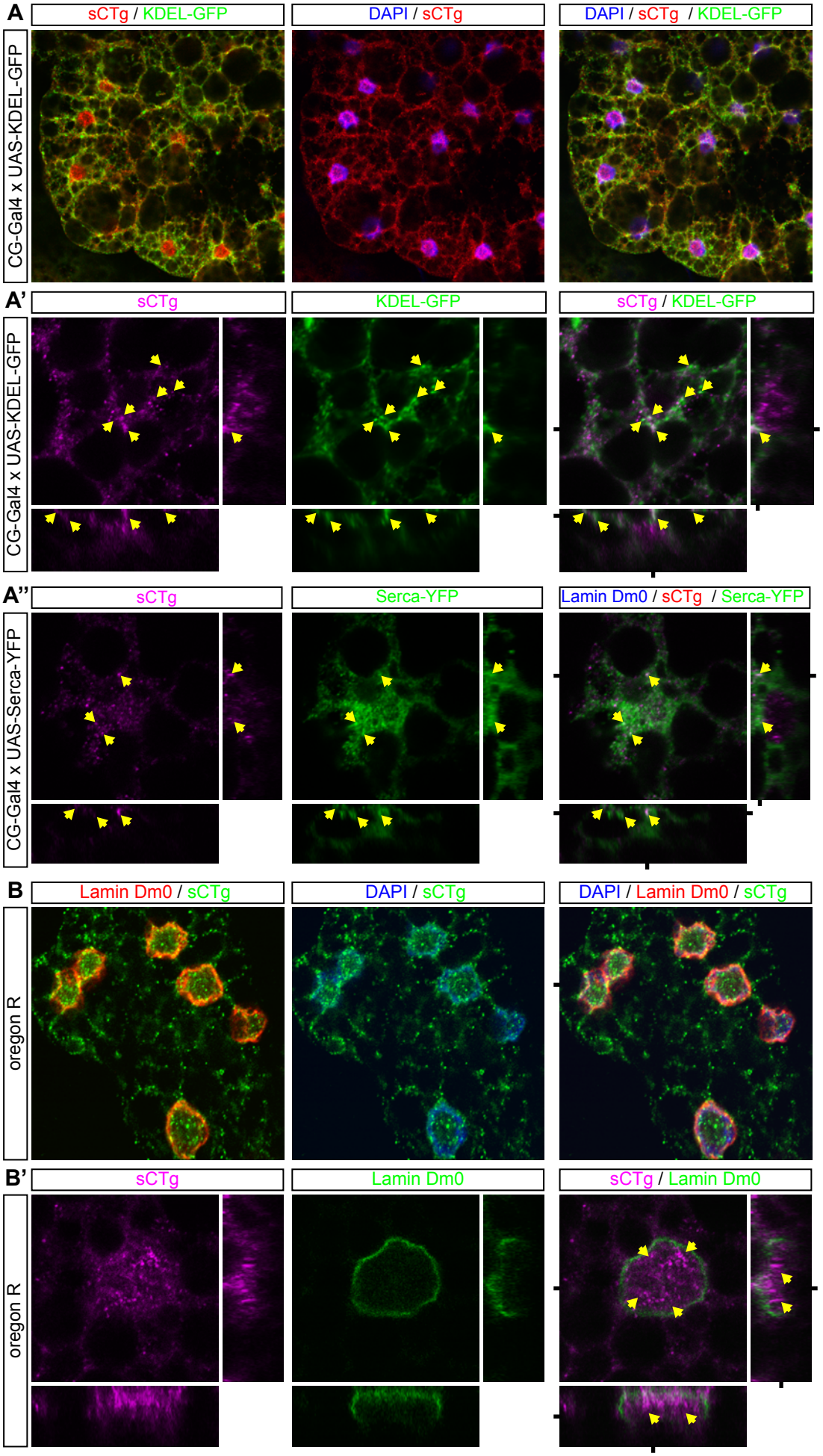
A
sCTg / KDEL-GFP
DAPI / sCTg
DAPI / sCTg / KDEL-GFP
CG-Gal4 x UAS-KDEL-GFP
A'
sCTg
KDEL-GFP
sCTg / KDEL-GFP
CG-Gal4 x UAS-KDEL-GFP
A''
sCTg
Serca-YFP
Lamin Dm0 / sCTg / Serca-YFP
CG-Gal4 x UAS-Serca-YFP
B
Lamin Dm0 / sCTg
DAPI / sCTg
DAPI / Lamin Dm0 / sCTg
oregon R
B'
sCTg
Lamin Dm0
sCTg / Lamin Dm0
oregon R

Figure 3.5 Endogenous Schlank protein is distributed in various subcellular pools, including endoplasmic reticulum and nucleus. A-B', images show co-stainings in fat body cells for Schlank (Schlank-CT guinea pig, sCTg; red in **A**, magenta in **A'** and **B'**, green in **B**) and subcellular markers for endoplasmic reticulum (ER-lumen, KDEL-GFP green; ER-membranes, Serca-YFP, green), inner nuclear membrane-lamina (Lamin Dm0) and DNA / chromatin (DAPI). **A** and **B** show fat body overview images, **A', A''** and **B'** depict orthogonal sections through 3D stacks of individual fat body cells. **A**, **A', A''** only a minority of the protein staining is found associated with the endoplasmic reticulum (yellow arrows). However, substantial amounts of Schlank protein is within the nucleus (**B** and **B'**, nuclear lumen is encircled by Lamin Dm0). Black bars next to the overlay images indicate the position of orthogonal sections. Y-Z sections are at the right hand side of the individual stack layers, X-Z sections are below.

3.6 Nuclear Schlank partly co-stains with INM markers, also within the nucleoplasm

The Schlank protein is a multi-transmembrane protein. Thus the punctate to tubular pattern within the nucleus is unlikely to be staining of free protein aggregates. It was previously shown that the inner nuclear membrane can produce two types of indentations (which combined are known as nucleoplasmic reticulum, NR). Type I indentations consist solely of folded INM membranes reaching inside the nucleus. Type II indentations are a combinatorial invagination of inner and outer nuclear membranes (INM and ONM) that are coated with Lamin (Broers et al, 1999; Malhas et al, 2011; Lamin B-variants can be stained by Lamin Dm0 antibody, Schulze et al, 2009), thereby visualizing type II indentations, in contrast to type I invaginations that are not covered by Lamin (Malhas et al, 2011). To see, whether or not Schlank would be inserted in the INM, fat body cells were co-stained for membrane-integral INM markers Otefin and Bocksbeutel (Wagner et al, 2004) (Fig. 3.6).

Co-staining of either SchlankCT or Schlank-homeodomain (Fig. 3.6 A, C) antibodies shows a partial co-localization with INM-marker Otefin in punctate to tubular structures in the nucleoplasm, which are not lined by Lamin Dm0 (Fig. 3.6 A). A similar pattern can be observed for a co-staining with INM-marker Bocksbeutel (Fig. 3.6 B). These data indicate that Schlank seems indeed to reside in type I INM invaginations.

This localization necessitates a nuclear import of the Schlank protein. Translocation of proteins into the nucleus is usually mediated by the α-Importin/ß-Importin mechanism that recognizes nuclear targeting sequences in proteins designated for nuclear import. Thus, the possibility that the Schlank protein should contains a region that would be necessary for its import was further explored.

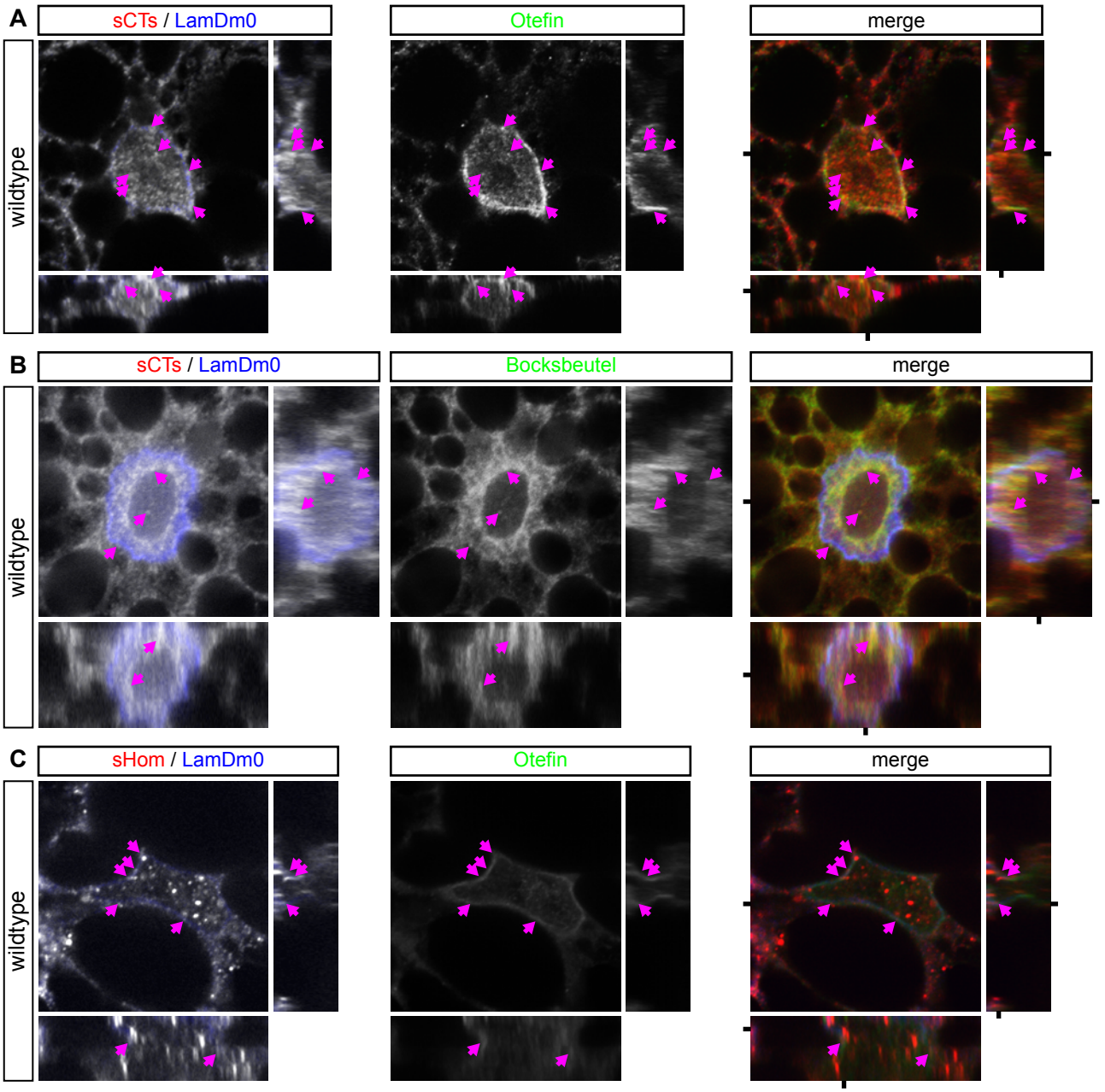

Figure 3.6 Schlank partly co-localizes with marker for the inner nuclear membrane. A-C, Orthogonal sections through fatbody cells marked for inner nuclear membrane markers Otefin (green) and Bocksbeutel (green). Schlank antibodies directed against its C-terminus (**A-B**, sCTs, red) and the homeodomain (**C**, sHOM, red) show co-staining (arrows) with INM markers at the nuclear envelope (marked by Lamin Dm0, blue) as well as in tubular structures (arrows in orthogonal views in A and B) reaching into the nucleoplasm.

3.7 Schlank protein regions determining nuclear import

To analyze, which part of the protein confers signal necessary for nuclear import, a series of overlapping Schlank protein version and deletions was generated.

3.7.1 The Schlank homeodomain mediates nuclear enrichment

N-terminal constructs of varying lengths were fused to an N-terminal eGFP and expressed in *Drosophila* Schneider cells (Fig. 3.7 A). While free eGFP freely diffuses between cytoplasm and nucleoplasm and can thus be found uniformly throughout the cell, the location of the Schlank derived fusion constructs is more restricted. To quantify a potential nuclear enrichment of an eGFP-tagged construct (Fig. AP3.7A), cell borders were marked in the DIC image channels (AreaC) and nuclei in DAPI channels (AreaN). Cytoplasmic fluorescence intensity was determined by subtracting nuclear eGFP intensity from whole-cell intensity. The ratio between cytoplasmic and nuclear eGFP-intensity was used as a statistical measure for nuclear enrichment (Fig. AP 3.7 A-C).

While an N-terminal encompassing the first transmembrane domain (aa1-63) is found in a vesicular and perinuclear pattern, constructs that either only contain the homeodomain (aa64-138, aa73-133) or start at the N-terminus and contain the homeodomain but not the second transmembrane domain (aa1-138) are nearly exclusively localized to the nucleus (in contrast to free eGFP; 1:3-1:5 ratio vs. 1:1.5). Constructs that also contain the second transmembrane domain are not exclusively enriched in the nucleus (ration ~1 to 1:1.5). With this tagging system however, it is not possible to distinguish between a partly nuclear localization with an accompanying cytoplasmic pool and the free eGFP contribution. This is due to the ubiquitous distribution pattern of the eGFP. Nevertheless, it is well suited to identify strong nuclear accumulation (Fig. 3.7 A; Fig. AP3.7 B).

Having identified the homeodomain as the protein stretch that contains nuclear import information, it stands to reason that there might be nuclear localization sequences (NLS) within the homeodomain.

3.7.2 Mutation of nuclear localization sequence (NLS)-like stretches in the homeodomain prevents exclusive nuclear enrichment

When the Schlank protein sequence is analyzed via WoLF PSORTII (Nakai & Horton, 1999; Nakai & Kanehisa, 1992) and cNLS-Mapper(Kosugi et al, 2009b; Kosugi et al, 2009a), two NLSs are predicted. The first stretch, RPKK, is recognized as four-residue pattern (pat4) NLS sequence. A second longer sequence is flagged as a bipartite NLS (Fig. 3.7 B). It starts with a RLDKKK stretch and spans to the highly conserved RxxRxRR region. NLSs are known to mediate nuclear import via Importin proteins. To address whether or not they also contribute this function for Schlank, NLSs

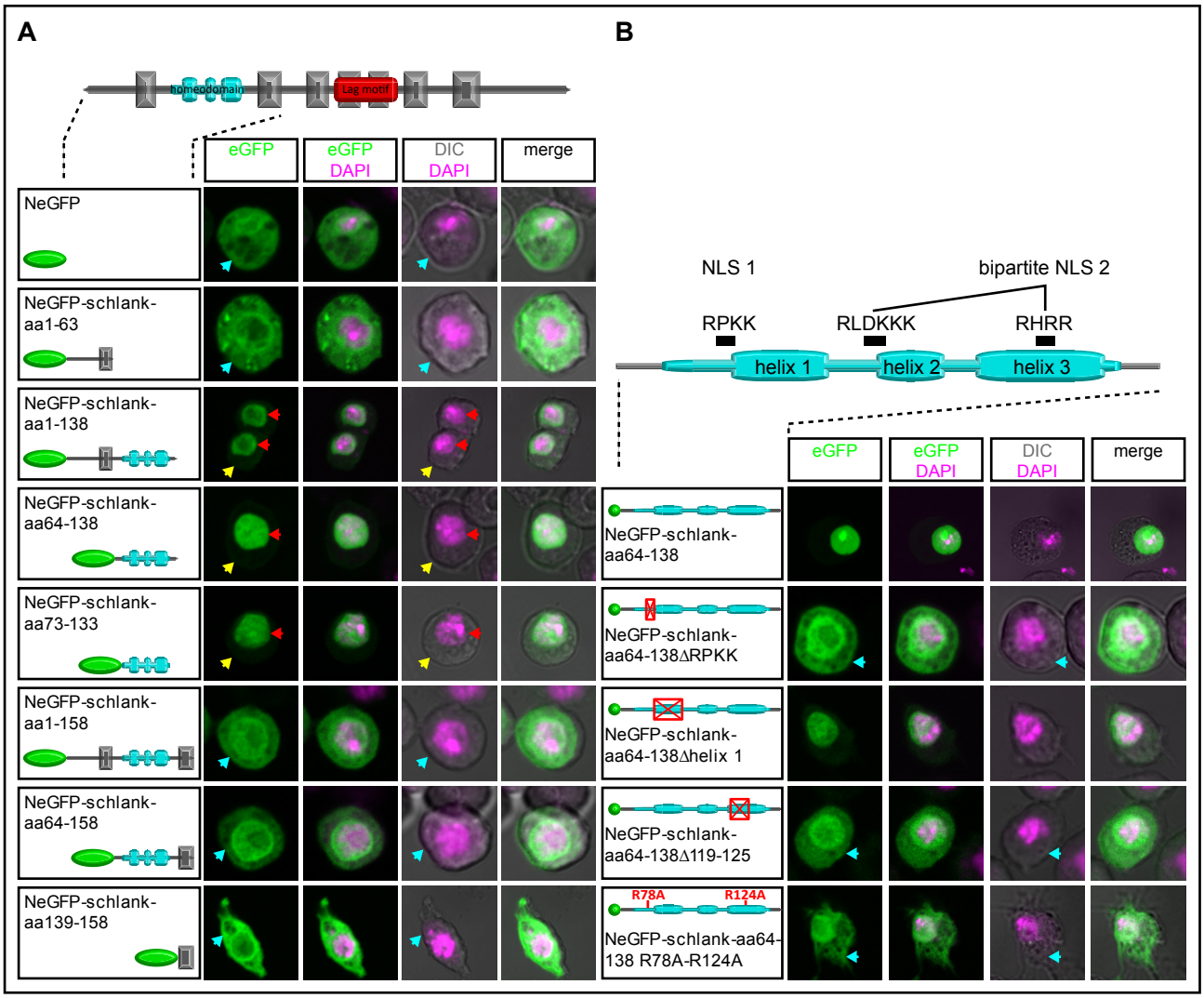

Figure 3.7 The Schlank homeodomain codes for functional nuclear localization sequences (NLSs). A-B, Native eGFP fluorescence was imaged, DNA was visualized by DAPI staining and cell borders were visualized by differential interference contrast (DIC). **A**, N-terminally eGFP-tagged constructs of different sizes covering Schlank amino acid region 1-158 were expressed in S2 cells. Schematic representation gives an overview of the region of the protein covered. In the scheme, the homeodomain is depicted in blue, eGFP in green. Free eGFP is distributed in cytoplasm and nucleus. eGFP-Schlank fusion proteins up to the second transmembrane domain that contain the homeodomain lose the cytoplasmic distribution (red arrows) and are almost exclusively translocated to the nucleus (yellow arrows). Schlank constructs either not containing the homeodomain or containing the second transmembrane domain retain the cytoplasmic staining (blue arrows). **B**, The schematic drawing depicts the Schlank homeodomain; boxes indicate the helices and predicted NLSs are marked on top. Potential NLSs were predicted by Wolf's PSORT II and cNLS mapper. Deletions in the eGFP-tagged homeodomain construct covering amino acids 64-138 are marked by crossed boxes, point mutations by amino acid substitution letter code. When either of the predicted NLSs is mutated, nuclear enrichment is decreased and cytoplasmic staining occurs (blue arrows). A construct with a deletion of Schlank homeodomain helix 1, which still codes for both NLS, retains the string nuclear accumulation.

were mutated in a Schlank-homeodomain construct that is exclusively localized to the nucleus (aa64-138).

Deletion of either the first NLS (ΔRPKK) or part of the bipartite NLS (IERWWRL; Δ119-125) leads to an additional accumulation of the eGFP-tagged constructs in the cytoplasm that is not statistically different from free eGFP but highly different from the intact homeodomain construct. In contrast, deletion of the first helix without affecting any of the NLSs (Δhelix1) does not change the exclusive nuclear accumulation.

Point mutation of R78 and R124 within the homeodomain to alanine (R78A R124A), which should affect both NLSs, also changes the exclusivity of nuclear enrichment to a localization of the construct throughout the whole cell (Fig. 3.7 B, Fig. AP3.7 C).

Taken together, mutation of either NLS-like stretch weakens the nuclear enrichment of Schlank homeodomain constructs.

3.8 Schlank is found in Importin-ß positive regions in cytoplasm and INM

The mutational analysis described above indicates that there are functional NLSs in the Schlank protein that are needed for its import into the nucleus. It can therefore be inferred that Schlank is imported via the classical nuclear import pathway.

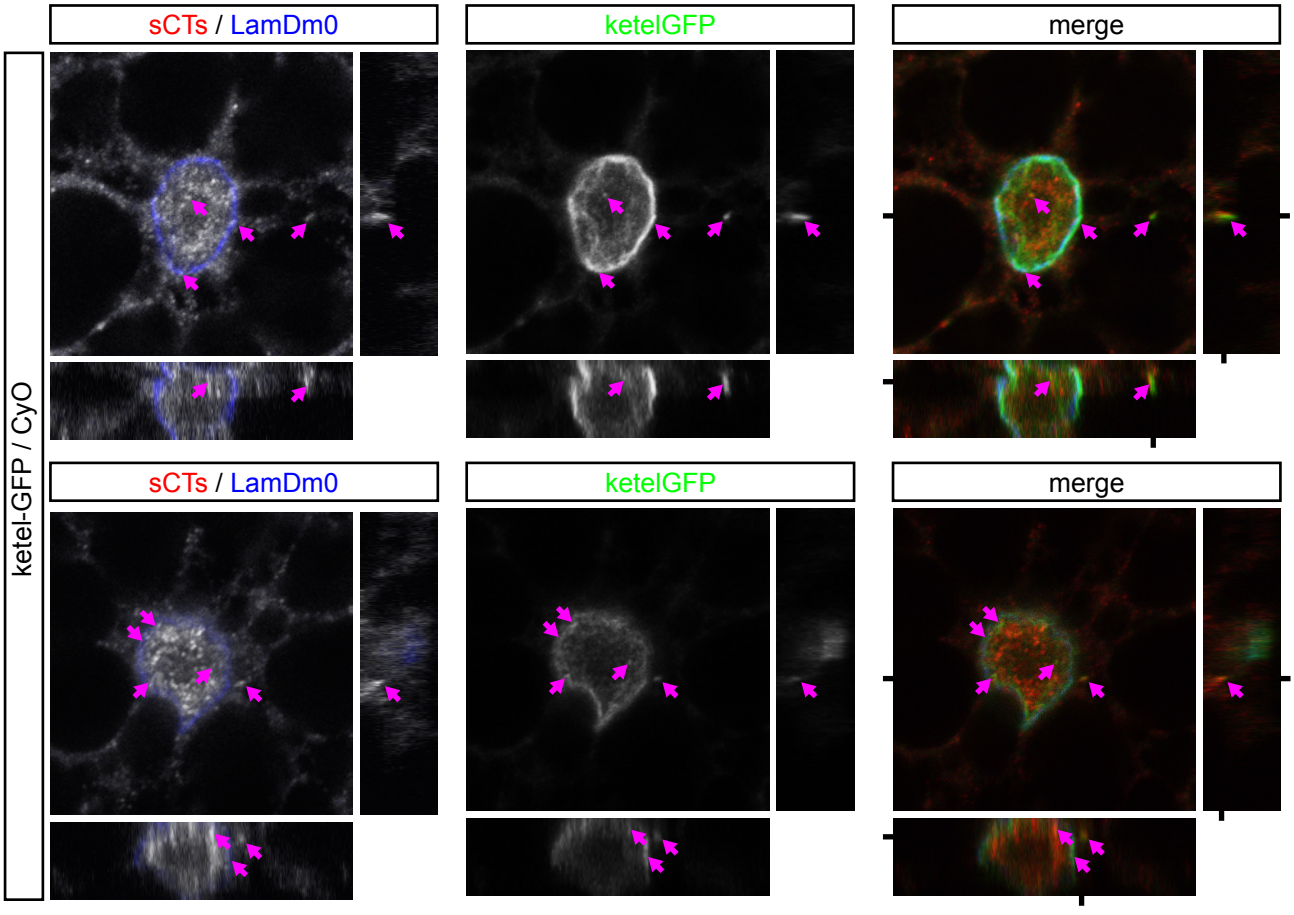

Figure 3.8 Importin-ß co-localizes with a part of the cytoplasmic and nuclear Schlank protein pool. Ketel-GFP (green) expressing fat body cells were stained for Schlank (sCTs, red) and nuclear envelope marker Lamin Dm0 (LamDM0,

blue). Ketel-GFP associated with a Schlank at the nuclear envelope, in nucleoplasmic structures and in cytoplasmic compartments at various distances from the nucleus. Images show orthogonal sections through fat body cells. Black bars next to the overlay images indicate the position of orthogonal sections. Y-Z sections are at the right hand side of the individual stack layers, X-Z sections are below.

Two mechanism have been described that allow nuclear translocation: 1) NLSs within the target protein are bound by Importin-α family members in the cytoplasm and this complex is then bound by Importin-ß and transported to the nuclear pore complex and finally to the inside of the nucleus. 2) ß-Importin itself binds NLSs within the target protein and transports it to the nucleus.

Both mechanisms are dependent on ß-Importin. Co-stainings of Schlank and the GFP-tagged ß-Importin homolog Ketel shows partial colocalization of both proteins at the nuclear membrane but also at structures within the cytoplasm (Fig. 3.8) in fat body cells (for Ketel-GFP tissue distribution, see Fig. AP 3.8). This would be consistent with a scenario in which Ketel binds Schlank at cytoplasmic structures (e.g. the ER) and transports it to the INM. More supporting evidence could be obtained by disturbing Ketel expression or function and analyzing Schlank localization.

3.9 The *Drosophila* Importin-ß homolog Ketel mediates nuclear import of endogenous Schlank

The Importin-ß homolog *ketel* was knocked down in a clonal fashion in the fatbody. To verify that the RNAi-flyline used is valid, *UAS-ketelRNAi* was driven by *actin-GAL4* and the *ketel* expression determined by realtime-RT-PCR. *ketelRNAi* line 27567 lead to a reduction of *ketel* transcript down to 35 % (Fig. AP 3.9 A). To verify that the clonal expression and RNAi response themselves would not affect Schlank expression or localization, an unrelated control RNAi (*pex19RNAi*) was expressed with the clonal expression system. There are no obvious changes in Schlank distribution upon *pex19RNAi*, validating the system for analysis (Fig. AP 3.9 B).

ketel-knock down clones (marked by a dotted line in Fig. 3.9 A) show a strong reduction in nuclear Schlank staining. There is no change in wildtypic sister clones (compare white and yellow arrows in Fig. 3.9 A). A detailed analysis of the nuclear Schlank staining via confocal microscope stacked images and a representation of the 3D volume by orthogonal sections shows that wildtypic nuclei contain filamentous Schlank-positive structures from INM to the inside of the nucleus (Fig. 3.9 B).

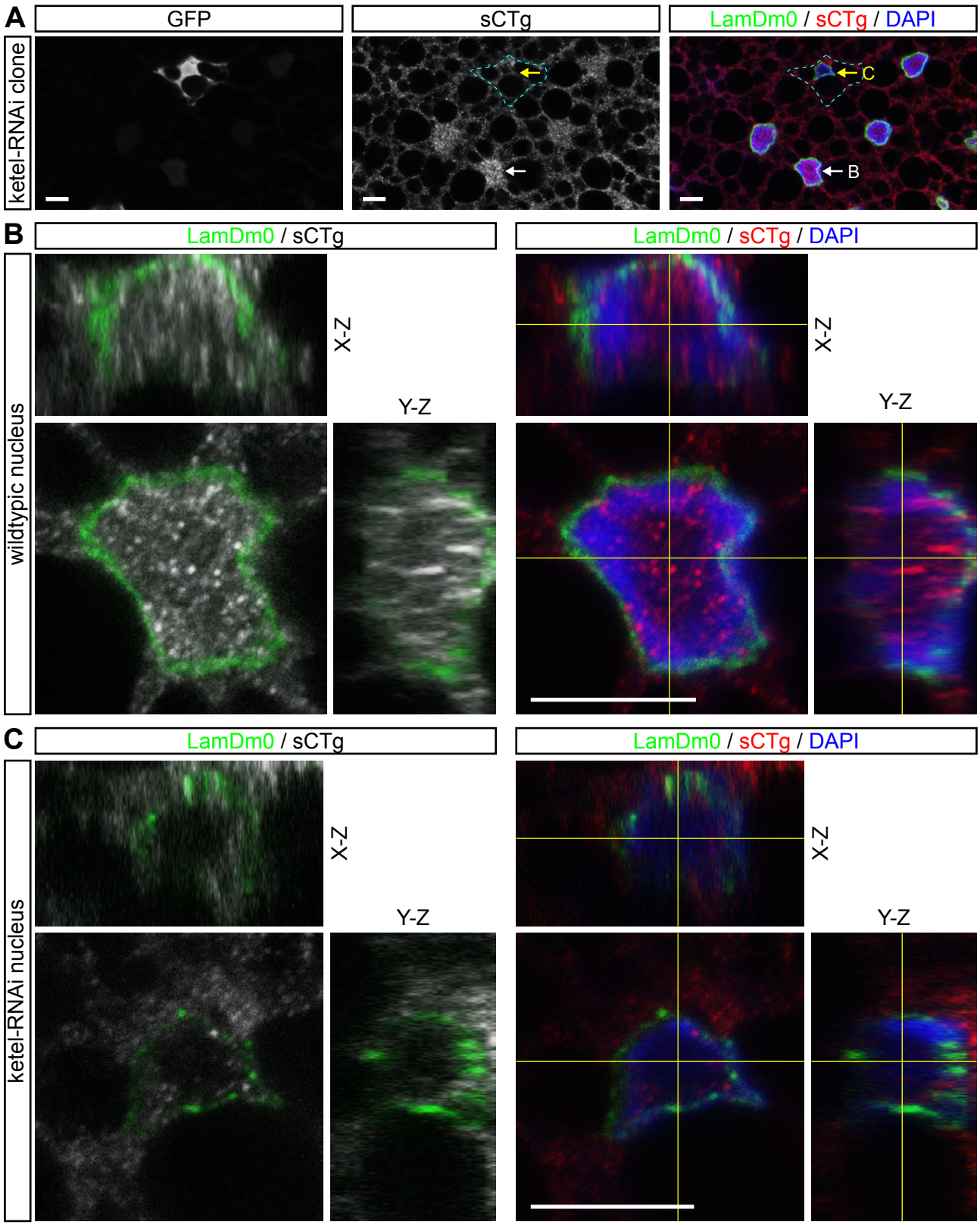

Figure 3.9 Ketel mediates nuclear import of native Schlank. A, *ketel* was knocked down in a clonal manner in the fatbody via an RNAi construct. *ketel*-RNAi clones (cell borders marked by a blue dashed line) show a strong reduction of nuclear Schlank staining (sCTg, yellow arrow) compared to control nuclei (white arrow). **B** and **C**, Orthogonal sections of wildtypic (B) vs. RNAi clones (C) show, that Schlank is not transported efficiently to the nuclear filamentous structures anymore. Lamin Dm0 is marked in green, Schlank in red and DAPI in blue. Position of orthogonal sections is

marked by yellow lines. Y-Z sections are at the right hand side of the individual stack layers, X-Z sections are on top. Scale bar is 10 μm.

Those structures, especially in the nucleus, are lost almost completely in *ketel*-knock down clones (Fig. 3.9 C).

Taken together, there is evidence that Schlank protein is imported from cytoplasm to nucleus in a NLS/Ketel-dependent mechanism. It should be investigated next whether the function of the Schlank homeodomain is mainly to harbor the NLS stretches or if there is DNA interaction as was shown to be the essential feature of other homeodomains.

3.10 Schlank homeodomain has a low level affinity for randomized double stranded DNA

To address whether or not the Schlank homeodomain would at all be capable to bind DNA, purified GST-tagged Schlank homeodomain and, as a control, pure GST was expressed in BL21 bacteria, purified by a GST column, biotinylated and bound to magnetic streptavidin beads (selection protocol of dsDNA SELEX, Bernhard Wulffen, Günter Mayer, Bonn, Germany).
Upon incubation with a randomized radioactively labeled 43-mer dsDNA library (flanked by 18 & 19 base pair primer compatible sequences 5' and 3' of the randomized sequence), GST-Schlank-aa65-138 bound up to 70% of the dsDNA library, while the GST control did only bind up to 3%, initially (before wash steps). The low amount of DNA bound to the GST-beads could be washed off, while it stayed on at the GST-Schlank-homeodomain construct and could be eluted by heat denaturation (Fig. 3.10 A).

This DNA binding could be competed by increasing the concentration of heparin, an unspecific DNA competitor (Fig. 3.10 B). The heparin EC50 concentration for outcompeting dsDNA is near a 1.5fold molar ratio of heparin to Schlank (heparin in excess; Fig. 3.10 C). At a 1 : 10 molar ratio of GST-Schlank aa65-138 : heparin, 3% of the DNA remained bound to Schlank after wash steps. Similar properties were observed with salmon sperm DNA as competitor. While with 10 fold molar excess of salmon sperm DNA there is still a total of ~6% of the dsDNA library bound to the Schlank protein, increase of the salmon sperm amount to an excess of 100 to 300 fold decreases the amount of dsDNA bound to the Schlank-homeodomain beads to 1 - 2 % (Fig. 3.10 D).

The salmon sperm DNA / heparin competition experiments show that the homeodomain-DNA binding is not due to unspecific charge interaction. However, it also shows that the interaction with the DNA-library *in vitro* is of low affinity.

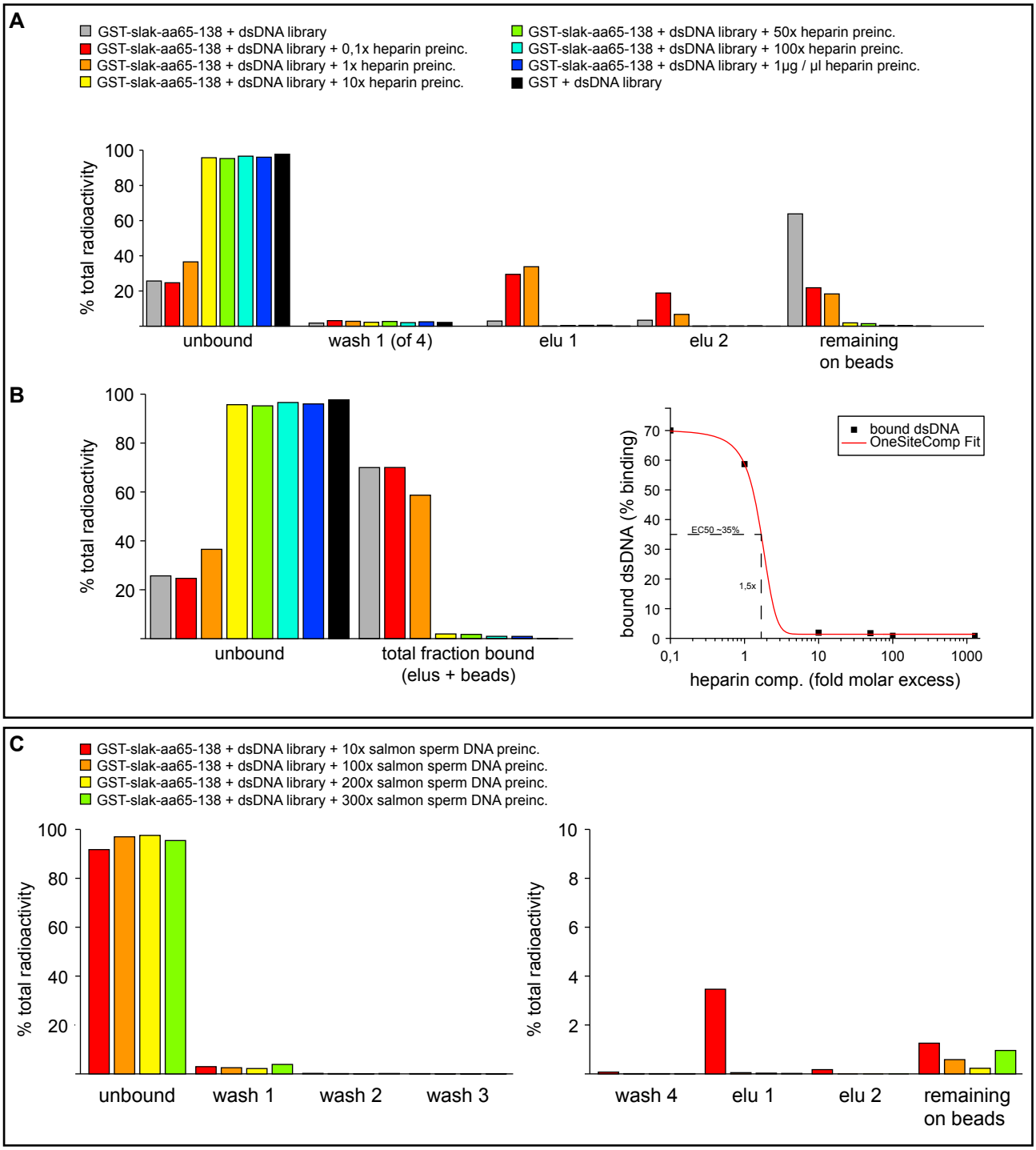

Figure 3.10 Schlank homeodomain can bind randomized DNA. A, Affinity-purified GST-Schlank-aa65-138 (homeodomain) was biotinylated and coupled to magnetic beads Streptavidin beads. Beads were then incubated with a radioactively labeled DNA library (D3) of a randomized 30mer flanked by primer sequences. Affinity purified and coupled GST alone did not bind any of the DNA, which was washed off the beads. GST-Schlank-aa1-138, however, bound a total of 70% of the DNA. Binding could be reduced with increasing amounts of heparin which competes for DNA and masks positive charges at the protein. When the heparin concentration was increased to more than a 10-fold molar excess, DNA binding was abolished. **B**, One-site competition fit calculations show that 50% of the DNA binding would still be bound at a 1.5 molar heparin excess. This correlates in numbers with a complete 1:1 aspect ratio between negative heparin charges and positive charges in the GST-tagged homeodomain, indicating that the DNA

binding might not be entirely due to charge interactions. **C**, Similarly, DNA binding to the Schlank homeodomain can be decreased with a preincubation of the homeodomain-carrying beads with up to a 300 molar excess of salmon sperm DNA. While at a 10-fold molar excess of salmon sperm DNA 10 % of the DNA-library still bind, binding is reduced to 2% with a 300-fold molar excess.

3.11 Short term induction of eGFP-Schlank homeodomain represses *lipase 3* transcription

In order to evaluate whether or not a homeodomain-containing construct itself might mediate the observed *lipase 3* transcript repression, eGFP-Schlank-aa1-138 was expressed via a mifepristone inducible tubulin-Gal4 (tubulin-GeneSwitch) system (Bahadorani et al, 2010; induction for 2 hours with 1 µg / mL mifepristone in agar yeast paste).

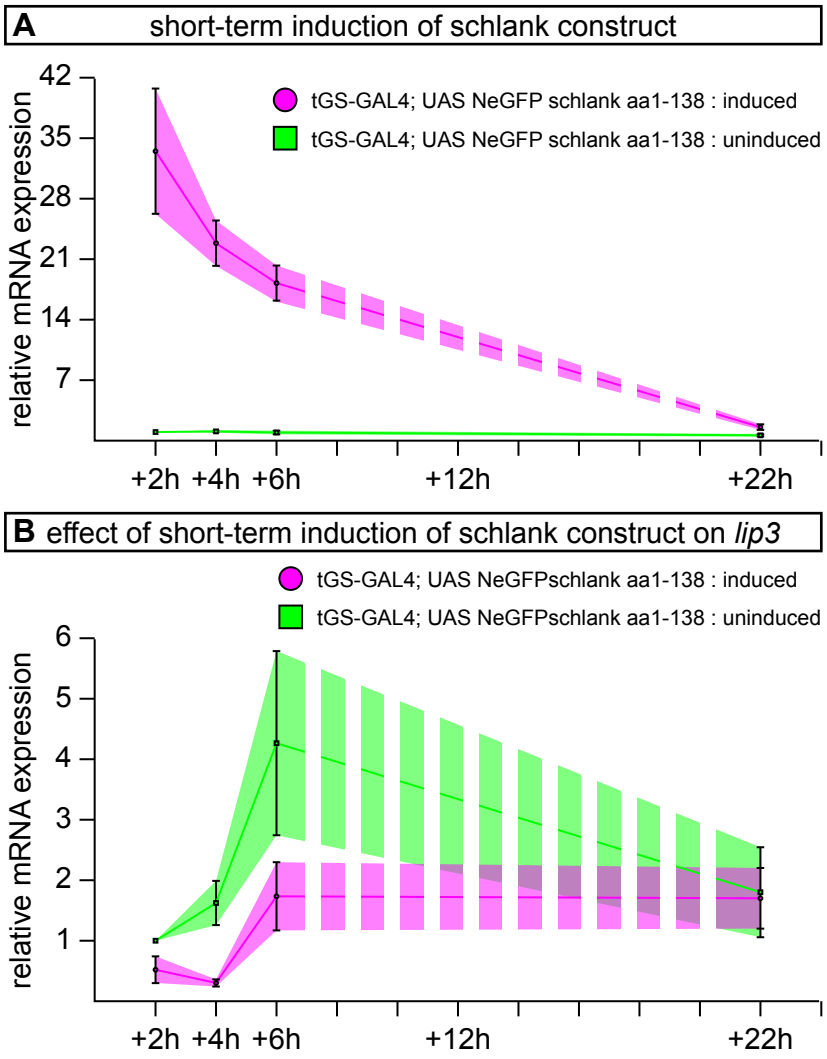

Figure 3.11 Overexpression of Schlank constructs can decrease lip3 expression 4h after induction. NeGFP-Schlank-aa1-138 was expressed via the Mifepristone-inducible gene-switch-GAL4-system (tGS-Gal4). Transcript levels were determined by realtime-qRT-PCR in 5 independent experimental setups for each condition. Transcript regulations were determined for timepoints 2, 4, 6 and 22 hours after induction of construct expression. Transcript expression of

hormone-fed animals (magenta) was compared to that of siblings which were fed without hormone (green). **A**, Expression of the Schlank construct was strongest shortly after 2 hour induction-period and steadily decreased until it was barely detectible 22 hours after induction. **B**, Slightly time-delay to the expression of the Schlank construct, lip3 expression was strongest reduced 4 hours after Schlank induction and then steadily normalized afterwards, in parallel to the Schlank levels.

Compared to an uninduced control of the same genotype (2 to 6 hours after induction), a 3-fold repression of *lipase 3* transcript can be observed that normalized 22 hours after induction, coinciding with the time when the expression of the eGFP-construct was shut off (Fig. 3.11). This indicates that the *lipase 3* regulation is due to the induction of the construct and that a INM-bound Schlank homeodomain might be sufficient to silence *lipase 3* transcription in either direct or indirect fashion.

3.12 RNA-sequencing comparison of Schlank full length vs. aa1-138 constructs identifies potential new Schlank target genes

Schlank levels have a strong effect on the transcription of *lip3* and *akh.* An RNA sequencing approach was chosen to identify new target genes that would be regulated by the homeodomain function. Two aspects are important to separate indirect transcriptional effects and direct homeodomain-mediated transcriptional changes: A) Transcriptional changes should be moderately fast (the pre-experiment suggested 2 – 4 hours would be enough for Schlank to regulate *lip3*). B) If the membrane bound homeodomain would be sufficient for gene regulation, expression of full length Schlank should affect the same genes as expression of Schlank aa1-138 (Schlank-N-terminus including the homeodomain). To account for position effects by the integration of the constructs into the genome, the inducible gene-switch system was used. Due to the fact that induced and uninduced states have the same genotype, there should be no bias by the integration position. Wildtypic larvae were treated with and without mifepristone in the same manner as the gene-switch animals to identify any effects that mifepristone treatment itself might have on the transcriptome. Genes that would be commonly regulated by Schlank full length and Schlank aa1-138 expression are thought to indicate genes that might be directly regulated by the activity of the homeodomain.

Principle component analysis (PCA) of the RNAseq experiment shows that there are only minor changes in transcript levels upon mifepristone induction alone (Fig. 3.12 A). Full length

induction shows some minor changes in overall transcription while expression of the 1-138 construct shows a stronger impact on the transciptome. The direction of change upon full length

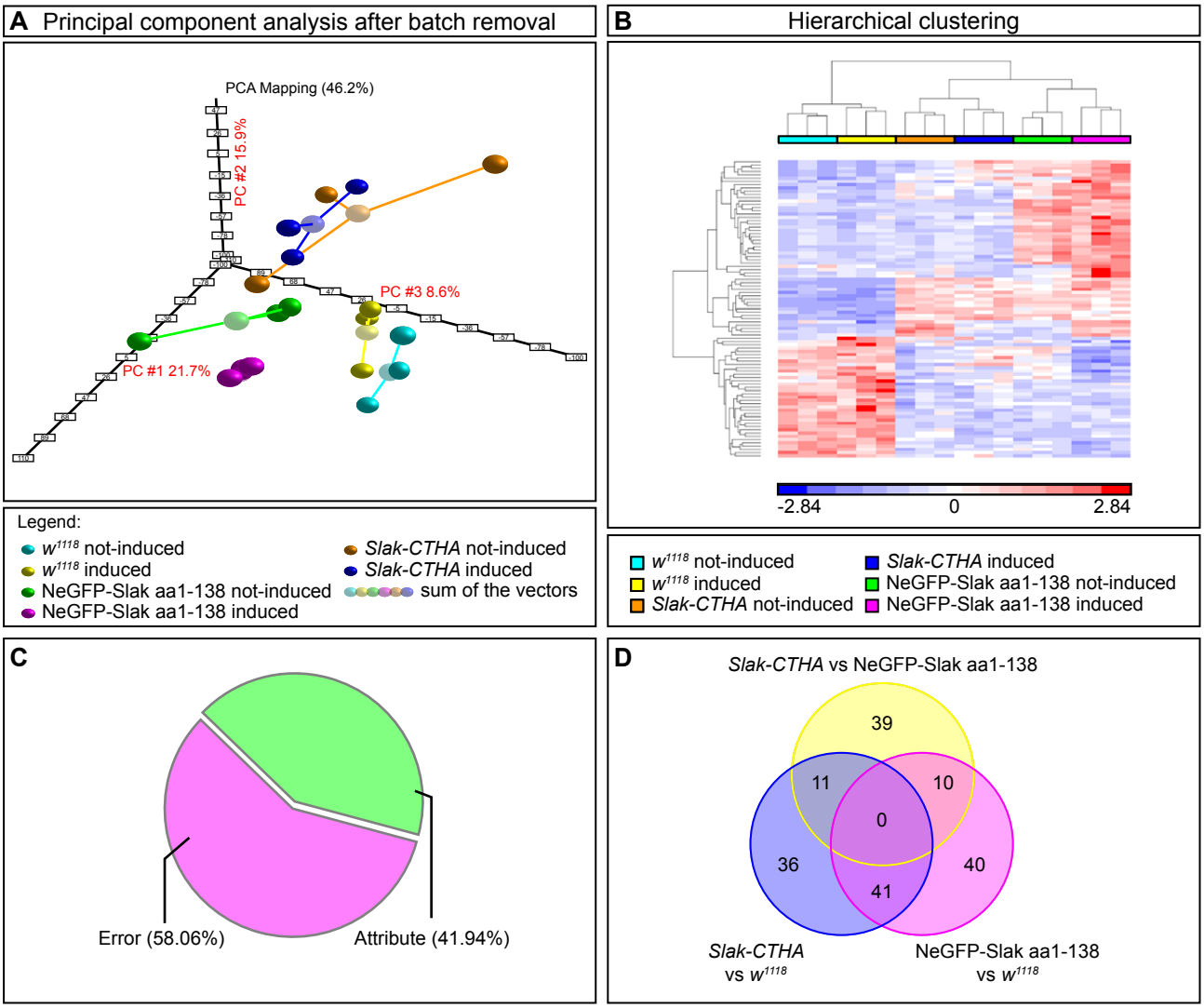

E Gene Symbol	CG Number	Mean (w^{1118})	Mean (w^{1118} induced)	Mean (NeGFP-Slak-aa1-138)	Mean (NeGFP-Slak-aa1-138 induced)	Mean (Slak-CTHA)	Mean (Slak-CTHA induced)	FoldChange (w^{1118} induced vs. NeGFP-Slak-aa1-138 induced)	p-value (w^{1118} induced vs. NeGFP-Slak-aa1-138 induced)	FoldChange (w^{1118} induced vs. Slak-CTHA induced)	p-value (w^{1118} induced vs. Slak-CTHA induced)	FoldChange (Slak-CTHA induced vs. NeGFP-Slak-aa1-138 induced)	p-value (Slak-CTHA induced vs. NeGFP-Slak-aa1-138 induced)
NeGFP-Slak-aa1-138 specific regulation													
	CG17047	1.95	1.06	1.08	3.31	0.74	0.54	-3.11	8.10E-05	1.96	1.70E-01	-6.09	1.40E-05
	CG42808	21.27	19.39	23.78	50.73	15.50	21.21	-2.62	1.50E-04	-1.09	7.40E-01	-2.39	2.40E-04
	CG31313	136.57	193.37	255.63	480.65	125.11	230.96	-2.49	3.20E-04	-1.19	5.00E-01	-2.08	9.00E-04
	CG15369	235.74	282.27	253.10	688.73	184.77	287.31	-2.44	1.50E-05	-1.02	9.20E-01	-2.40	1.70E-05
	CG5653	2.90	2.12	1.05	0.86	2.87	1.98	2.48	2.90E-04	1.07	5.60E-01	2.31	6.90E-04
Slak-CTHA specific regulation													
	CG33723	0.39	0.06	0.44	0.20	0.85	1.49	-3.12	5.50E-01	-23.06	6.90E-05	7.39	1.60E-04
fit	CG17820	0.06	0.07	0.00	0.19	0.00	0.58	-2.91	1.50E-01	-8.80	8.70E-05	3.02	7.60E-04
	CG13982	0.56	0.38	0.38	1.10	0.51	3.34	-2.85	6.90E-02	-8.67	7.20E-06	3.04	7.70E-05
	CG11437	0.72	0.49	0.74	0.78	0.96	2.80	-1.58	4.90E-01	-5.72	1.80E-04	3.61	5.00E-04
	CG30283	0.34	0.72	0.61	0.97	0.51	0.28	-1.34	1.50E-02	2.60	3.50E-04	-3.48	9.20E-06
common regulation by NeGFP-Slak-aa1-138 and Slak-CTHA													
Hsp70Bb	CG31359	0.72	0.82	3.01	74.90	2.47	61.83	-91.05	7.20E-07	-75.16	4.20E-06	-1.21	8.30E-02
Lag1	CG3576	25.12	26.85	22.70	335.33	28.61	495.51	-12.49	1.20E-06	-18.45	2.40E-08	1.48	3.30E-04
ssSPTb	CG34194	3.59	2.66	5.00	32.66	2.25	20.93	-12.26	1.10E-05	-7.85	6.17E-04	-1.56	1.03E-02
	CG13051	2.45	1.96	2.29	14.12	1.34	11.63	-7.22	3.50E-05	-5.95	2.30E-04	-1.21	1.80E-01
Tig	CG11527	13.70	14.64	13.20	98.06	15.85	84.52	-6.70	1.94E-04	-5.78	7.35E-04	-1.16	3.75E-01
bnb	CG7088	30.20	28.01	36.30	180.35	25.48	146.75	-6.44	1.44E-04	-5.24	9.43E-04	-1.23	2.20E-01
	CG3097	1.91	1.32	2.15	8.40	2.45	10.89	-6.35	7.00E-08	-8.23	3.80E-09	1.30	6.20E-04
	CG6409	286.64	242.02	438.09	1413.56	443.90	1334.02	-5.84	4.60E-06	-5.51	8.60E-06	-1.06	5.60E-01
	CG13067	9.50	11.07	18.05	58.77	16.47	55.67	-5.31	8.20E-06	-5.03	1.50E-05	-1.06	6.00E-01
Tsp42Eo		12.50	9.62	10.59	43.73	10.20	43.47	-4.54	6.70E-05	-4.52	7.10E-05	-1.01	9.60E-01
	CG4325	3.71	4.08	2.33	16.89	2.91	17.11	-4.14	1.40E-04	-4.19	1.20E-04	1.01	9.20E-01
	CG13177	56.98	51.56	52.62	188.78	31.57	214.31	-3.66	8.10E-05	-4.16	1.90E-05	1.14	2.60E-01
	CG6891	72.14	73.40	109.68	181.89	126.64	202.38	-2.48	2.40E-05	-2.76	5.20E-06	1.11	1.90E-01
Dic1	CG8790	11.69	12.37	17.18	29.46	19.97	26.24	-2.38	1.00E-04	-2.12	5.10E-04	-1.12	2.70E-01
7B2	CG1168	9.78	6.32	8.05	13.73	8.01	15.00	-2.17	3.30E-05	-2.37	8.40E-06	1.09	2.50E-01
	CG14572	32.57	31.13	29.95	66.96	30.06	65.34	-2.15	2.40E-04	-2.10	3.50E-04	-1.02	8.10E-01

Figure 3.12 Trancriptome-changes upon Mifepristone-induced expression of Schlank full-length and homeodomain constructs. Expression of Schlank-full length and Schlank aa1-138 was induced with the gene-switch-GAL4 system.

Three independent RNAs each were isolated 4 hours after induction from induced and not induced wildtypic larvae and larvae that can express the constructs. RNAs were sequenced via next-gen-sequencing on an Illumina platform and analyzed with Partek Genomics Suite 6.5 (M. Kraut, M. Beyer, J. Schultze). **A**, Principle component analysis of induced and uninduced animals shows that the differences in transcriptome changes between genotypes are more prominent than between induced and not-induced states. However, there is a clear directional shift upon induction of the constructs. PC # % = percent variance in principle component number indicated. **B**, Hierarchical clustering of regulated genes show that the transcriptome difference between the genotypes are tremendous but that there are also a number of genes that are differentially regulated by expression of the constructs. The color code indicates the strength of normalized expression, with blue being 2.84-fold downregulated and red being 2.84-fold upregulated. **C**, Source-variation analysis shows that ~60% of the observed gene regulations are not due to biological changes. **D**, Venn-Diagram analysis shows that there are 41 potential target genes regulated by the expression of both of the Schlank-constructs and 11 full-length specific and 10 homeodomain-specific regulated genes. **E**, List of potential target genes either specific for the Schlank homeodomain (green header), the full length protein (blue header) or commonly regulated genes upon the expression of both Schlank constructs (golden header). Mean detection counts, relative expression change values and p-value changes for the regulation are listed next to the gene-name and gene-collection number (CG).

or 1-138 expression compared to the uninduced states is similar. However, the PCA also shows that there are strong variances in the three independent repeat samples of each induced condition (except for wildtype controls) (Fig. 3.12 A). Hierarchical clustering of the analyzed transcripts reveals that there are genes specifically up or downregulated in either full length or 1-138 expression conditions but there are also genes that are regulated the same way in both situations but not in the induction controls. In addition there are some genes exclusively regulated by each construct (Fig. 3.12 B).

The error rate due to biological variance is near 58% and only ~42% can be evaluated as attribute (Fig. 3.12 C). A Venn-Diagram shows that there are 41 candidate genes regulated by both the full length and the 1-138 construct. There are 36 genes only regulated upon full length expression and there are 40 genes specifically regulated by the homeodomain (Fig. 3.12 D).

Top candidates for the regulation by both constructs include ssSPTb, the small subunit of Serine-palmitoyl-transferase, the first enzyme in the Ceramide Synthase enzymatic cascade, as well as Tigrin (Tig) and Bangles and beads (Bnb), both genes involved in neuronal and glia cell development (Fig. 3.12 E).

3.13 Realtime-qRT-PCR fails to validate RNAseq-derived potential Schlank target genes

Putative Schlank target genes identified via RNAseq were chosen to be validated by realtime qRT-PCR.

3.13.1 GAL4 itself regulates expression of more than 1000 Drosophila genes and masks regulation of putative Schlank target genes

Literature research about the potential target genes raised the issue that GAL4 itself is able to regulated gene expression in *Drosophila*: Liu & Lehmann, 2008 recently demonstrated that expression of GAL4 in salivary glands regulates about 1000 *Drosophila* genes and raised the question if there might be even more genes that they could not account for due to the limited expression pattern of GAL4 used in the experiment.

To at least in part account for those regulations, all GAL4 target genes identified by Liu *et al.* were discarded from the candidate list, while at the same time the false discovery rate was relaxed. This left 19 genes potentially regulated by both Schlank constructs and 45-63 genes (depending on the construct) that were individually regulated. When the stringency was raised again by re-introducing a false discovery of rate <0.1, that list was narrowed down to 7 common and 2-13 individual targets, depending on the construct. *ssSPT*, *tig* and *bnb* remained in the new candidate list (Fig. 3.13 A).

3.13.2 RNAseq derived top target genes commonly regulated in animals expressing either of the Schlank constructs are GAL4 regulated

To verify the top candidate genes left after discarding known GAL4 targets, the constructs used in the RNAseq approach were again expressed the same way, but this time compared to animals that only expressed GAL4 without the constructs. In addition, NLS-tagged GFP itself was expressed to account for targets that might be regulated by GFP itself. Putative target genes were individually analyzed by realtime-qRT-PCR (Fig. 3.13 B, C). In a pre-screen, expression of the candidate genes upon induction of the tubGS driver line itself was analyzed and the expression level compared to the mean RNAseq regulation to account for GAL4 dependent effects (Fig. 3.13 B). Genes regulated the same way as in the RNAseq upon expression of the Schlank constructs were flagged as ‘GAL4-regulated’ (Fig. 3.13 D).

To account for a potential effect of GFP itself, expression of target genes not regulated by GAL4 were tested in a system were GFP.nls was expressed by the gene-switch system (Fig. 3.13 C). Genes that were not regulated upon GAL4 activation but were regulated upon induction of GFP.nls the same way as in the RNAseq were flagged as ‘GFP-regulated’ (Fig. 3.13 D).

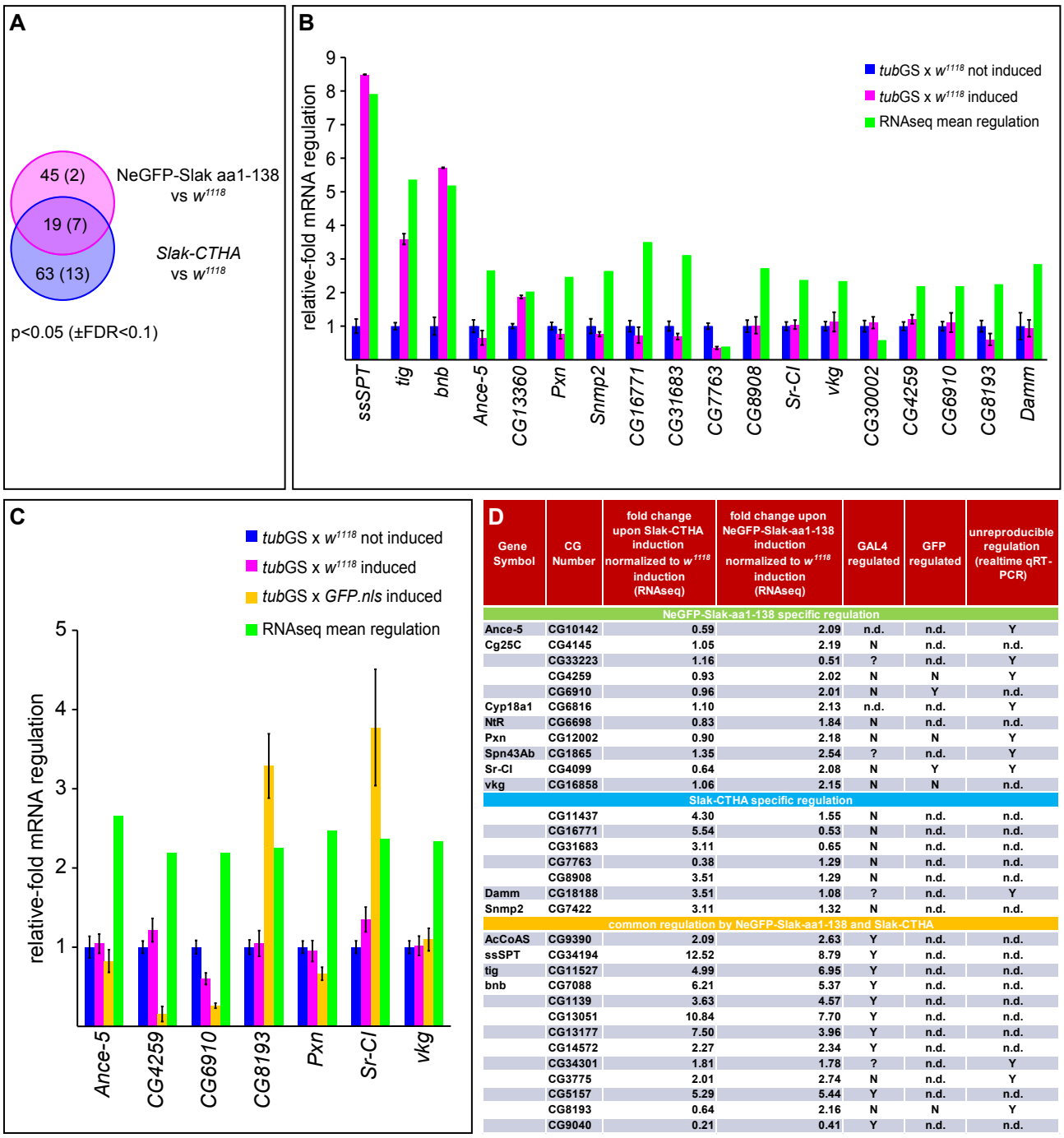

D

Gene Symbol	CG Number	fold change upon Slak-CTHA induction normalized to w^{1118} induction (RNAseq)	fold change upon NeGFP-Slak-aa1-138 induction normalized to w^{1118} induction (RNAseq)	GAL4 regulated	GFP regulated	unreproducible regulation (realtime qRT-PCR)
NeGFP-Slak-aa1-138 specific regulation						
Ance-5	CG10142	0.59	2.09	n.d.	n.d.	Y
Cg25C	CG4145	1.05	2.19	N	n.d.	n.d.
	CG33223	1.16	0.51	?	n.d.	Y
	CG4259	0.93	2.02	N	N	Y
	CG6910	0.96	2.01	N	Y	n.d.
Cyp18a1	CG6816	1.10	2.13	n.d.	n.d.	Y
NtR	CG6698	0.83	1.84	N	n.d.	n.d.
Pxn	CG12002	0.90	2.18	N	N	Y
Spn43Ab	CG1865	1.35	2.54	?	n.d.	Y
Sr-CI	CG4099	0.64	2.08	N	Y	Y
vkg	CG16858	1.06	2.15	N	N	n.d.
Slak-CTHA specific regulation						
	CG11437	4.30	1.55	N	n.d.	n.d.
	CG16771	5.54	0.53	N	n.d.	n.d.
	CG31683	3.11	0.65	N	n.d.	n.d.
	CG7763	0.38	1.29	N	n.d.	n.d.
	CG8908	3.51	1.29	N	n.d.	n.d.
Damm	CG18188	3.51	1.08	?	n.d.	Y
Snmp2	CG7422	3.11	1.32	N	n.d.	n.d.
common regulation by NeGFP-Slak-aa1-138 and Slak-CTHA						
AcCoAS	CG9390	2.09	2.63	Y	n.d.	n.d.
ssSPT	CG34194	12.52	8.79	Y	n.d.	n.d.
tig	CG11527	4.99	6.95	Y	n.d.	n.d.
bnb	CG7088	6.21	5.37	Y	n.d.	n.d.
	CG1139	3.63	4.57	Y	n.d.	n.d.
	CG13051	10.84	7.70	Y	n.d.	n.d.
	CG13177	7.50	3.96	Y	n.d.	n.d.
	CG14572	2.27	2.34	Y	n.d.	n.d.
	CG34301	1.81	1.78	?	n.d.	Y
	CG3775	2.01	2.74	N	n.d.	Y
	CG5157	5.29	5.44	Y	n.d.	n.d.
	CG8193	0.64	2.16	N	N	Y
	CG9040	0.21	0.41	Y	n.d.	n.d.

Figure 3.13 RNAseq-determined target genes thought to be commonly regulated by the expression of the Schlank constructs are regulated due to the transcriptional activity of the activated GAL4 itself. A, Genes known to be direct targets of the GAL4-protein (~1000) were discarded from the RNAseq list. Stringency of the analysis reduced to an error rate lower than 5% (p<0.05). The Venn-Diagram shows that there are 19 commonly regulated genes left and 45 homeodomain-specific as well as 63 Schlank-full length-specific genes. Adjusting the false discovery rate to 10% (FDR<0.1) reduces the number of potential target genes to 7, 2 and 13, respectively. **B**, To validate remaining potential target genes for a GAL4-derived regulation, tGS-GAL4 flies were crossed with wildtype flies and changes in gene-expression upon feeding the inducer (Mifepristone) were determined. Gene-expression in the uninduced state (blue) is normalized to 1. Regulation upon induction is shown in magenta. RNAseq derived mean regulation is depicted as green bar. Error bars show s.e.m. **C**, To account for a potential regulation by the GFP-tag in the homeodomain construct, nuclear targeted GFP was induced via the tGS-GAL4-gene-switch system for genes not regulated by GAL4

itself. Uninduced state is depicted in blue, induced non-expressing state in magenta, GPF.nls induced state in yellow and the RNAseq regulation in green. **D**, The table summarizes the transcript changes of the remaining genes in the RNAseq and indicates whether or not they are due to GAL4 or GFP expression itself. All genes regulated by the expression of both Schlank constructs are either GAL4 regulated or their regulation is not reproducible. A small number of homeodomain-specific target genes is indeed regulated by the expression of the GFP-tag. n.d: not done, Y: yes, N: no.

All candidate target genes of both Schlank constructs turned out to be either GAL4 regulated, or their change in expression could not be reproduced in the realtime-RT-PCR experiments. Two potential target genes of the homeodomain construct itself seem to be directly GFP-regulated while target genes specific for either construct are not GAL4 regulated, but half of them are not reproducibly regulated (Fig. 3.13 D). Taken together, all top candidates for a 'common' regulation have to be evaluated as unspecific, but there might still be valid candidates for a regulation by the individual constructs.

Nonetheless, there are still two top candidates that can be analyzed for a potential Schlank homeodomain interaction: *lip3* and *akh* (see also Introduction) were regulated in all experiments where Schlank levels were changed. Thus those two might still be good candidates to address in biochemical Schlank-DNA-interaction experiments, which do not rely on the UAS-GAL4 system.

3.13.3 GST-tagged Schlank homeodomain binds Schlank-consensus-binding-site-containing lipase 3 and akh promoter fragments in electromobility shift assays

An unbiased bacterial-one-hybrid screen of all Drosophila homeodomains conducted by Noyes *et al*. (2008) identified a consensus DNA binding site for the Schlank homeodomain. *In silico* screening of the 1kb region upstream of the transcription start of the two most promising candidates, *lip3* and *akh*, revealed that there are sequence stretches consistent with the Schlank consensus (Fig. 3.14 A-D green boxes, marked genomic sites in red). Two sets of oligonucleotides were designed for electromobility shift assays (EMSA):

For non-radioactive EMSAs, 30-32 base stretches of the respective Schlank consensus containing potential regulatory regions of *lip3* or *akh* genes were synthesized with biotin-end label at one strand (Fig. 3.14 C). For radioactive EMSAs, 34 base long *lip3* regulatory region stretches containing the Schlank consensus were synthesized and radioactively end-labeled (Fig. 3.14 C).

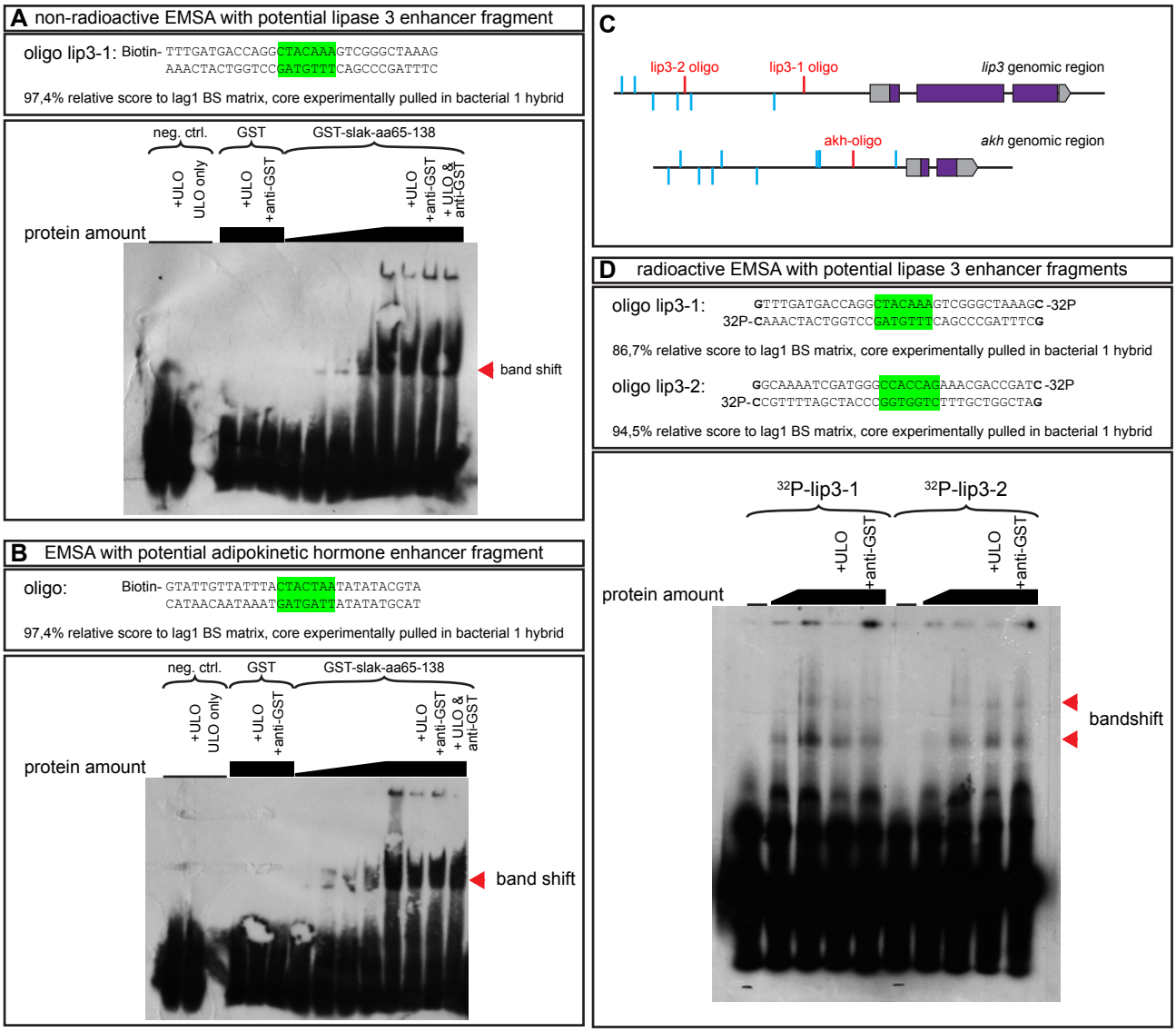

Figure 3.14 Schlank homeodomain binds to promoter fragments of *lip3* and *akh* that contain the Schlank binding consensus. A and **B** Non-radioactive electromobility shift assay with biotin-labeled oligonucleotides covering a ~30mer promoter fragment of *lipase 3* (**A**) and *adipokinetic hormone* (**B**) that contains the Schlank consensus binding site (Noyes et al, 2008a). Upper panel shows the oligonucleotide used for the EMSA. The green box highlights the consensus binding site. The band shift is indicated by arrows. Negative controls were labeled and unlabeled oligos without protein as well as oligo-incubations with purified GST-tag. GST alone does not bind to the oligonucleotides. With increasing GST-Schlank-homeodomain concentration (GST-slak-aa65-138), the amount of bound and thus retarded DNA increases. **C**, Analyzes of the 1kb region preceding the *lip3* and *akh* transcriptional start sites. Untranslated exon regions are depicted in grey, coding sequences in purple. Bars indicate the position of Schlank consensus binding sites that conform to >85 % to the matrix. Bars on to indicate sites in forward orientation towards the transcript start, bars below indicate sites in reverse orientation. Red bars indicate the position of consensus-site containing regions used for EMSA experiments. **D**, To exclude unspecific interaction of the biotin-labeled oligo with the Schlank-homeodomain via the biotin-moiety, EMSAs were done in parallel with radioactively end-labeled oligos. Upper panel shows the oligonucleotides used for the EMSA. The green box highlights the consensus binding sites. Band shift occurs when the oligos are incubated with Schlank-homeodomain in a concentration-dependent manner. For lip3-oligo-1, unlabeled oligo in 100-fold molar excess can outcompete the radioactively labeled oligo (staining

reduced to ~50 %) and incubation with GST-antibody leads to a decrease of shifted bands intensity to ~60 %. Lip3-2 oligo is also bound in a concentration-dependent manner but cannot be outcompeted by unlabeled oligo or shifted by adding GST-antibody. **A-D**, ULO = unlabeled oligo, anti-GST = Glutathione-S-transferase antibody, bar height indicates the protein amount.

Purified glutathione-S-transferase (GST)-labeled-Schlank homeodomain protein was incubated with labeled oligos in binding buffer on ice. Afterwards, the mixture is run on a non-denaturing tris-borate-EDTA (TBE) acrylamide gel. The free unlabeled oligos enter the gel first, however, if binding between the protein and the oligo occurs, entry to the gel is retarded. This leads to upwards shifted bands after visualization of the location of the oligo in the gel (band shift).

Non-radioactive EMSAs show that:

a. purified GST itself does not bind the labeled oligos containing the Schlank consensus binding site,
b. GST-Schlank homeodomain is able to bind the labeled oligos which leads to the occurrence of band shifts (Fig. 3.14 A, B, C red arrows), and
c. that with increasing protein concentration but steady oligo concentration, the amount of shifted oligo / Schlank-homeodomain complex increases. Thus the amount of DNA-oligo interaction-complexes is concentration-dependent (Fig. 3.14 A, B)

Competition experiments with unlabeled oligos and supershift experiments with GST-antibodies did not result in obvious changes in the amount of shifted oligos for the biotin-labeled oligos.

Radioactively-labeled *lip3* oligos are also bound by purified GST-Schlank homeodomain in a concentration dependent manner (Fig. 3.14 D), ruling out that the oligo-Schlank homeodomain-interaction in the non-radioactive assays would be due to an unspecific binding to the biotin moiety. In addition, EMSAs with ^{32}P-labeled *lip3* oligo 1 show a decrease in the amount of bound labeled oligo and addition of the GST antibody leads to an upward-shift of the oligo-protein complex, resulting in an increase of the staining intensity in the gel-pocket and a decrease in the amount of the oligo-Schlank homeodomain complex (Fig. 3.14 D). For *lip3* oligo 2 there are no obvious changes to the oligo-Schlank homeodomain complex upon addition of the cold competitor oligo or the GST-antibodies.

All in all the EMSA experiments show that there is indeed binding of the Schlank homeodomain to regulatory regions of *lip3* and *akh* that contain a Schlank consensus binding site.

This binding is not due to either biotin or GST-moieties but specific to the homeodomain and the oligos and increases in a Schlank homeodomain-amount dependent manner. Binding conditions are still sub-optimal, evident in the fact that unlabeled competition and supershift of the protein-oligo complexes does not work in all experimental setups.

4 Discussion

Previous work had shown that decreased levels of Schlank lead to a fat storage phenotype which is accompanied by an upregulation of *lipase 3* and *brummer* transcription as well as a decrease of SREBP target transcription. This indicates that there is an effect on both processes that are thought to mainly control fat stores: lipolysis and lipogenesis (André Völzmann, 2007; Bauer et al, 2009).

Cell culture data, however, show that there is a bias towards the *lipase 3* misregulation: knock down of *lipase 3* transcript can rescue the fat storage phenotype observed upon schlank dsRNA treatment in S2 cells (Ute Schepers, Reinhard Bauer, personal communication). This indicates that *lipase 3* regulation might be the main factor altering fat storage in *schlank* mutants. Consistent with the mutant data, it was observed that overexpression of *schlank* leads to an increase in storage fat levels.

In order to identify whether or not the observed misregulations are due to the metabolites produced in the Ceramide Synthase reaction or due to an independent protein activity, a point mutated Schlank version that is unable to enzymatically react (H215D), was overexpressed.

Most interestingly, this mutated version was still able to change fat stores, which indicates that it would indeed be a CerS-activity independent function of Schlank that mediates the observed misregulations.

In this thesis, the possibility of a functional role of the Schlank homeodomain in mediating the observed fat store and *lipase 3* expression changes was examined. In summary, the following was observed:

- A detailed alignment and phylogenetic approach shows that there is strong sequence conservation between CerS homeodomains and that they were fused to a (type I) CerS probably with the emergence on Filozoa, before Metazoans evolved.
- In addition, experimental 3D structure data (RIKEN project, Japan, Wada & Tanaka, 2002) show that CerS homeodomains are structurally conserved to all other classical homeodomains and a 3D modelling of Schlank predicts a similar structure.
- A pool of endogenous Schlank protein is localized to the nucleus, at the inner nuclear membrane and potential type I INM invaginations.

- The Schlank homeodomain itself encodes nuclear localization signals needed for its nuclear import.
- Schlank nuclear translocation is depending on an Importin-ß (Ketel) mediated transport mechanism.
- Expression of an N-terminal Schlank fragment that is membrane bound and contains the homeodomain alters *lipase 3* expression.
- Purified Schlank homeodomain can bind DNA, specifically *lipase 3* promoter fragments / regulatory elements containing the previously published Schlank binding consensus (Noyes et al, 2008a)

Overall, there are two central dogmas that had been established in the last years concerning Ceramide Synthases:

1) CerS are found in the ER, where they are enzymatically active.
2) The CerS homeodomain has no function except in supporting/enhancing CerS activity.

4.1 Endogenous CerS Schlank protein is distributed in various subcellular compartments

While the first claim that CerS are found in the ER is partly supported by mammalian data on subcellular fractionations, *in vitro* enzyme activity and co-localization staining, there is growing evidence that CerS are not limited to the endoplasmic reticulum. It was found that CerS can at least in part also localize to mitochondria (Shimeno et al, 1998). Evidence presented in this thesis indeed break the ER paradigm – in the *Drosophila melanogaster* fat body cells, only the minority of the CerS Schlank protein pool is found in the ER, roughly 30-40 % can be found in the nucleus and approximately 50 % of the protein is localized to yet unidentified subcellular compartments (from the mammalian data, mitochondrial localization would be rather likely). This distribution might be dependent on the cell type and could be different from tissue to tissue. The amount the nuclear Schlank protein pool is e.g. much lower in the central and peripheral nervous system, where Schlank is overall enriched but mainly localized to the cytoplasm (Fig. AP4.1.1 - 4.1.12).

Mammalian localization studies were so far mostly done by overexpressing tagged CerS protein versions. It has been reported for other proteins that there might be differences in the subcellular localization between endogenous and overexpressed protein variants. (Krumins et al, 2004; Jia et al, 2007). Therefore, in contrast to studies in mammals, the subcellular CerS

localization presented here addresses the distribution of endogenous protein with the help of a series of newly generated antibodies. To that end, highly specific antibodies, directed against the Schlank C-terminus, were generated. Overall, imaging of endogenous Schlank shows a punctate, spheroid to tubular pattern. While the ER protein pool is punctate to spheroid, the nuclear pool can be punctate but tends to be more tubular. Those tubular structures mostly seem to originate at the inner nuclear membrane and fold inwards. Overlaps at the nuclear envelope are positive for Ketel, Otefin, Lamin and Bocksbeutel defining them as inner nuclear membrane (INM), while tubular elongations reaching into the nucleoplasm partly co-stain for INM markers like Otefin or Bocksbeutel but not Lamin, indicating type I indentations.

The multi-transmembrane-nature of the Schlank protein renders it very unlikely that the protein would be pulled out of the membrane and be able to freely distribute in the nucleoplasm, due to the sheer number of hydrophobic protein regions. Although a similar mechanism has been indicated for the epithelia growth factor receptor (EGFR), which is imported into the nucleus as membrane bound-receptor and upon reaching the INM is then completely pulled out of the INM by the Sec61ß translocon (Wang et al, 2010).

We observed that there is cleavage of the Schlank protein within the homeodomain (Reinhard Bauer, Tristan Wirtz, Simon Healy, personal communication), which would also have allowed a model in which only part of the Schlank protein (e.g. the homeodomain) would be released from the membrane via protease cleavage, but this model did not hold true: the cleavage occurs within the homeodomain (Anna-Lena Klemm, personal communication) and cleavage products cannot be found within nuclear fractions. However, Western Blot analyzes show that they seem to be enriched in mitochondrial-membrane and vesicle enriched fractions (Reinhard Bauer, Raija Sophie Ebert, Anna-Lena Klemm). Nuclear fractions are nearly devoid of cleaved fragments and favor the full length proteins. Thus, cleavage has to occur with a different Schlank protein pool and not take place in the nucleus. Summed up, the protein cleavage seems not to be relevant for a facilitation of nucleoplasmic localization of Schlank.

While an EGFR-like translocation / membrane-removal mechanism cannot yet be ruled out with the currently available data either, it seems more likely, that the tubular Schlank-positive structures are INM-invaginations. Two types of nuclear membrane-invaginations have been described:

Type I are defined as direct INM invaginations of the INM into the inside of the nucleus. Type II, which are invaginations of both INM and ONM as double membrane are, in contrast to

type I invaginations, lined with Lamins (Malhas et al, 2011). Schlank positive invaginations don't show Lamin enrichment and could thus be classified as type I INM-invaginations.

Lipid stains (e.g. CM-DiI) were not able to penetrate the fat body nuclei with established protocols and thus could not be used to identify nuclear membrane invaginations themselves (Linde & Stick, 2010). However, immune-gold electron microscope imaging should be able to allow a better analysis of the Schlank distribution in the nucleus in respect to the INM in future approaches.

Nuclear translocation of the Schlank protein itself could be addressed by clonal analysis of the main nuclear importer Importin-ß (Ketel) as well as mutagenesis analysis of a GFP-tagged Schlank homeodomain construct.

Knockdown of *ketel* transcript leads to a loss of the nuclear but not cytoplasmic Schlank pool. Also, there is some association of Ketel with Schlank in the cytoplasmic pool. This could hint to a mechanism where Ketel binds part of the cytoplasmic / ER Schlank protein pool and transfers it via the nuclear pore to the inner nuclear membrane, from where it is distributed to type I INM-invaginations.

Importin-ß (Ketel)-dependent nuclear translocation mechanisms rely on nuclear localization sequences within the cargo protein. Structure function analyzes revealed that the information for a nuclear import is encoded with in the homeodomain. N-terminal eGFP-tagged Schlank constructs that contain the homeodomain are nearly exclusively found in the nucleus. This seems to be a general CerS feature, as HA-tagged CerS5-homeodomain in mammalian cell is also strongly enriched in the nucleus (B. Fuß, personal communication).

The Schlank homeodomain is predicted to contain two nuclear localization sequences. When either one of them is mutated or deleted, there is strong loss of nuclear accumulation of the GFP-tagged Schlank homeodomain. These data provide more evidence that supports the Importin-ß-mediated nuclear translocation model for Schlank.

In addition, protein topology predictions (Fig. 3.2) as well as glycosylation scanning mutagenesis (Anna-Lena Klemm, personal communication, for method see van Geest & Lolkema, 2000) suggest that the homeodomain would face the cytosol when inserted into the ER membrane. Thus, NLSs would be accessible for nuclear importers. This topology also translates into the homeodomain facing the nucleoplasm when Schlank is inserted into INM-invaginations and could be potentially accessible to DNA/Chromatin and other nuclear proteins.

These data can be summed up in the following nuclear translocation model (Fig. 4.1):

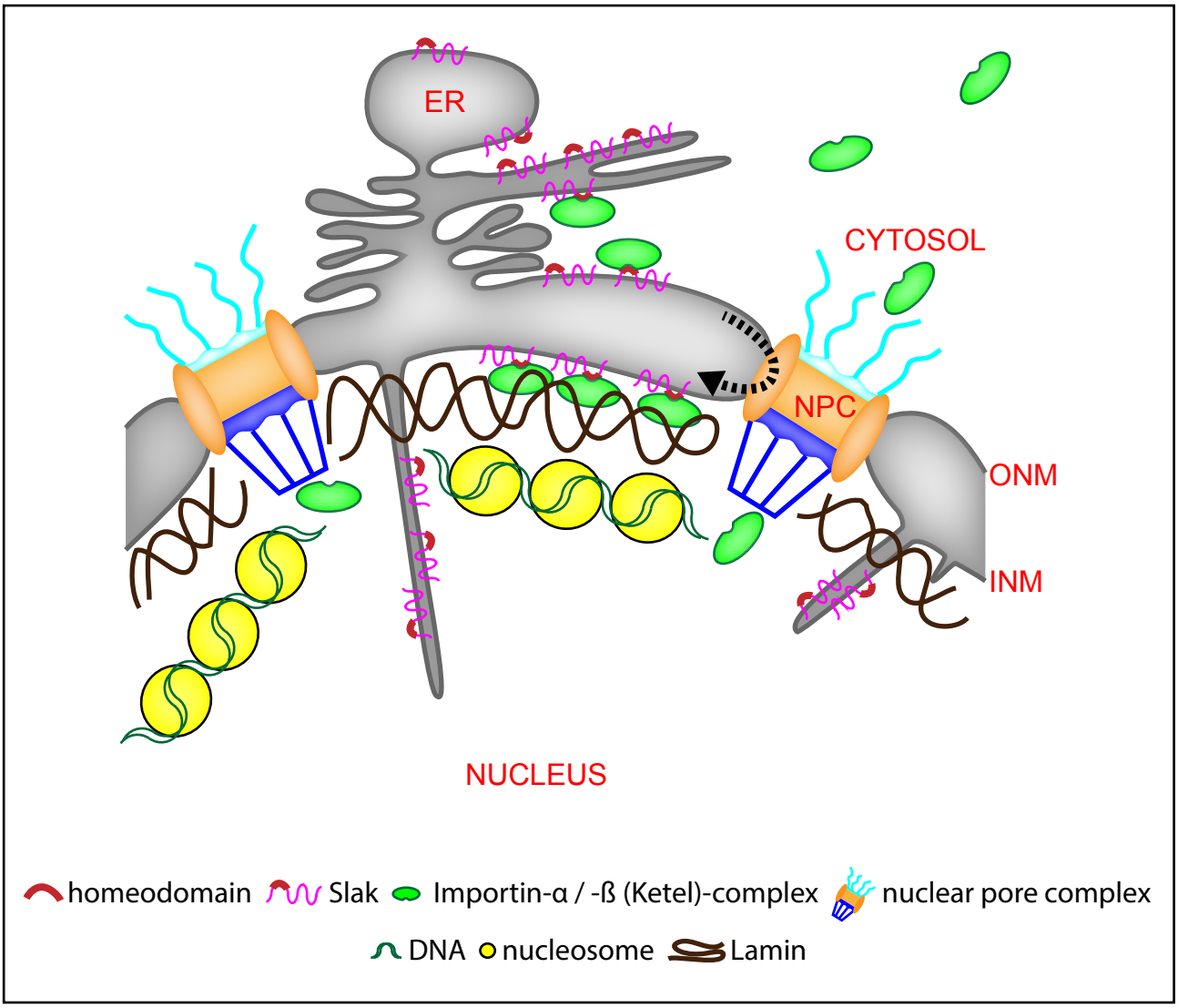

Figure 4.1 Model of Schlank nuclear translocation. A part of the Schlank protein pool within the endoplasmic reticulum membrane is bound via its nuclear localization sequences by an α-ß-Importin complex or ß-Importin (Ketel) itself. In a Ketel-dependent mechanism, Schlank is then transported in its membrane-bound state through the nuclear pore complex to the inner nuclear membrane. It then distributes to INM-identations. According to topology predictions, the homeodomain faces the cytosol when Schlank is inserted in the ER membrane and would face the nucleoplasm upon reaching the INM. Schlank could then potentially recruit specific DNA stretches via its homeodomain. Subcellular compartments and borders are indicated.

Whether or not there could be a functional relevance to the homeodomain, was addressed by a series of experiments shedding light on Schlank homeodomain properties and in essence invalidated the second Ceramide Synthase paradigm.

4.2 The Schlank homeodomain can interact with DNA

4.2.1 Amino acid sequence deviation in CerS homeodomains does not preclude DNA-binding

The second paradigm proposed for Ceramide Synthase properties states that CerS homeodomains would be non-functional except for supporting ceramide synthesis (Mesika et al, 2007). This is basically not supported at all by any experimental data, neither found in literature nor indicated by data acquired and summarized in this thesis.

Three arguments have been raised to conclude a supposed incapability of CerS homeodomains to bind DNA:

a. There is amino acid sequence exchange in Ceramide Synthase homeodomains compared to the homeodomain consensus (Mesika et al, 2007; Levy & Futerman, 2010).
b. Prosite alignment-based domain prediction programs start to recognize the homeodomain-like stretch from amino acid 15 on, only (Mesika et al, 2007; Levy & Futerman, 2010).
c. Exhange of homeodomain amino acid 51 from Asn to other amino acids abolishes DNA binding (Mesika et al, 2007).

4.2.2 The Schlank homeodomain conforms to the classical homeodomain consensus

Although the consensus sequence of homeodomains is quite useful to predict homeodomain-like structures and highlight important features and functional stretches within the homeodomain (Bürglin, 1994), amino acid exchange in respect to the consensus in general is quite common. Conservations in functional homeodomains can range from e.g. 63.3 % identity and 73.3 % similarity in *Homo sapiens* PDX1 homeodomain down to 21.7 % identity and 33.3 % similarity in *Drosophila melanogaster* Prospero homeodomain, when aligned via Emboss Stretcher-Software (Myers & Miller, 1989). Taking into account only the percentage identity and similarity, the Schlank homeodomain scores 23.3% and 48.3% respectively. Thus in raw numbers, it would even be a better fit to the homeodomain consensus than the well characterized Prospero homeodomain. This illustrates quite well that a dismissal of DNA-binding properties on similarity scores would be rather short-sighted.

Sequence alignment logo of human homeodomains shows a strong conservation of helix 3 but also only a minor sequence conservation of the N-terminal part of homeodomains (Fig. AP 4.2.1) similar to the conservation pattern in CerS homeodomains (Fig. 3.4 B). The assessment that the first 15 amino acids of the CerS homeodomain would be 'missing' was based on the assumption that the Prosite homeobox recognition pattern would be more stringent than the SMART HOX recognition pattern and thus better suited for homeodomain predictions (Mesika et al, 2007). However, it is noteworthy that the Prosite-pattern cannot even recognize the *bona fide* homeodomains of *Drosophila melanogaster* Prospero or *Homo sapiens* ADNP2. Also, the homeodomain of *Homo sapiens* ADNP is recognized from amino acid 16 on only, same as for the Ceramide Synthase homeodomains. Thus, failure of the Prosite-pattern to predict the entirety of homeodomains does not indicate non-functionality nor missing amino acids.

4.2.3 CerS homeodomains have the same 3D-folding as classical homeodomains

More important to functional aspects of a homeodomain is the 3-helix folding, with the helices arranged at specific angles by the loop-regions between them. Homeodomain helical folding and angles allow the third helix to contact bases at a DNA groove and the N-terminal arm in front of helix 1 to contact bases and the DNA-backbone. Thus both N-terminal arm and helix 3 determine the base-specificity of the consensus site of a homeodomain. This stereotypic helix pattern is well conserved in Ceramide Synthase homeodomains. Overlay of 3D structural data of CerS5 / 6 homeodomains gathered by NMR and classical homeodomain structures resolved by X-ray crystallography show that there are 3 helices in CerS homeodomains that are at the same angles to each other as in classical homeodomains. These homeodomain backbones can virtually not be told apart. SWISS-MODEL-predictions for the Schlank homeodomain predict the same helical pattern as for CerS5/6 homeodomains.

4.2.4 Once thought-to-be-mandatory Asparagine-51 is only present in some CerS homeodomain variants but was shown not to be essential for homeodomain-DNA interactions in some classical homeodomains

DNA-amino acid interaction is fundamentally linked to the biochemical properties of both molecule classes and is universal for all life on earth. Homeodomains show a fundamental similarity to bacterial mating class helix-turn-helix DNA interaction proteins in both structure and

DNA-interaction dynamics. The homeodomain DNA-interaction is so basic that homeodomains are found in plants and animals alike identifiable by the same amino acid and structure pattern (three helices connected by two loops/turns) and following the same DNA-amino acid interaction rules (Mukherjee et al, 2009).

Amino acids side chains, especially in the third helix, are important for direct homeodomain-DNA interaction. Side chains either contact the phosphate backbone or specific DNA bases. Thus a specific DNA recognition pattern is established that relies on the specific sequence of the homeodomain. It was suggested that Asn-51 is crucial for most homeodomains that bind a TAAT DNA-core sequence. Here, Asn-51 is thought to contact the second adenosine of the TAAT core (Noyes et al, 2008a)). Asn-51 is indeed exchanged in the Schlank homeodomain for a Leucine (L) and in most other Ceramide Synthases for arginine (R), glutamine (Q) or histidine (H). It is noteworthy that there are also exceptions for Ceramide Synthases: *Ciona intestialis* CerS UPI0000561E41, *Pteropus vampyrus* CerS3, *Danio rerio* UPI0001E9288F (CerS4b, et al. 2013 for nomenclature) code for Asn-51.

It is of utmost importance that there are also examples of other *bona fide* homeodomains that do not rely on asparagine (Asn, N) at position 51 for specific DNA interaction at all:

For Oct-4, an important homeodomain-transcription factor important in cell fate decisions, it has been shown that an exchange of Asn-51 (position within the homeodomain) to Arg does not change affinity of the Oct-4 homeodomain to its consensus binding site (ATGCAAAT) but in addition allows for an additional recognition of an alternative binding site (ATGCAAGG; Smith & Ford, 2005). In addition, DNA-interaction of the two homeodomains in *Zea mays* Hox2a does not rely on Asn at position 51 at all but there is either Serine (Ser, S) or Glycine (Gly, G) leading to a core consensus site of TCCT and GATC (Kirch et al, 1998). This is quite revealing as Asn-51 has been mapped to bind adenosine at the third base in four-base core consensi. N51R exchange in Oct-4 and N51S/G exchange in *Zm*Hox2a yield a consensus shift to guanine/cytosine/thymine, respectively. Taken together, this indicates that Asn-51 exchange to other amino acids might not disqualify DNA-interaction in general but might indicate a shift of the consensus binding site from adenosine to other DNA bases, perhaps leading to specific but more derivative DNA consensus binding sites.

This assumption was ultimately proven in a large-scale bacterial-one-hybrid-screen involving most *Drosophila melanogaster* homeodomains, including the Schlank homeodomain. Out of a randomized set of DNA sequences, the Schlank homeodomain bound those sequences that have a specific consensus motif roughly conforming to C[T/C]AC[C/T]A[A/G/T] (matrix

MA0193.1 Noyes et al, 2008b, JASPAR database Mathelier et al, 2013; some variation of the 'fixed' bases may occur, see matrix). The Schlank consensus binding site is richer in cytosines than average DNA binding sites.

4.2.5 Schlank homeodomain is able to bind DNA in vitro

When an affinity purified GST-tagged Schlank homeodomain is incubated with radioactively labeled 43 bp randomized 60 mer oligos, a high percentage (~80 %) of the DNA-library is bound. The DNA-binding is not due to the GST-tag as purified GST does not bind the double stranded DNA library at all. This indicates that per se DNA binding is possible. The binding can be disrupted / reduced by heparin or salmon sperm DNA, which are competitors for homeodomain interactions by charge. However, the inhibitory concentration where 50 % of the DNA binding to the randomized library is gone is equal to a 1.5 molar ratio of heparin over GST-Schlank-homeodomain. This would roughly correspond to the amount of charges needed to completely nullify all positive charges in the homeodomain construct. Put in other words, when all positive charges are masked there is still 50 % of the DNA-library binding to the Schlank homeodomain. Higher excess of heparin abolishes DNA binding but this is perhaps not surprising due to the fact that there would be an extremely low amount of DNA molecules in the library that corresponds to the potential Schlank consensus.

Competition with salmon sperm DNA is somewhat similar but allows 1 - 2 % of the DNA library to still bind the Schlank homeodomain even in a 300 fold molar excess.

In order to identify more *bona fide* Schlank homeodomain targets, an RNA sequencing (RNAseq) approach was chosen. A full length version and a construct that ranges from the Schlank N-terminus until after the homeodomain were expressed by a hormone-inducible GAL4-system (tubulin GeneSwitch GAL4, tGS-Gal4) in larvae. This has the advantage that control (uninduced) and experiment (induced) conditions would have the exact same genotype thus eliminating a transcriptome change due to different sites of construct insertions. Wildtypic animals were used to identify potential off-targets due to the feeding of the hormone itself. Following comparisons were chosen to identify homeodomain-specific and non-specific target genes:

a. *indirect* (not homeodomain mediated) target genes should be regulated by expression of the full length but not the N-terminal construct.
b. *homeodomain-specific* targets should be regulated by the N–terminal construct only.

c. *direct* physiologically relevant target genes should be regulated by both constructs.

Obviously, this necessitates that the N-terminal construct is itself functioning as transcription factor. This was shown in a pre-experiment: expression of the N-terminal construct decreases *lip3* expression in a time-dependent manner: four hours after a two hour induction with the hormone, *lip3* expression decreases the strongest, which is roughly two hours after the expression peak of the construct itself. This time-frame would allow the construct to be translated and act to repress the potential target gene *lip3*. When the expression of the construct has decreased, also the repression of *lip3* is gone. Thus, the time-point four hours after induction seemed suitable for the RNAseq analysis.

While there were a number of indirect and homeodomain-specific target genes, the post-RNAseq realtime-qRT-PCR-based validation of direct physiologically relevant target genes failed due to only recently reported problems inherent to the GAL4-expression system itself.

All commonly regulated target genes were shown to be unspecifically regulated by the transcription-inducer GAL4 itself. While it was previously believed that the yeast GAL4-protein would not be active on the fly genome unless a UAS-sequence was supplied, it was only recently shown that this is not the case. GAL4 apparently can induce more than 1000 *Drosophila* melanogaster genes by directly binding regulatory elements within the fly genome. Thus the frame of reference in the RNAseq approach is wrong, leading to a strong transcriptional noise level that led to the identification of GAL4-target genes instead of the direct Schlank targets, even when the so far known GAL4-targets were discarded from the list of regulated genes.

This error can be easily rectified by using a different baseline-reference condition:
The inducible tGS-GAL4 construct itself without UAS-effector. Induction of the tGS-GAL4 should activate the DNA binding capacity of the GAL4 itself and already up- and downregulate the respective GAL4 targets. When this transcriptome is used as a reference for the transcriptome upon overexpression of the Schlank constructs, the identification of specific Schlank targets should be possible. All genes that are up- or downregulated upon expression of both Schlank constructs relative to the induced tGS-GAL4 transcriptome (not the induced wildtypic transcriptome) would be the proper target genes if they are shown not to be regulated by feeding the hormone itself.

4.2.6 Schlank homeodomain binds lip3 and akh regulatory regions in vitro

Lip3 and *akh* are two genes that are strongly upregulated in the mutants and can be suppressed by the overexpression of Schlank, even when the Ceramide Synthase activity is abolished in the expressed Schlank constructs. Both proteins are intimately linked to lipid storage: Akh activates a G-coupled protein receptor cascade that activates triacyl- and diacylglycerol lipases and allows them access to lipid droplets and Lipase 3 is a lipase.

In silico analysis of the potential promoter region for both genes (approx. 1000 bp region upstream of the transcription start) indicated the presence of Schlank consensus binding sites.

When ~30mers were used that code for those regulatory elements, the purified GST-tagged Schlank protein but not GST alone was able to bind those oligos, leading to a band shift in an electromobility shift assay. Occurrence of bands indicates that a homeodomain-DNA complex has formed, which retards entry of the DNA-oligo into the gel. Overall binding conditions in the EMSAs are not optimal yet, as illustrated by the fact that only a minor amount of oligo was bound by the purified protein and that competition with unlabeled oligos and antibody supershifts don't consistently work. Binding affinity of homeodomains to DNA oligos is strongly influenced by the binding buffer composition as well as interacting co-factors (perhaps even Schlank dimers) that might be needed to stabilize or enhance the homeodomain-DNA interaction. To that end, future EMSA approaches should make use of partly purified Schlank protein from *Drosophila melanogaster* lysates instead of bacterial lysates. New and perhaps more affine binding sites and in parallel new target genes could be identified via DNAse I protections assays, protein binding micro arrays or Chromatin-immunoprecipitation-like assays in combination with DNA-sequencing analysis. A Schlank-ChIP assay was established in this thesis (Fig. AP 4.2.2) but was not combined with a DNAseq approach yet due to missing opportunities to determine specific DNA enrichment in the pulldown as well as inconsistent chromatin shredding. Usage of a Misonix Ultrasonic processor or enzymatic digestion should give a more reproducible DNA fragmentation than a dip-in sonicator rod. Qubit high sensitivity DNA dye can be used to estimate lowest amounts of DNA. Overall DNA enrichment (but not gene specificity) in ChIP-like pulldown experiments in comparison to isotypic antibody controls can indicate DNA pulldown. However, it cannot replace a gene-specific enrichments control. Now that *lip3* is established as potential Schlank target gene, qRT-PCRs over *lip3* promoter regions containing the consensus binding site can help estimate a gene-specific enrichment.

Potential TF-ChIP targets can in turn be cross-correlated with the Schlank binding site consensus identified by (Noyes et al, 2008a) as well as the target genes of the *Apis mellifera* Schlank homolog (Lag1) which were identified via comparative transcriptomics analysis (Chandrasekaran et al, 2011).

Taken together, there is evidence that the Schlank homeodomain can interact with DNA, which was found with two independent approaches: Schlank-homeodomain-matrix based binding of a radioactively labeled randomized DNA library and electromobility shift assays with specific Schlank-consensus sequence-based oligonucleotides.

4.3 Potential modes of operation for a Schlank-homeodomain mediated transcriptional regulation

If there would indeed be a direct transcriptional regulation by the Schlank homeodomain, three modes of action would be plausible:

a. transcriptional regulation by a transactivation domain / interaction with transactivator
b. transcriptional regulation by a repressor domain / interaction with a repressor
c. gene-specific recruitment of a chromatin-stretch to the inner-nuclear membrane in an Emerin-like fashion

Modes of operation one and two cannot be ruled out, however transactivator and repressor domains could not be identified, yet.

There is some more supporting evidence for mode three, however. Emerin is a prominent example for an INM-inserted transmembrane protein that is involved in transcriptional regulation: Emerin, which is tightly linked to Lamin A, lines the inside of the nuclear envelope. While Emerin itself cannot directly bind DNA, current models propose that it is a bridging protein between the INM-Lamina, DNA-binding protein cKrox and Histone deacetlyase 3 (HDAC3). Specific GAGA-rich DNA sequences (Lamin-associated sequences [LAS] or Lamin-associated domains [LAD]) are bound by the GAGA-associated factor cKrox and HDAC3 which both recruit those DNA-stretches to the nuclear Lamina / INM by an Emerin and Lap2ß interaction (Zullo et al, 2012). Subsequent gene-silencing is mediated via Emerin's interaction with the transcriptional repressors Germ cell-less (GCL) as well as Histone deacetylase 3 (HDAC3; Holaska et al, 2003; Demmerle et al, 2012). HDAC3 is a central part of the nuclear co-repressor (N-CoR) complex.

In summary, for the Emerin-based gene-silencing mechanism, the following principal components are needed: a DNA-interactor that is recruited to the INM along with a bound DNA-stretch by interaction with Emerin and transcriptional repressors like HDAC3 that silence the recruited genomic region.

Analogously, for Schlank this would translate into the following mechanism with a shortcut for DNA-binding: Schlank, integrated into the INM, would bind DNA stretches (perhaps even sequence-specific) via its homeodomain and thus recruit them to the INM-Lamina. An associated or nearby transcriptional repressor would then silence gene expression or a transcriptional activator would activate gene expression. Alternatively, recruitment of chromatin-modifiers could change the chromatin state (condensed or decondensed chromatin). Interaction partner candidates that might be involved in chromatin modification or transcriptional regulation were already identified by yeast-2-hybrid approaches 10 years ago: transcription factor No-ocelli (noc) was pulled with a full-length Schlank cDNA clone (Giot et al, 2003) and the structural chromatin component and modifier Decondensation factor 31 (Df31) was pulled with hSos-fused Schlank-aa65-145 (Bauch, 2003). Df31 was in addition verified by GST-Schlank-aa65-145-mediated pulldown of ^{35}S-labeled *in vitro* transcribed Df31 protein (Bauch, 2003).

Potential regulatory complexes would still need to recruit DNA stretches towards Schlank. To visualize target gene DNA stretches that might be recruited to the INM-Schlank region, an immunostaining-complemented fluorescent *in situ* hybridization (immunoFISH, Reddy et al, 2008) could be applied that would allow visualization of the target gene in relation to the Schlank protein.

4.4 Potential physiological relevance of nuclear localization, homeodomain as well as enzymatic activity

Sphingolipids were shown to be major structural components of membranes as well as essential signaling molecules that even have their own receptors and signaling cascades (e.g. Sphingosine-1-phosphate, Rosen et al, 2009; Granado et al, 2009). In general, these lipids have been implicated in a wide range of cellular processes, ranging from the modulation of apoptosis (Young et al, 2013) and immune function (Olivera & Rivera, 2005; Lahiri & Futerman, 2007) to effects on carcinogenesis (Riley et al, 2001; Ryland et al, 2011) and occurrence of neuropathies (Eckhardt, 2010{Yu 2012 #327van Echten-Deckert & Walter, 2012).

Ceramide Synthases are thought to be right at the center of the synthesis and recycling of all complex sphingolipids. We could show that at least in *Drosophila melanogaster*, in addition to the aforementioned effects, CerS might have an effect on general fat storage that could be independent from its enzymatic function and thus independent of sphingolipids as effector molecules. It turned out that the most important factor for the modulation of fat store levels, in situations where Schlank levels are changed, would be the level or activity of Lipase 3. Normalization of *lipase 3* levels was sufficient to restore the fat store in cell culture experiments. This necessitates for future analyzes of Schlank activities and mutant phenotypes to dissect and tell apart various molecular biological aspects:

a. Which protein pool within a given cell is modulated?
b. Are there changes in the dynamics of protein localization?
c. Is the enzymatic activity or another protein function affected, like homeodomain activity or protein interaction?

There are various approaches underway addressing this issue: genomic engineering will allow to modify the Schlank coding sequence in its genomic locus in a way that either the enzymatic activity (H215D mutation), DNA binding (homeodomain mutations) or the nuclear import (NLS mutations) will be individually affected without changing the expression level or tissue distribution. In addition, rescue experiments with different constructs abolishing different aspects of molecular Schlank function will give valuable insights into which domain function would be needed in which tissue. So far, rescue experiments suggested that the enzymatic activity is needed for the developmental timing, since H215D mutated protein versions cannot rescue the developmental delay. Whether or not they could rescue fat storage aspects remains to be seen.

Although it is quite tempting to attribute the observed transcriptional changes seen upon the modulation of Schlank protein levels to the homeodomain activity only, especially in light of the H215D mutation data, it should not stay unmentioned that sphingolipids are differentially distributed in nuclear domains (Lucki & Sewer, 2012) and have been shown to be involved in nuclear architectures, spindle formation during mitosis (Gillies et al, 2009; Fyrst & Saba, 2010), nuclear protein import (Faustino et al, 2008) and transcriptional regulation itself (Hait et al, 2009). This might have severe implications for nuclear Schlank functions warranting further dissection of the different domain activities. Sphingosine was shown to be phosphorylated to sphingosine-1-phosphate (S1P) by a nuclear Sphingosine-Kinase 2 (SphK2, Igarashi et al, 2003) which also binds

histone 3 as well as histone modifiers HDAC1/2 (Hait et al, 2009). It was shown that S1P inhibits HDACs acetylation activity and thereby changes transcription of specific target genes (*p21* and *c-fos*, Hait et al, 2009). Enzymatic activity of Neutral Sphingomyelinase, Ceramidase (Tsugane et al, 1999) and Sphingomyelin Synthase (Albi & Magni, 1999) in nuclear fractions suggest that there is a network of enzymes involved in sphingolipid synthesis located within the nucleus.

The finding of various sphingolipids in the nucleus, including sphingosine, sphingosine-1-phosphate as well as glycosphingolipids GD1a and GM1 (Wu et al, 1995) has prompted the speculation that there might be various nuclear sphingolipid domains (Ledeen & Wu, 2008; Fyrst & Saba, 2010). The set of identified sphingolipid metabolism-related enzymes might thus not be surprising and even allow for a model in which there is local synthesis in addition to a sphinglipid transfer from ER / Golgi to the nucleus (Ledeen & Wu, 2008).

Schlank as a CerS with a nuclear pool would complete this picture in a way that it might be involved in nuclear ceramide synthesis as well, adding to the maintenance and modulation of the nuclear sphingolipid environment. Whether or not there would be an additional contribution to the homeodomain function of this ceramide synthesis activity in combination with the SphK2-based transcriptional regulation by the modulation of S1P levels cannot yet be composed into a holistic model due to the sheer wealth of newly identified and unknown variables.

Taken together, the data derived and summed up in this thesis open the door not only for new directions in research for the whole CerS enzyme family, especially in respect to the activity of the different protein domains and the enzyme localization. They also raise more questions towards the overall nuclear architecture, the local maintenance of the nuclear lipid environment and give an additional layer of depth to sphingolipid-mediated transcriptional regulation.

5 Appendix

AP1 *schlank* mutations affect the development of the compound eye

Ceramide levels and changes in CerS activity have been previously described to induce or suppress apoptotic processes (depending on the ceramide species (Bose et al, 1995; Acharya et al, 2003; German et al, 2006; Mullen et al, 2011; van Brocklyn & Williams, 2012).

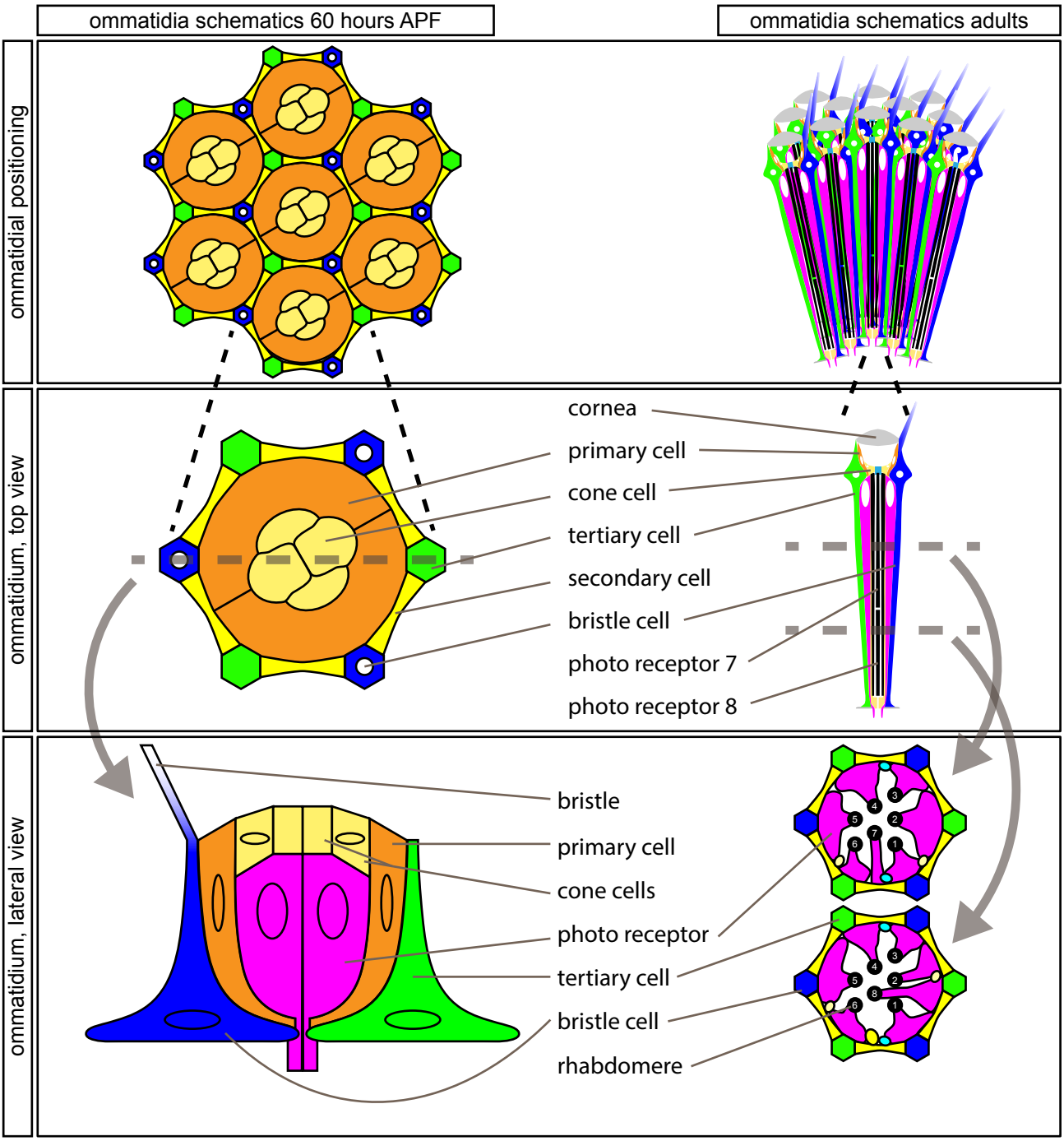

Figure AP 1.1.1 Schematic representation of ommatidial arrangement 60 hours after puparium formation and at adult stages. Horizontal and lateral sections are shown. The arrangement is stereotypic with three tertiary cells, three

bristle cells, six secondary cells, two primary cells and four cone cells that surround the eight photoreceptors (with photoreceptor 8 below photoreceptor 7).

In *Drosophila*, one of the major systems to address an involvement of a protein in apoptosis and neurodegeneration is the development of the compound eye (Song et al, 2000; Takemura & Adachi-Yamada, 2011; Loewer et al, 2004; Lu, 2009). A modifier screen for eye development identified *schlank*^{G0365} as being involved in proper eye development (Ida et al, 2009). In this study, the system was used to analyze whether or not Schlank is involved in naturally occurring apoptotic processes, as was suggested by data obtained in mammals (Novgorodov et al, 2011; Véret et al, 2011; Bieberich et al, 2001; Herget et al, 2000).

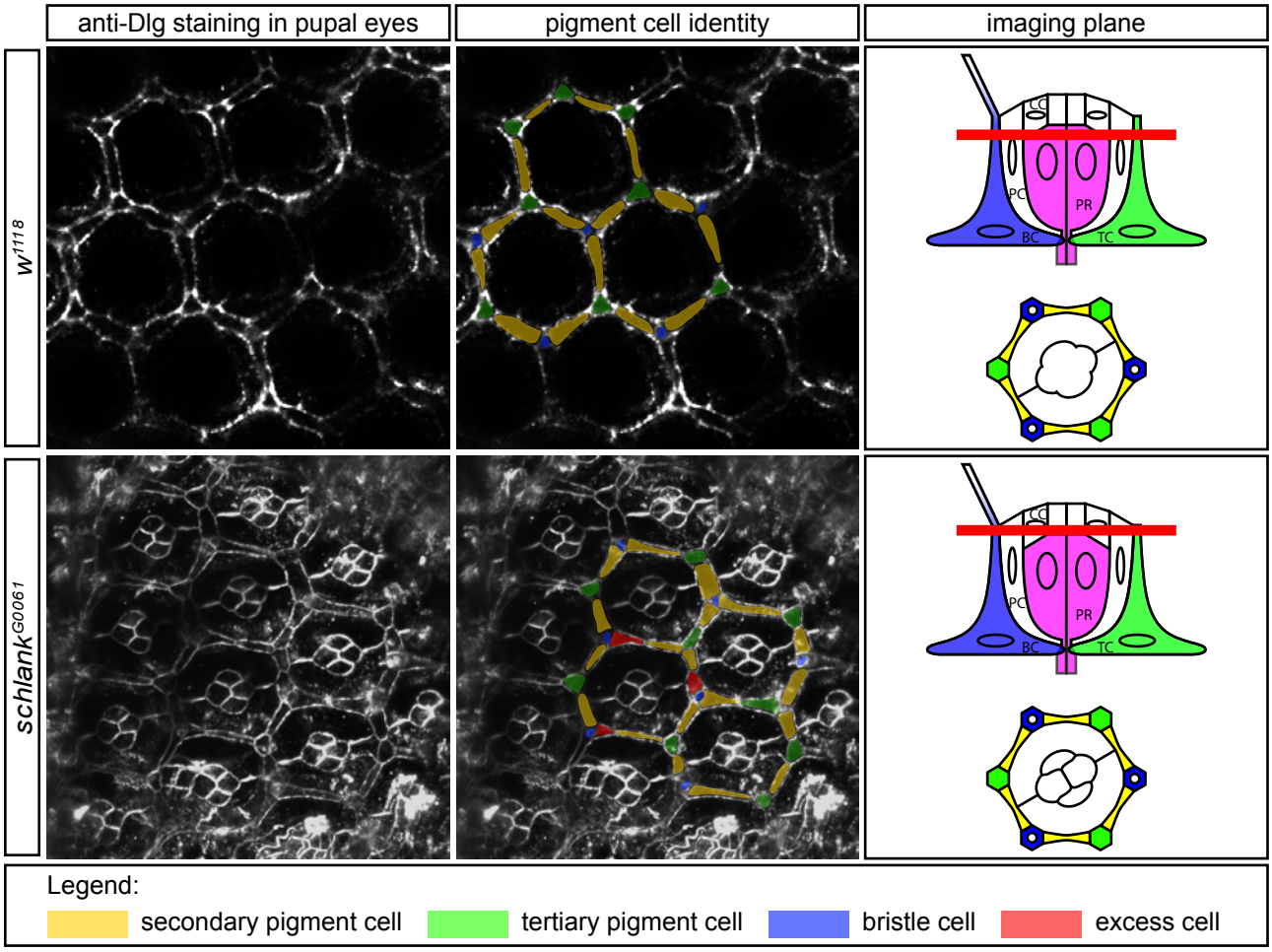

Figure AP 1.1.2 *schlank*^{G0061} mutants show excess pigment cells at the end of pupal development. Discs large (Dlg) antibody staining on wildtypic (upper panel) and *schlank*^{G0061} mutant (lower panel) pupal eyes 60 hours after puparium formation. Tertiary cells are highlighted in green, bristle cells in blue, secondary cells in yellow and excess cells in red. Schematic representations show the imaging planes. BC, bristle cell; TC, tertiary cell; PR, primary cell; PC, pigment cell; CC, cone cell

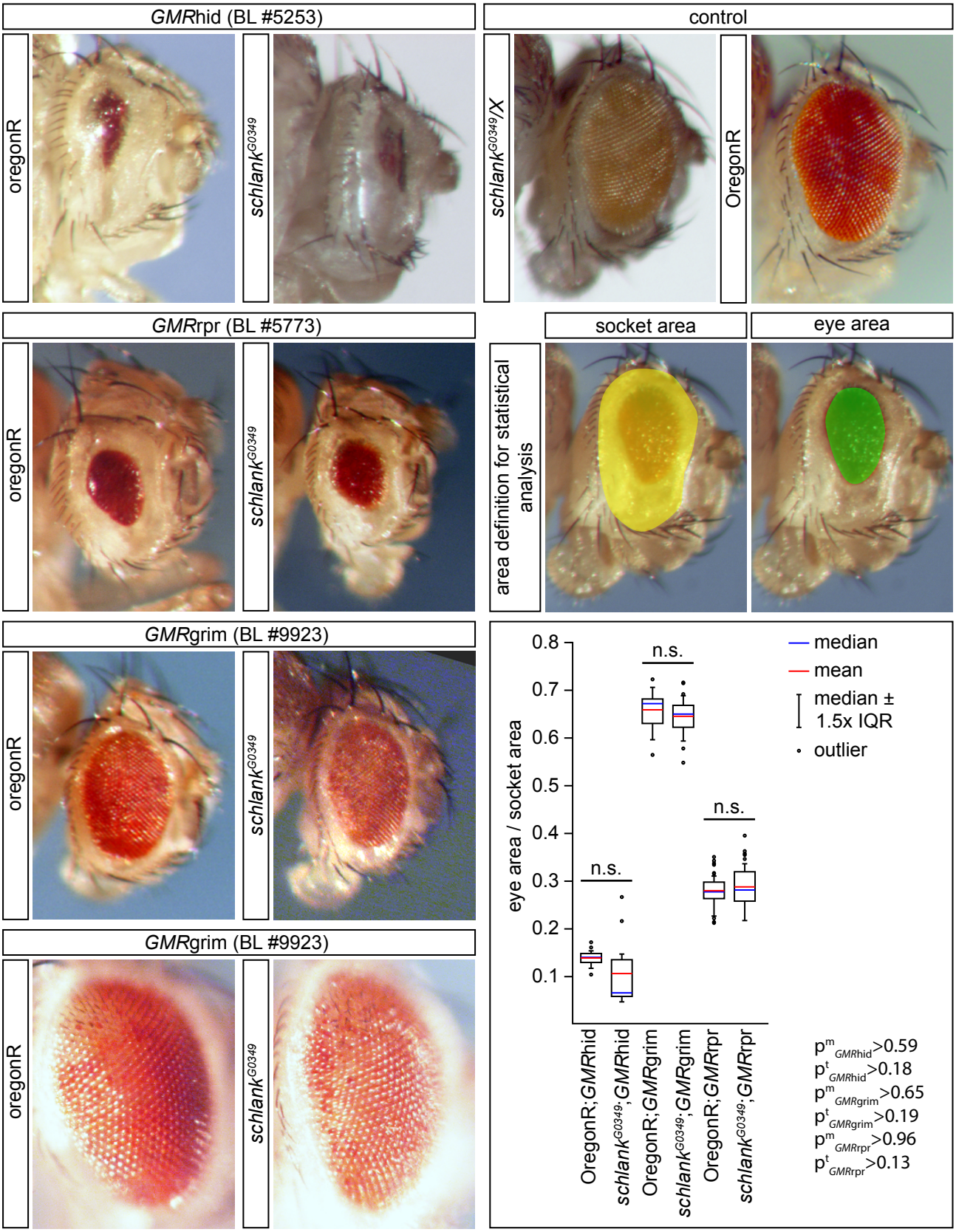

Figure AP 1.1.3 Schlank mutation does not have any modulatory effect on the activity of apoptosis initiators Rpr, Hid and Grim. Glass Multimer Reporter (GMR)-driven initiators of apoptosis Reaper (rpr), Wrinkled (hid) and grim were crossed into the Schlank mutant background. Heterozygous combinations do not significantly change the eye size. To determine the relative eye size independent from varying imaging angles, the ommatidia-carrying area was measured relative to the eye socket area. Quantifications are shown as boxplots. Distributions were analyzed via T-Test (p^t) and Mann-Whitney-U-Test (p^m). None of the eye size distributions are significantly different. This indicates

that either Schlank is not involved in the classic apoptotic pathway, acts upstream of the RHG (Reaper, Hid, Grim) family or downregulation of *schlank* is not sufficient to have any effect. Median is marked in blue, mean in red, outliers outside the 1.5x interquantile range (IQR) are shown as dots.

The compound eye develops from undifferentiated cells set aside during embryonic development that, in larvae and early pupae, have formed the eye-antennal imaginal disc.

Differentiation of these cells starts in late stage 3 larvae (Morante et al, 2007). A wave of differentiation, called morphogenetic furrow, sweeps across the disc from posterior to anterior. During this process, photoreceptors R1 to R8 are defined (starting with R8; Jarman et al, 1994; Strutt & Strutt, 1999) that later also instruct cone cell formation, while pigment cells derive from remaining undifferentiated cells (Graham et al, 2010; Fig. AP 1.1.1). After two 45° rotation steps, photoreceptor clusters are aligned to each other in a fixed invariant pattern relative to the horizon (Strutt & Mlodzik, 1995; Chou & Chien, 2002). During pupal development, the number of pigment cells surrounding photoreceptor clusters becomes fixed to a stereotypic pattern: each photoreceptor cluster is surrounded by six secondary pigment cells, three tertiary pigment cells and three bristle cells (Fig. AP 1.1.1). All excess pigment cells and undifferentiated cells die via apoptosis to give this fixed pattern (Dos-Santos et al, 2008; Hays et al, 2002; Rusconi et al, 2000). Thus, the number of remaining pigment cells can be used as model to study apoptotic processes and at the same time, photoreceptor development is used as a model to study neuron differentiation.

Cell membranes in pupal eyes of the same age were stained by discs large (Dlg). This allows the identification of secondary and tertiary pigment cells as well as cone cells if imaged at the appropriate z-level. The staining of *schlank*^{G0061} mutant eyes showed that the pattern is disturbed and there are excess secondary pigment cells (Fig. AP 1.1.2). This indicates that Schlank might be involved in pigment cell apoptosis as a positive regulator.

To identify the position in the apoptotic cascade, epistasis experiments were carried out. To that end, either Oregon R or *schlank*^{G0349} (stronger allele) were crossed into fly lines carrying constructs that express either *hid*, *grim* or *reaper* in the eye. Hid, grim and reaper block activity of the '*Drosophila* inhibitor of apoptosis' (Diap) and thus if overexpressed, activate the apoptotic cascade. Expression of these genes via the 'glass multiple reporter' (GMR) promoter leads to smaller eyes, because photoreceptors and pigments cells undergo apoptotic cell death.

To score for any effect of *schlank* mutation on apoptotic processes, the size of eye area relative to the remaining socket area was quantified. There were no significant differences in the size of eye to socket area between transheterozygous *schlank-hid/rpr/grim* mutants and Oregon R

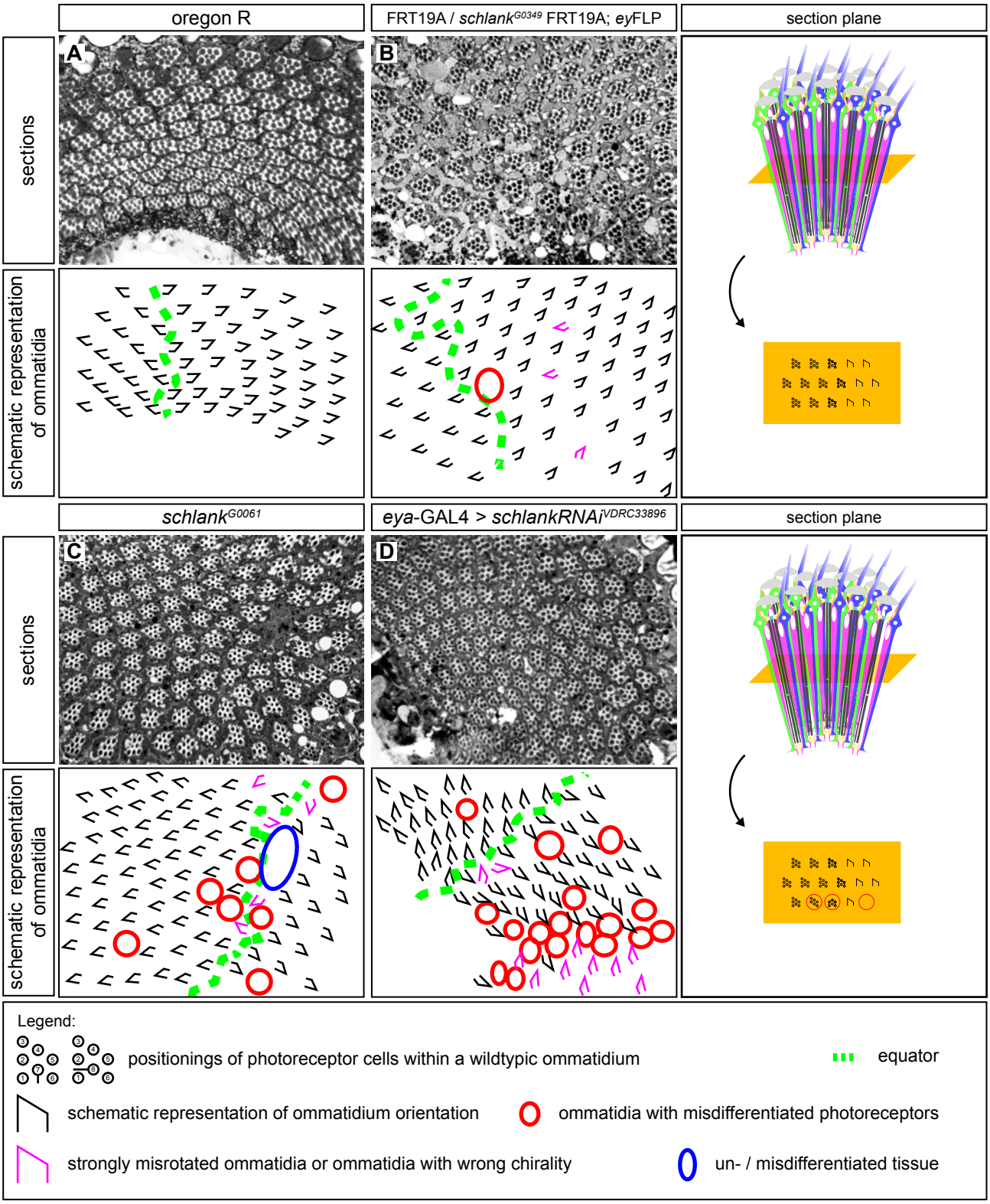

Figure AP 1.1.4 Modulation of Schlank levels during eye development leads to ommatidial rotation defects, undifferentiated tissue and misdifferentiated ommatidia. A-D, Sections of adult eyes stained with methylene/toluidine blue and embedded in DEPEX solution. Upper panel shows the sections, lower panel shows schematic representation of photoreceptor cell clusters - each trapezoid representing one ommatidium. Schemes to the right indicate the section plane in respect to the photoreceptors. **A**, Wildtypic eyes show a stereotypic photoreceptor pattern with ommatidia aligned in parallel, mirrored at the equator (green dashed line). **B**, *schlank*^{G0349} mutant clones initiated with the eyeless driven flippase expression show rotation defect (magenta trapezoids) and

misdifferentiated ommatidia (red circles, wrong number of photoreceptors). **C**, *schlank*^{G0061} mutant eyes show misrotation and misdifferentiation but also undifferentiated tissue (blue ellipses), especially near the equator. **D**, *Eyes absent* (*eya*)-driven *schlankRNAi* (VDRC33896) shows severe misrotation and misdifferentiation of ommatidia.

- *hid*/*rpr*/*grim* animals (Fig. AP 1.1.3). Thus the effect of Schlank on apoptotic processes during this process remains inconclusive. Adult eye sections show that the observed phenotypes were not due to a developmental delay: Eyeless-driven flipout clones of *schlank*^{G0349}, *schlank*^{G0061} mutant eyes and eyes-absent- driven *schlankRNAi*^{33896} showed both misdifferentiated and misrotated ommatidia (Fig. AP 1.1.3). This phenotype is usually observed upon differentiation defects during larval and early pupal stages of eye development. Additionally, *schlank*^{G0061} mutant adult eyes and eyeless-driven *schlank*^{G0349} clones in adult eyes contain masses of undifferentiated tissue (Fig. AP 1.1.3).

AP3.3 Phylogenetic analysis of Ceramide Synthases shows multiple duplication events and secondary loss of homeodomain-carrying CerS in Nematodes

Over 218 Ceramide Synthase protein sequences from 66 species were aligned and their phylogenetic relationship analyzed via Bayesian algorithms (Fig. AP 3.3.1). Due to the complexity of the task, the number of species and the available resources, employment of neighbor-joining-based programs was not feasible (mainly due to the fact that they did not allow the continuation of interrupted calculations). The first 25 % of the trees were discarded (burn-in) and afterwards the consensus tree was calculated. The identification of the individual Ceramide Synthases already showed that the homeodomain is present in species at the root of the phylogenetic tree. Species like the unicellular *Capsaspora owczarzaki*, the sponge *Suberites domuncula*, cnidarians *Hydra magnipapillata* and *Nematostella vectensis* as well as the only recently sequenced *Mnemiopsis leidyi* (genes ML077640a and ML279810a with HOX recognition by SMART, albeit with very weak threshold), which is thought to reside at the very root of the animal kingdom, already have type II Ceramide Synthases. Of all the analyzed Nematode species, none show a type II CerS. However, there are several type I CerS that show specific clustering. While *C. elegans* lag-r clusters with other CerS1 variants, Hyl-1 and 2 seem to be rather divergent, clustering with the other arthropod CerS. In addition, sister groups of Nematodes, Trematodes, Insects and Crustacians all code for type II CerS. This makes it rather likely that type II CerS were lost secondarily in Nematodes than an uptake of the homeodomain several times in evolution. It is also noteworthy that most insects seem to have lost type I CerS variants. It has been proposed previously (Holland et al, 2007) that

CerS homeodomains would be close to ZHX, ZEB and HOMEZ homeodomains. Indeed, SMART-based prediction of the protein domains recognizes various CerS2, CerS3 and CerS4 homeodomain variants as HOMEZ-homeodomain. An alignment of the CerS homeodomains (Fig. 3.3 B) gives some indication of the amino acid stretches important in CerS homeodomains. Following this motif, it becomes apparent that also other species, where SMART and other programs cannot recognize a homeodomain, still code for a sequence stretch that in length and sequence is very close to the CerS homeodomains (putative homeodomains, annotated as put. HOX).

Quality control for phylogenetic inferences is always a major issue. To asses the probability of a consensus tree and the tree nodes and branch lengths, several independent analysis runs are necessary to judge if the tree topologies converge on the same space. To that end, the calculations were done in four independent runs. MrBayes gives some rough indications as to when the convergence might be reached: the standard deviation of split frequencies should approach 0.01 and the potential scale reduction factor should approach 1.0. Effective sample size (ESS) gives an idea of the balance between the length of the chain and how frequent the posterior was sampled during the run. It should be higher than 200. However, MrBayes diagnostic parameters are often lacking and were complemented with a quality assessment via AWTY (Are we there yet?). The compare function plots the bipartition frequency between different runs and should correlate linearly. All quality criteria were met by the analysis (Fig. AP 3.3.2).

Taken together the phylogenetic analysis shows that CerS are a protein family closely related but distinct from TRAM and CLN8 proteins and that the homeodomain was incorporated very early in evolution.

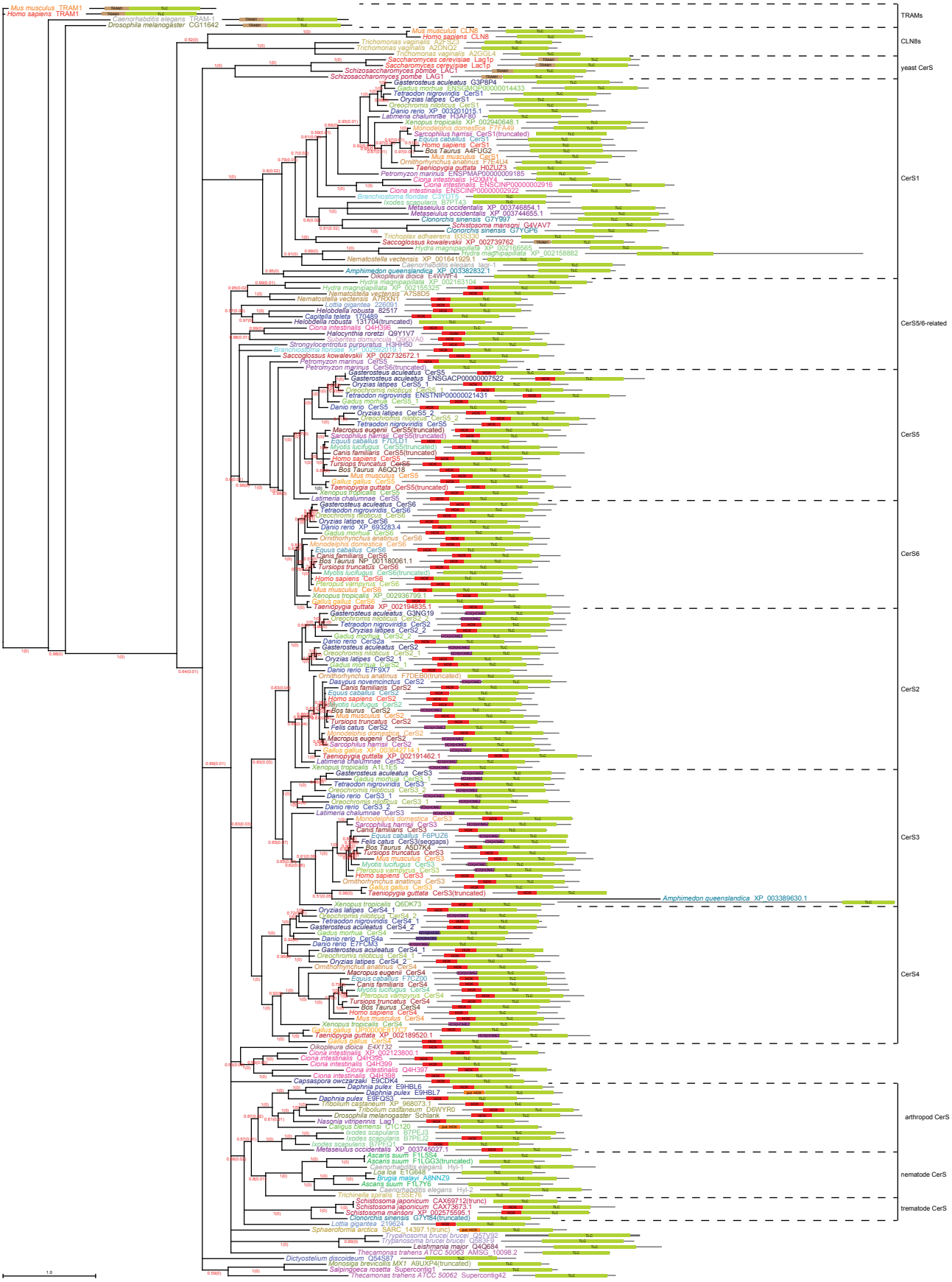

Justification of putative HOX domain annotations

species	gene	motif	E-value	motif		E-value
Sphaeroforma arctica JP610	SARC_14397.1	HOX	2.7	Blast:HOX	Q4SNB1_TETNG	5.0e-7
Caligus clemensi	C1C120			Blast:HOX	UPI0001560BB9	2.0e-5
Daphnia pulex	E9HBL7	HOX	301			

Figure AP 3.3.1 Phylogenetic tree for Ceramide Synthase full length protein sequences. 223 Ceramide Synthase full length sequences were aligned with ClustalW (for settings, see Materials and Methods part) and analyzed by Bayesian Markov Chain Monte Carlo algorithms (MCMC) with Jones amino acid exchange model with a burn-in of 25% for 1.28252 billion generations in MrBayes software in 4 independent runs with one cold and one heated chain each. The consensus tree of all runs is depicted via Archaeopteryx phyloxml viewer. Posterior probabilities are depicted in red numbers with standard deviations in brackets, species and protein symbols are given. Domain models for each protein are shown next to the gene symbol. Domains are annotated by boxes; the protein backbone is shown as grey line. Overlapping domains are depicted semi-transparently. All domain annotations are based on EMBL-SMART analysis, except for putative homeodomain sequences. CerS subfamilies are marked in brackets with dashed lines. SMART domain annotations: HOX, homeodomain; put. HOX, putative homeodomain [similar to CerS-homeodomain weblogo]; TLC, TRAM-LAG1-CLN8 domain; TRAM1, Translocating chain-associated membrane protein 1-domain; HOX | HOMEZ, HOMEZ-like homeodomain; HOX |BrkDBD, Brinker-DNA-binding-domain; Apt1, aberrant pollen transmission 1-domain; DUF, Domain of unknown function; Cornichon, cornichon-domain.

A

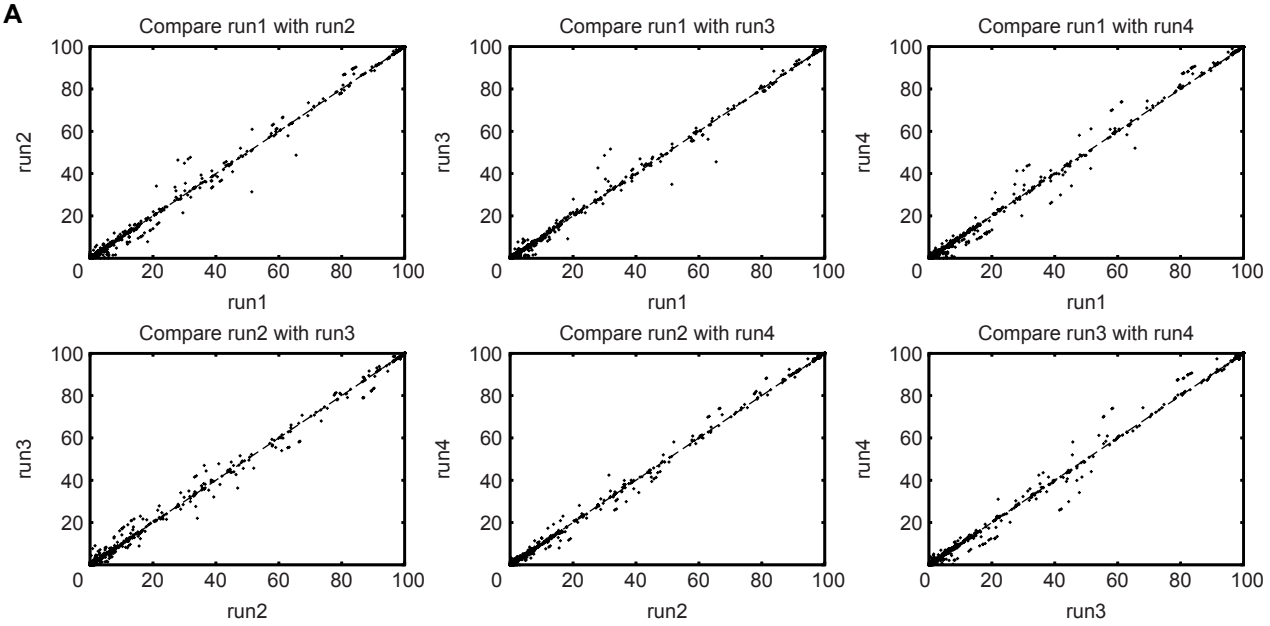

B

Parameter	Mean	Variance	Lower	Upper	Median	min ESS	avg ESS	PSRF
TL	94,207138	0,637229	92,641459	95,777503	94,199746	1655,22	4770,87	1,0000

C

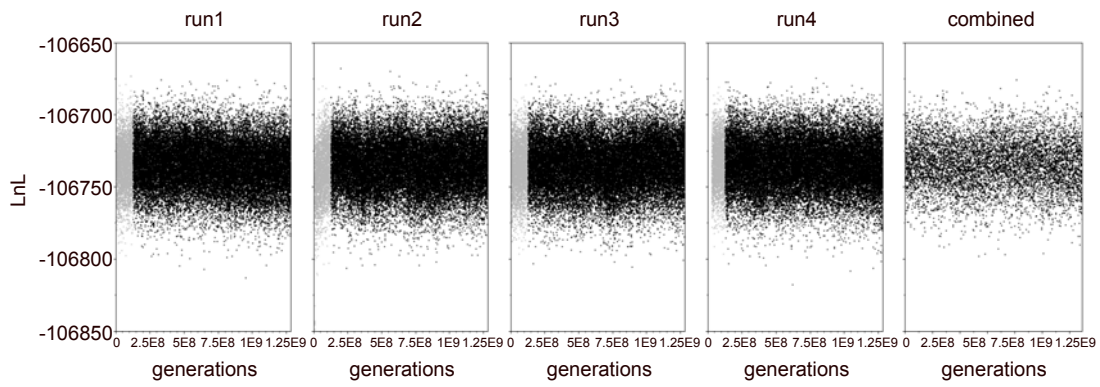

Figure AP 3.3.2 Quality control for phylogenetic consensus trees. Graphs depict AWTY (Are we there yet?) analysis comparing the convergence of all independent Markov Chain Monte Carlo (MCMC) runs. Tables show MrBayes parameter analysis of the runs with a burn-in of 25% at 95% highest probability density (HPD) interval. **A**, CerS full length protein sequence were calculated for 1.28252 billion generations in MrBayes. Linear regression in the AWTY compare output indicates convergence of the runs. TL total tree length, sum of all branches; ESS, estimated sample size (should be >100, otherwise undersampling); min, minimum; avg, average; PSRF, Potential Scale Reduction Factor (should approach 1.0 when runs converge; Gelman and Rubin, 1992) **B**, MrBayes statistical parameters. **C**, Tracer output for log-likelihood (LnL) through time (generations). ESS of the combined trace is ~500. Runs converge.

AP3.5 The 500bp genomic region upstream of the *schlank* transcriptional start directs expression in nervous system, fatbody and gut

Public data based on *in vitro* analysis suggests that the downstream region of Schlank as well as part of the first intron contain various transcription factor binding sites and might thus be a suitable region for enhancer/silencer identification (Fig. AP 3.5.1; flybase GBrowse, TFBS tracks).

To identify potential regulatory elements within the *schlank* locus, ~2 kb region downstream of the *schlank* transcriptional start was divided into overlapping parts of differing size (Fig. AP 3.5.1) and cloned into either the Gal4-containing pCaSpeR-AUG-Gal4-X or the LacZ-containing pCaSpeR-hsAUG-LacZ vector. After integration into the fly genome, the expression pattern was analyzed by crossing the Gal4 line with UAS-GFP containing fly lines or staining for LacZ activity via X-ß-Gal.

Overall, the longest constructs, spanning nearly the whole region, drive expression in multiple tissues: central nervous system (brain), oenocytes, gut, fatbody and trachea (Fig. 3.5.2). The expression in the fatbody and the gut (esp. proventriculus) is kept in pupal and adult stage. The common and differing expression patterns of overlapping constructs give some more detailed information on the regions tissue specificity:

Regions -2000 to -1206 and -1225 to -908 as well as -958 to -364 don't show any specific expression pattern. This region partly overlaps with the coding region of the gene spt6. This region might not be relevant for the expression pattern anyway, due to the fact that there is a native insulator element at position -321 to -311 (Fig. AP 3.5.1).

In contrast, region -448 to +49 (common between constructs 1552-2636, 3-2049 and 775-2049) mediates expression in the central nervous system (Fig. AP 3.5.2), more specifically neuroblasts, ganglion mother cells, intermediate neuronal progenitors and their progeny up to

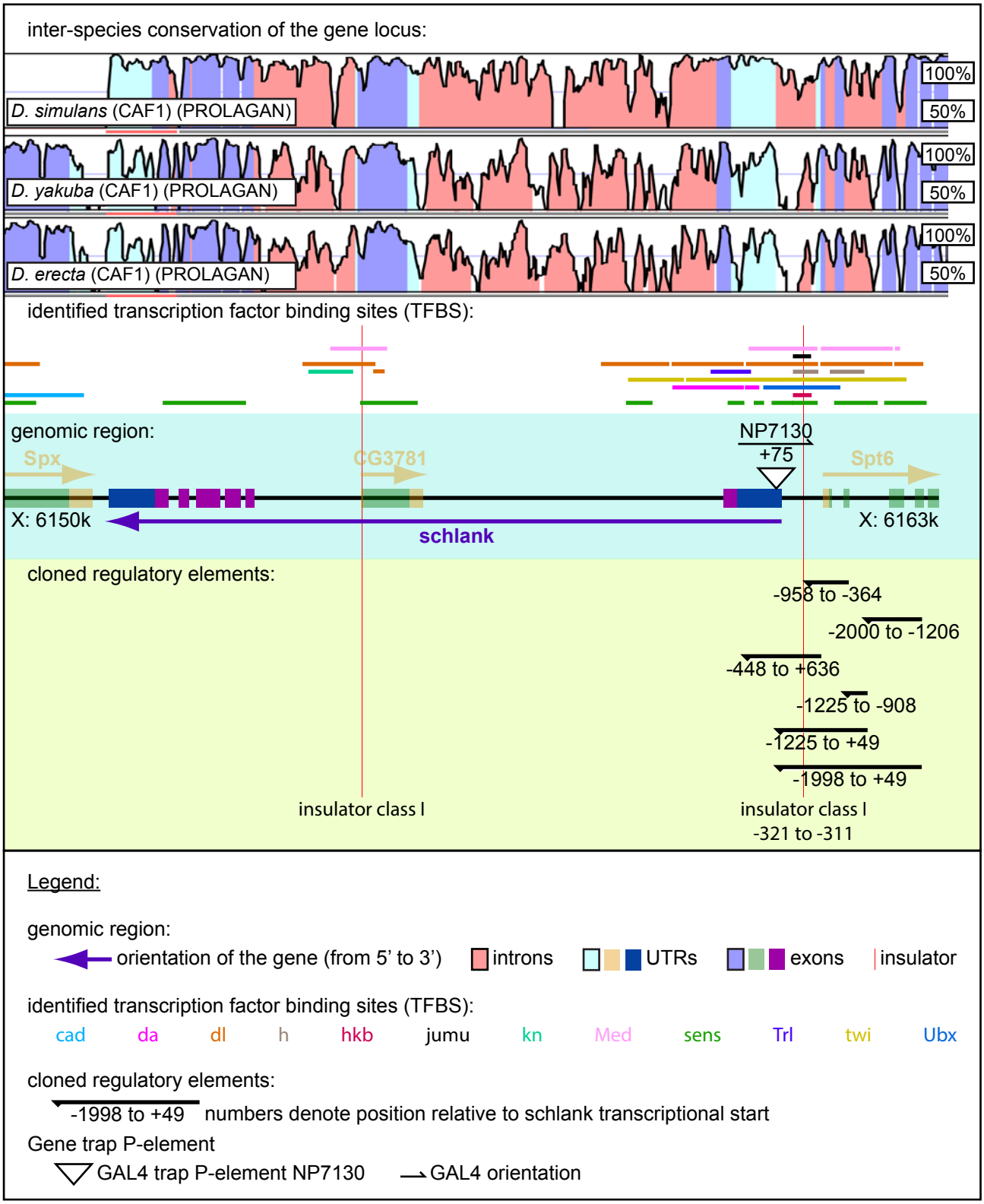

Figure AP 3.5.1 Transcription factor binding sites at the extended schlank gene locus. The schlank locus was analyzed for conserved regions via VISTA genome browser and correlated to GBrowse annotations. Exons are shown as colored boxes. Arrows above and below indicate gene orientations. Red vertical lines indicate the position of insulator elements; horizontal lines indicate transcription factor binding regions, vertical lines insulator elements. Arrows with numbers below indicate regions cloned into pCaSPer-AUG-Gal4 vector. The chromosomal region is indicated at the ends of the genomic locus. The 1 kb region in front of the *schlank* transcription start and intron one are conserved and rich in transcriptions factor binding sites.

oenocytes

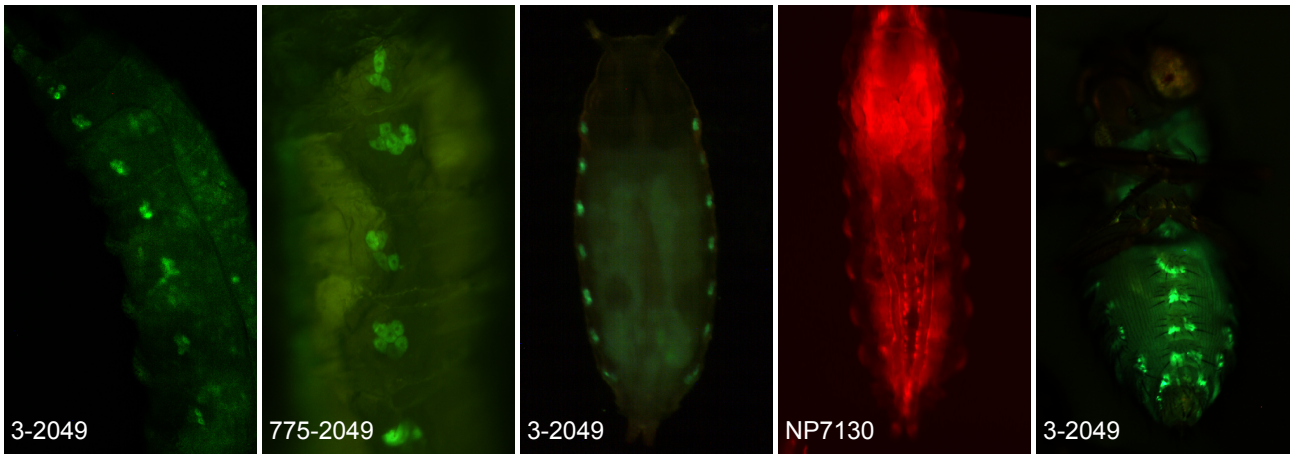

fatbody

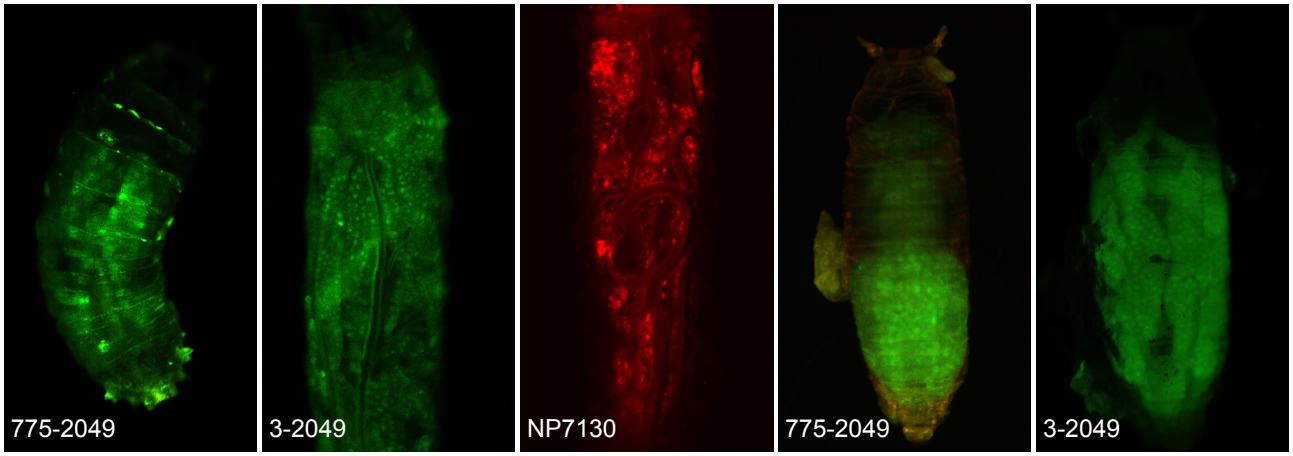

proventriculus

heart

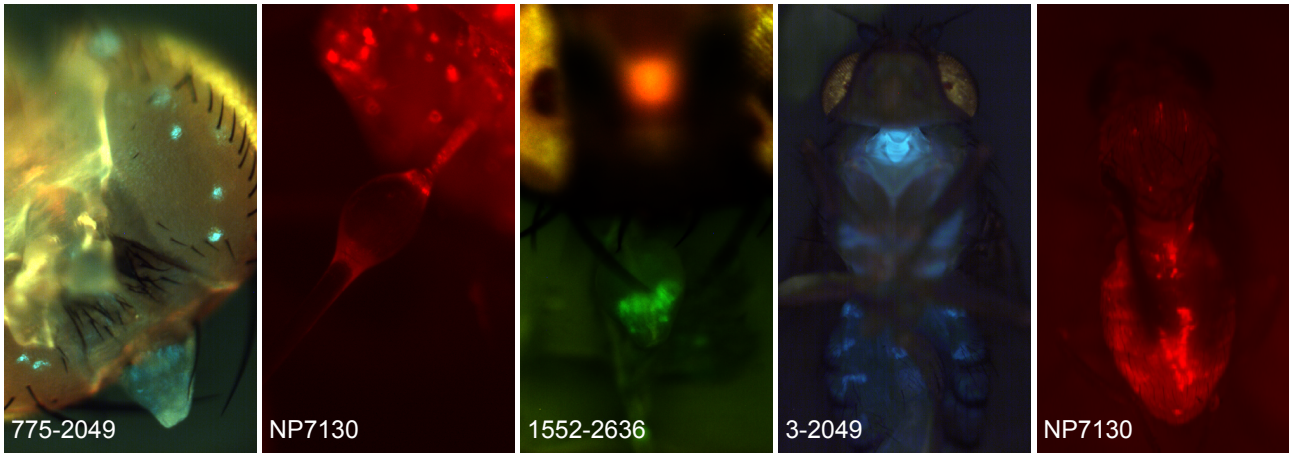

expression pattern analysis

		larva							pupa		adult			
construct	genomic region	brain	oenocyte	salivary gland	gut	near mouthhooks	fatbody	trachea	salivary gland	fatbody	fatbody	brain	prov	heart
0-794	-2000 to -1206									weak	weak			
755-1092	-1225 to -908									weak	weak			
1042-1626	-958 to -364					x								
1552-2636	-448 to +636	x								x			x	
3-2049	-1998 to +49	x	x	x	x		x	x	x	x	x	x	x	
775-2049	-1225 to +49	x	x		x		x	x		x	x		x	
NP7130	+75	?	x	x	x	x	x	x	x	x	x		?	x

Figure AP 3.5.2 The *schlank* promoter region drives expression in oenocytes, gut, proventriculus, fat body and trachea. Epifluorescence images of larvae expressing UAS-GFP under control of the indicated promotor fragment-GAL4-constructs and the schlank GAL4-enhancer trap NP7130 driving UAS-mRFP. The table summarizes the constructs, their genomic location relative to the schlank transcription start and expression patterns of the different constructs at different developmental stages. A ~500bp region directly in front of the transcription start is sufficient to direct nervous system expression.

one neuron per cluster (see Fig. AP 3.5.3). The same is true for expression in pupal fatbody and adult proventriculus / gut. However, expression in oenocytes, larval gut, fatbody and trachea can only be found in constructs that have region -1225 to +49 in common. E.g. the construct that spans region -448 to +636 but also the construct spanning -1225 to -908 do not drive expression in those tissues. This can indicate one of two things: various enhancer regions act co-dependently and removing one enhancer destroys the expression pattern and/or a silencer region is present in region +49 to +636. A more detailed analysis of the promoter regions is needed. Most interestingly, the commercially available enhancer trap line NP7130 drives expression in the central nervous system to some degree, in oenocytes, gut, fatbody, trachea, pupal fatbody and to some degree also in the adult gut / proventriculus (Fig. AP 3.5.2). Moreover, the enhancer trap derived LacZ in *schlank*^{G0349} heterozygous animals is expressed in fatbody and gut tissue of larvae (Fig. AP 3.5.4). Thus, the generated constructs covering the first 500bp before transcription start are in part consistent with the enhancer trap lines (Fig. AP 3.5.1).

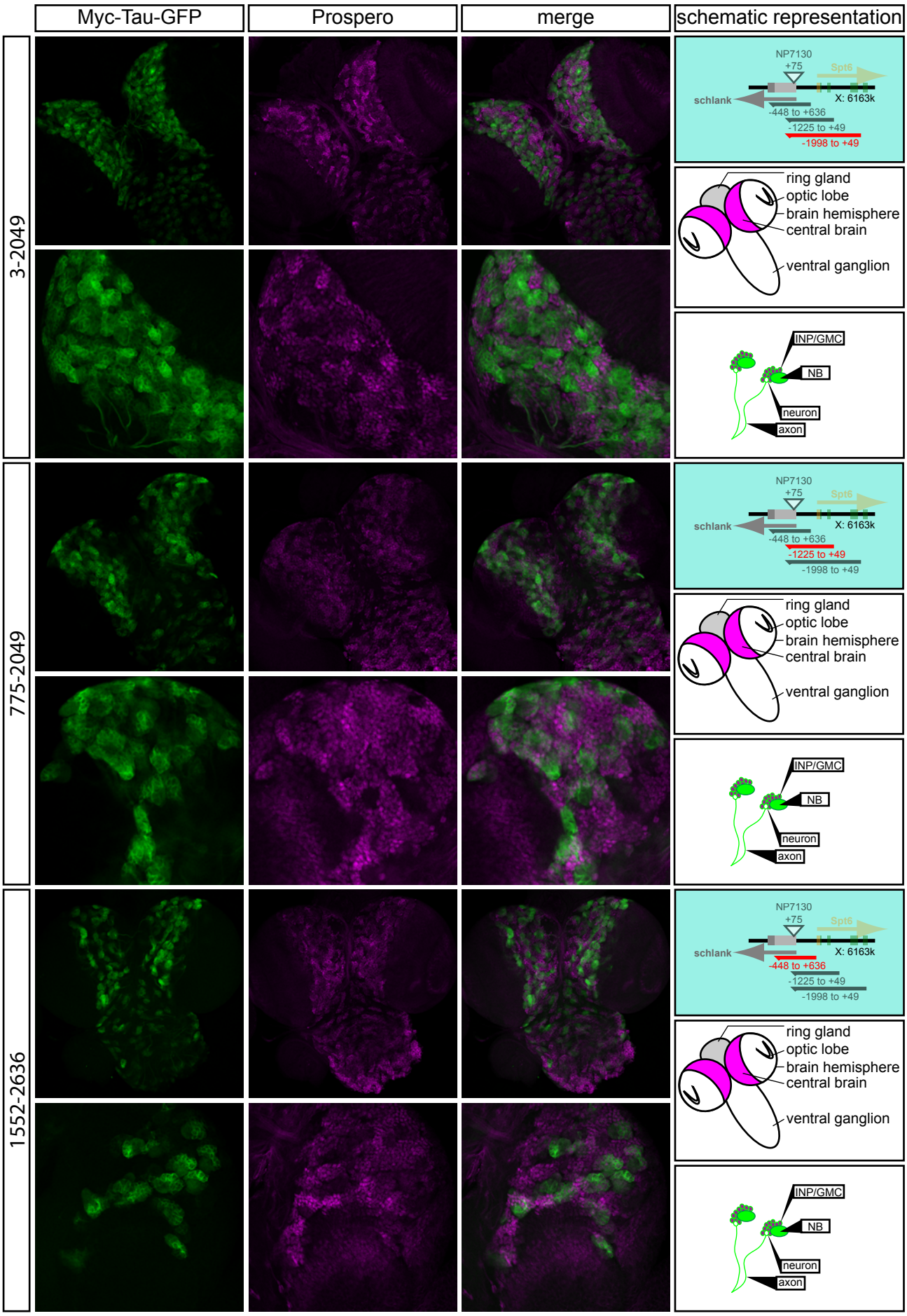
Myc-Tau-GFP
Prospero
merge
schematic representation
3-2049
775-2049
1552-2636
NP7130
+75
Spt6
schlank
X: 6163k
-448 to +636
-1225 to +49
-1998 to +49
ring gland
optic lobe
brain hemisphere
central brain
ventral ganglion
INP/GMC
NB
neuron
axon

Figure AP 3.5.3 Three *schlank* promoter constructs covering the 500bp region directly in front of the *schlank* transcription start direct expression in the larval brain. *schlank*-promotor-GAL4 lines were crossed to UAS-tauGFP-flies. Larval brains of progeny were stained for Prospero and the native GFP-fluorescence was detected. Schemes to the right indicate the position of the respective regulatory element, overview model of the brain as well as neuroblast-GMC clusters. NB, neuroblasts; INP / GMC, intermediate neuronal progenitor /ganglion mother cells

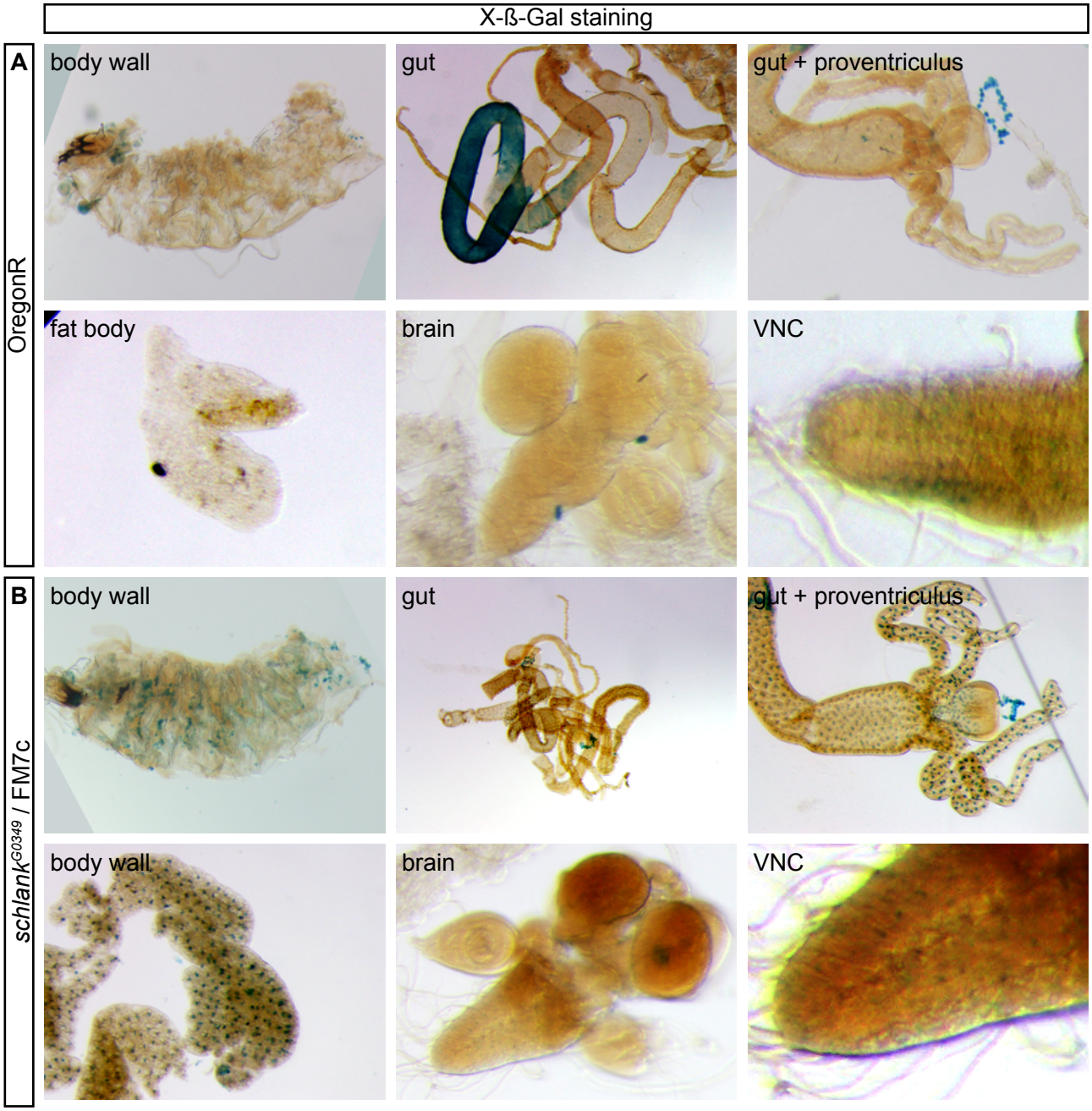

Figure AP 3.5.4 X-ß-Gal4 staining of a LacZ-enhancer trap line independently verifies expression in larval fat body and gut cells. A, X-ß-Gal staining on wildtype larval tissues. There is no staining in fat body, or proventriculus cells. There is unspecific staining in some gut regions which occur cytoplasmic and not nuclear. B, X-ß-Gal staining on *schlank*^{G0349} / FM7c heterozygous larvae LacZ enhancer trap (nuclear targeted ß-Galactosidase) shows specific expression in fat body, gut and proventriculus cells. VNC, ventral nerve cord.

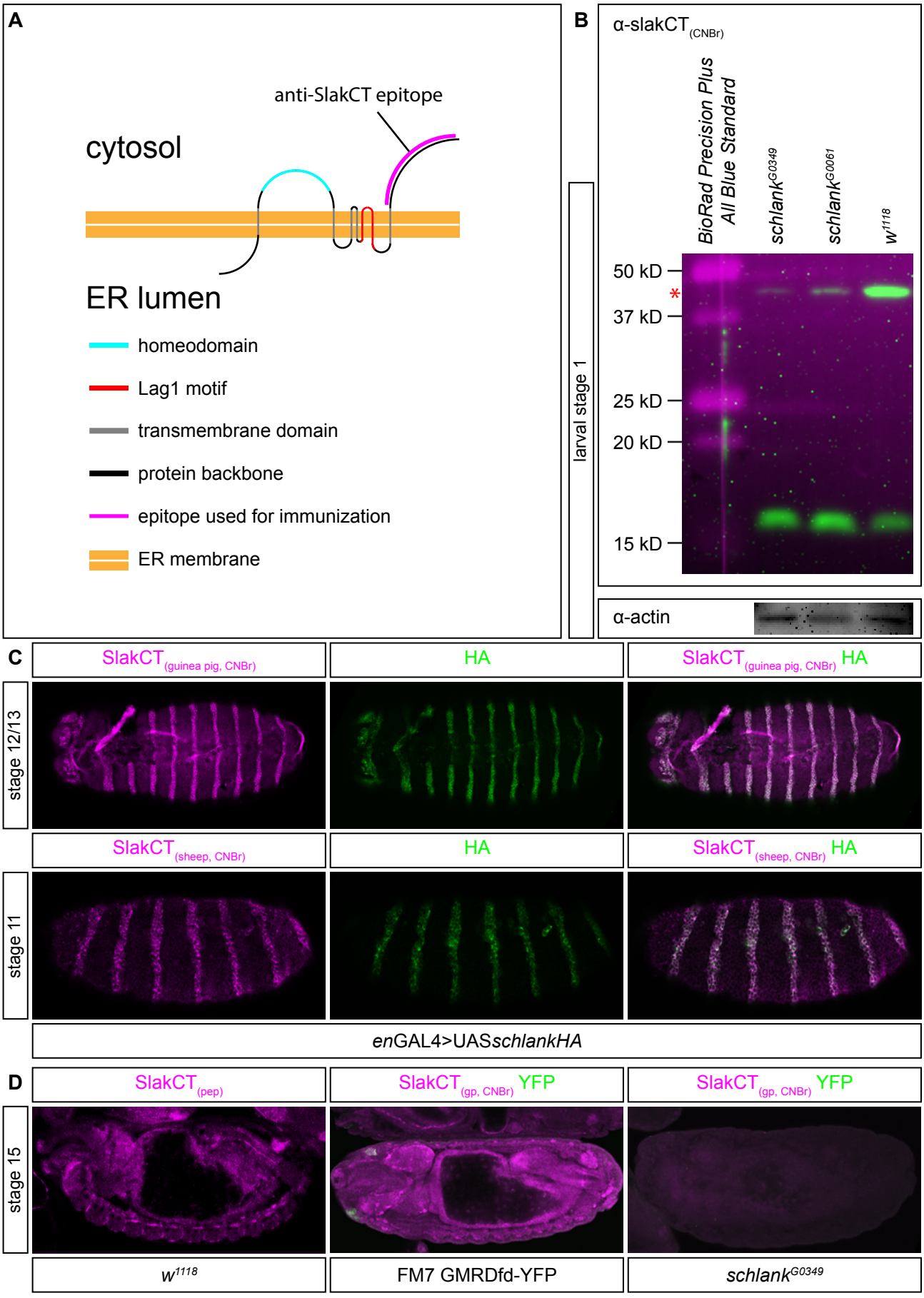
A
anti-SlakCT epitope
cytosol
ER lumen
homeodomain
Lag1 motif
transmembrane domain
protein backbone
epitope used for immunization
ER membrane
B
α-slakCT(CNBr)
BioRad Precision Plus All Blue Standard
schlankG0349
schlankG0061
w1118
50 kD
37 kD
25 kD
20 kD
15 kD
larval stage 1
α-actin
C
SlakCT(guinea pig, CNBr)
HA
SlakCT(guinea pig, CNBr) HA
stage 12/13
SlakCT(sheep, CNBr)
HA
SlakCT(sheep, CNBr) HA
stage 11
enGAL4>UASschlankHA
D
SlakCT(pep)
SlakCT(gp, CNBr) YFP
SlakCT(gp, CNBr) YFP
stage 15
w1118
FM7 GMRDfd-YFP
schlankG0349

Figure AP 3.5.5 Antibodies raised against the Schlank-C-terminus specifically recognize Schlank. A, Schlank domain model indicating the protein region used for immunization of two guinea pigs and one sheep. All antibodies were affinity purified by CNBr columns coupled with the SchlankCT-region depicted. **B**, Western blot on schlank mutants and wildtypic larvae 40 hours after egg laying. Actin was used as loading control. SchlankCT-antibody (α-SlakCT) derived from guinea pig #1 shows the downregultion of Schlank protein (~42kD) in mutants. The unspecific band at 16kD can only be observed with SchlankCT antibodies raised in guinea pig #1 but not guinea pig #2 (data not shown). **C**, SchlankCT-antibodies raised in guinea pig and sheep recognize ectopically (engrailed-pattern, *en*GAL4) expressed hemagglutinin (HA)-tagged Schlank protein in immunohistochemical stainings. HA in green, Schlank antibodies in magenta. **D**, SchlankCT antibodies recognize the embryonically expressed Schlank (magenta) in FM7 DfdGMR_YFP-balancer animals (second row, YFP in green). In hemizygous *schlank*^{G0349} mutants (third row) antibody staining is reduced. The antibody staining is heterozygous animals is consistent with a published peptide-based Schlank antibody (first row). Balancer and *schlank* mutant stainings were done in parallel and image with identical imaging settings.

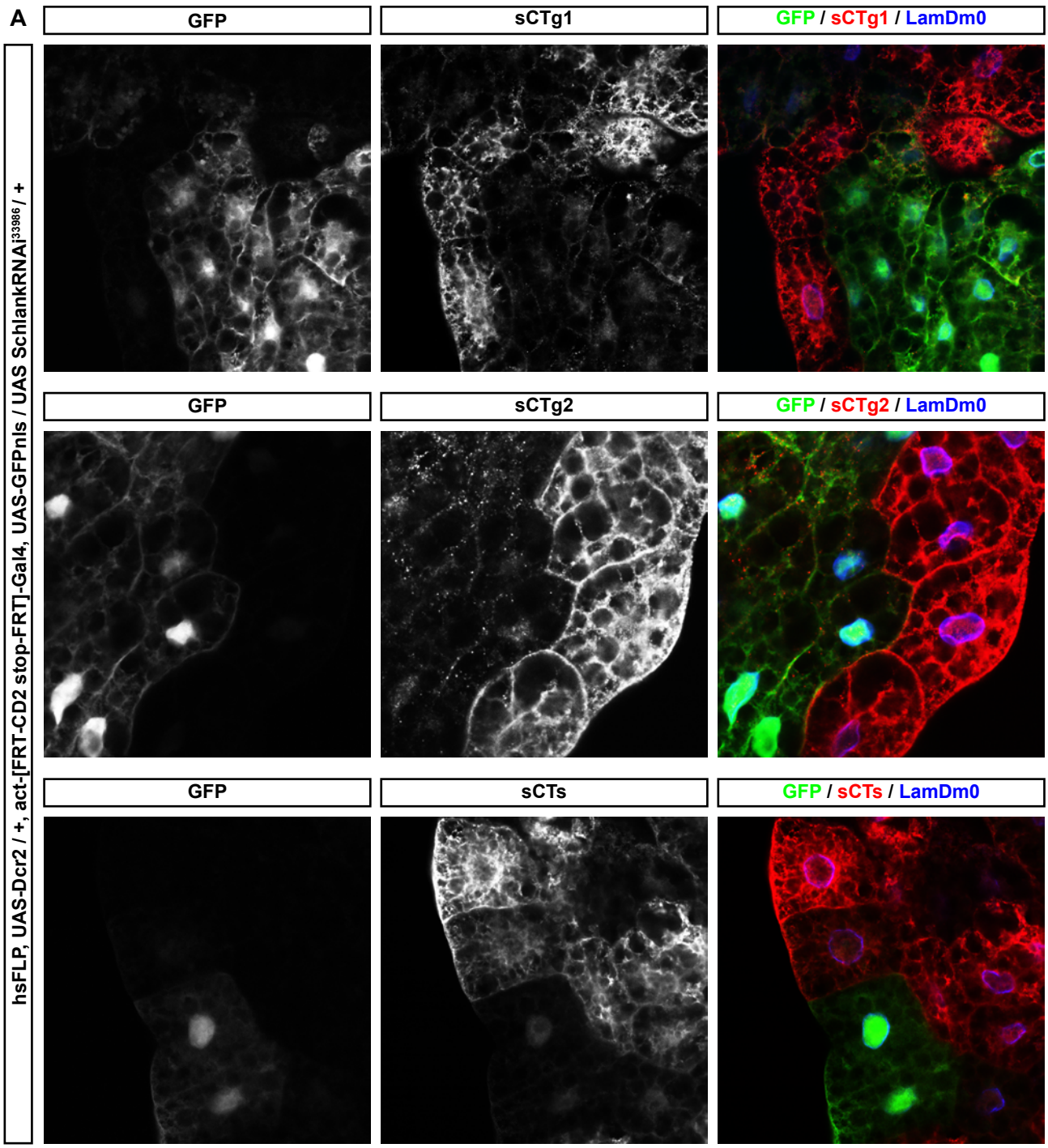
A
GFP
sCTg1
GFP / sCTg1 / LamDm0
GFP
sCTg2
GFP / sCTg2 / LamDm0
GFP
sCTs
GFP / sCTs / LamDm0
hsFLP, UAS-Dcr2 / +, act-[FRT-CD2 stop-FRT]-Gal4, UAS-GFPnls / UAS SchlankRNAi33986 / +

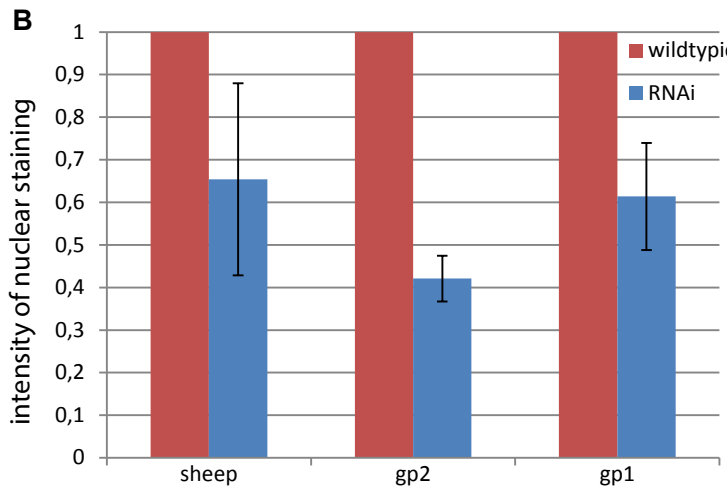
B
intensity of nuclear staining
1
0,9
0,8
0,7
0,6
0,5
0,4
0,3
0,2
0,1
0
wildtypic
RNAi
sheep
gp2
gp1

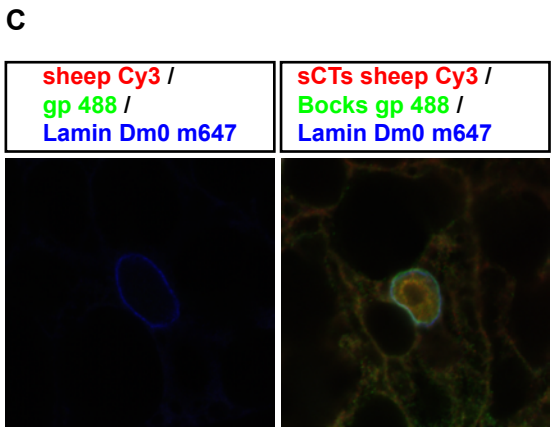
C
sheep Cy3 /
gp 488 /
Lamin Dm0 m647
sCTs sheep Cy3 /
Bocks gp 488 /
Lamin Dm0 m647

Figure AP 3.5.6 Schlank antibodies derived against the C-terminus show specific staining in fat body cells with cytoplasmic and nuclear pools. A, Schlank was downregulated in a clonal fashion with a heatshock flippase based GAL4 system expressing schlankRNAi33896 (hsFLP, UAS-Dcr2 / +, act-[FRT-CD2 stop-FRT]-Gal4, UAS-GFPnls / UAS SchlankRNAi33986 / +). Clones expressing the RNAi construct are marked by GFP-expression. Schlank was stained with SchlankCT-antibodies raised in guinea pig #1, #2 or sheep (sCTg1, sCTg2, sCTs; red). Native GFP fluorescence was detected without antibody staining (green). Lamin Dm0 was used as nuclear envelope marker (blue). All *schlankRNAi* clones show a strong loss of Schlank staining. **B**, To measure nuclear staining intensity, the nuclear region was defined as area encircled by Lamin Dm0. Staining intensity was measure for clonal cells expressing schlank RNAi and wildtypic sister cells. Mean intensity in wildtypic cells was normalized to one. There is substantial loss of nuclear Schlank staining in schlankRNAi clones. ≥8 clones per genotype were measured. Error bars indicate standard deviations. C, Larval fat bodies were fixed, washed and split for staining and in parallel secondary antibody control. For the secondary antibody control, Schlank antibodies (sCTs) and Bocksbeutel (Bocks) primary antibodies were omitted. Secondary antibody staining was done in parallel with the same antibody solutions. Images were taken with identical imaging setups.

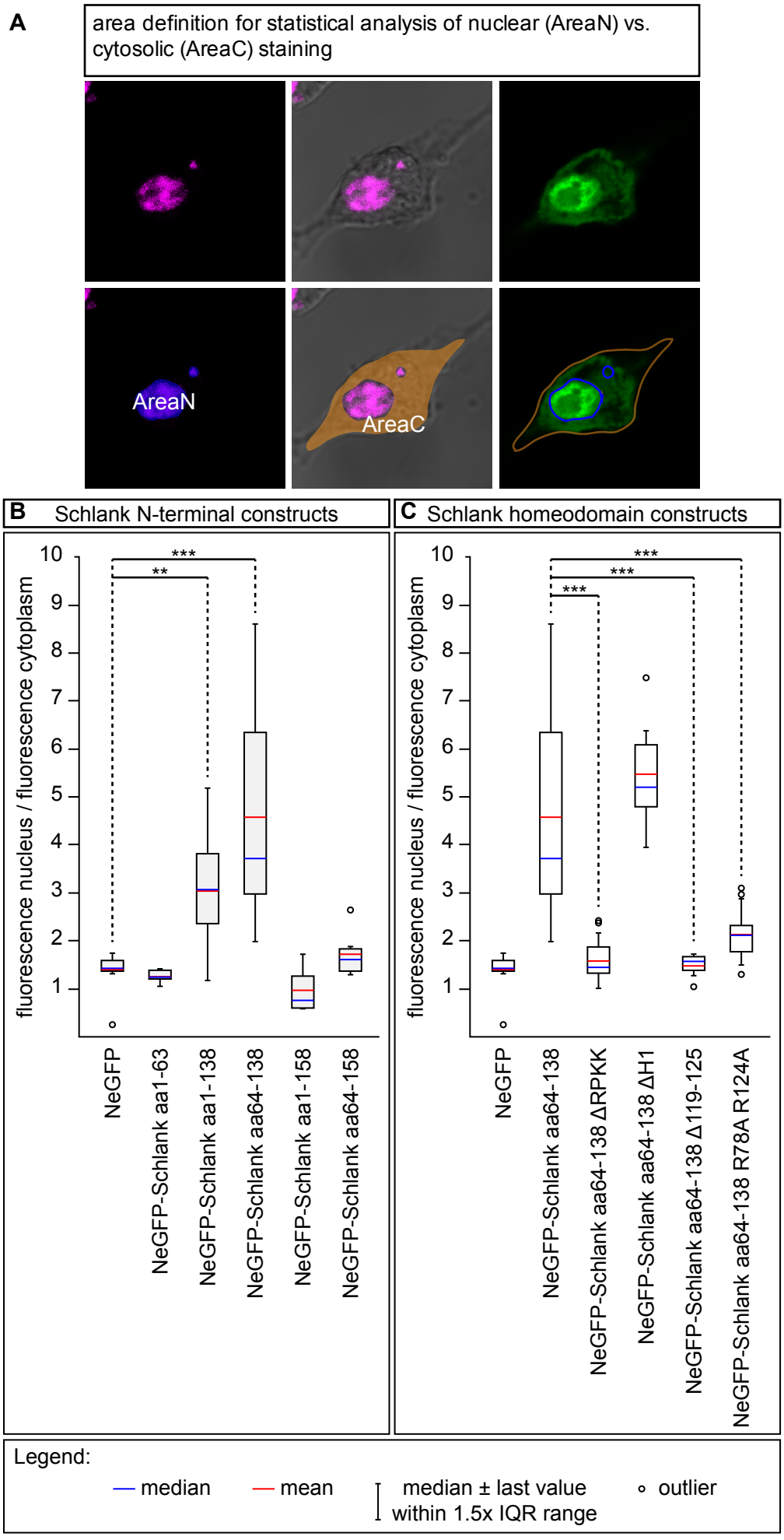
A
area definition for statistical analysis of nuclear (AreaN) vs. cytosolic (AreaC) staining
AreaN
AreaC
B Schlank N-terminal constructs
C Schlank homeodomain constructs
fluorescence nucleus / fluorescence cytoplasm
10
9
8
7
6
5
4
3
2
1
***
**
***
***
***
NeGFP
NeGFP-Schlank aa1-63
NeGFP-Schlank aa1-138
NeGFP-Schlank aa64-138
NeGFP-Schlank aa1-158
NeGFP-Schlank aa64-158
NeGFP
NeGFP-Schlank aa64-138
NeGFP-Schlank aa64-138 ΔRPKK
NeGFP-Schlank aa64-138 ΔH1
NeGFP-Schlank aa64-138 Δ119-125
NeGFP-Schlank aa64-138 R78A R124A
Legend:
median
mean
median ± last value within 1.5x IQR range
outlier

Figure AP 3.7 Quantification of nuclear accumulation of eGFP-tagged homeodomain-containing constructs and NLS deletions. A, To quantify nuclear accumulation, two areas were defined: AreaN, the nucleus area, which is stained by DAPI; AreaC, the cytoplasmic area, which is the staining within the cell membrane (DIC image) without AreaN. GPF-fluorescence in AreaN and AreaC was determined with Fiji and the ratio AreaN/AreaC calculated. **B**, Quantification of nuclear to cytoplasmic GFP fluorescence ratios upon expression of eGFP-tagged construct covering the N-terminal region of Schlank (aa-number indicates which Schlank amino acid region is coded by the constructs). NeGFP-schlank aa1-138 and aa64-138 show a significant increase in nuclear staining. **C**, NeGFP-Schlank aa64-138 construct was mutated to impair potential nuclear localization signals. Deletion (ΔRPKK, Δ117-123) or point mutation (R6A-R54A) of either NLS led to a significant decrease in nuclear eGFP staining, while deletion of helix 1 (ΔH1), which does not alter any NLSs is still accumulated in the nucleus. ** $p<0.01$ ***$p<0.001$, p-values were calculated via t-test.

AP3.8 Ketel-GFP trap expression pattern

To verify, that Ketel is expressed in larval tissues, native Ketel-GFP (generous gift from János Szabad) fluorescence was detected after a co-staining with the INM marker LamDm0 and the DNA marker DAPI. In third larva, *ketel-GFP* is expressed in fatbody, gut, malpighian tubules and trachea (Fig. AP 3.8). Thus Ketel might be viable candidate for Importin-ß nuclear import function in fat body cells. This warrants the use of *ketelRNAi* to determine the effect of the impairment of classical nuclear import on subcellular Schlank distribution.

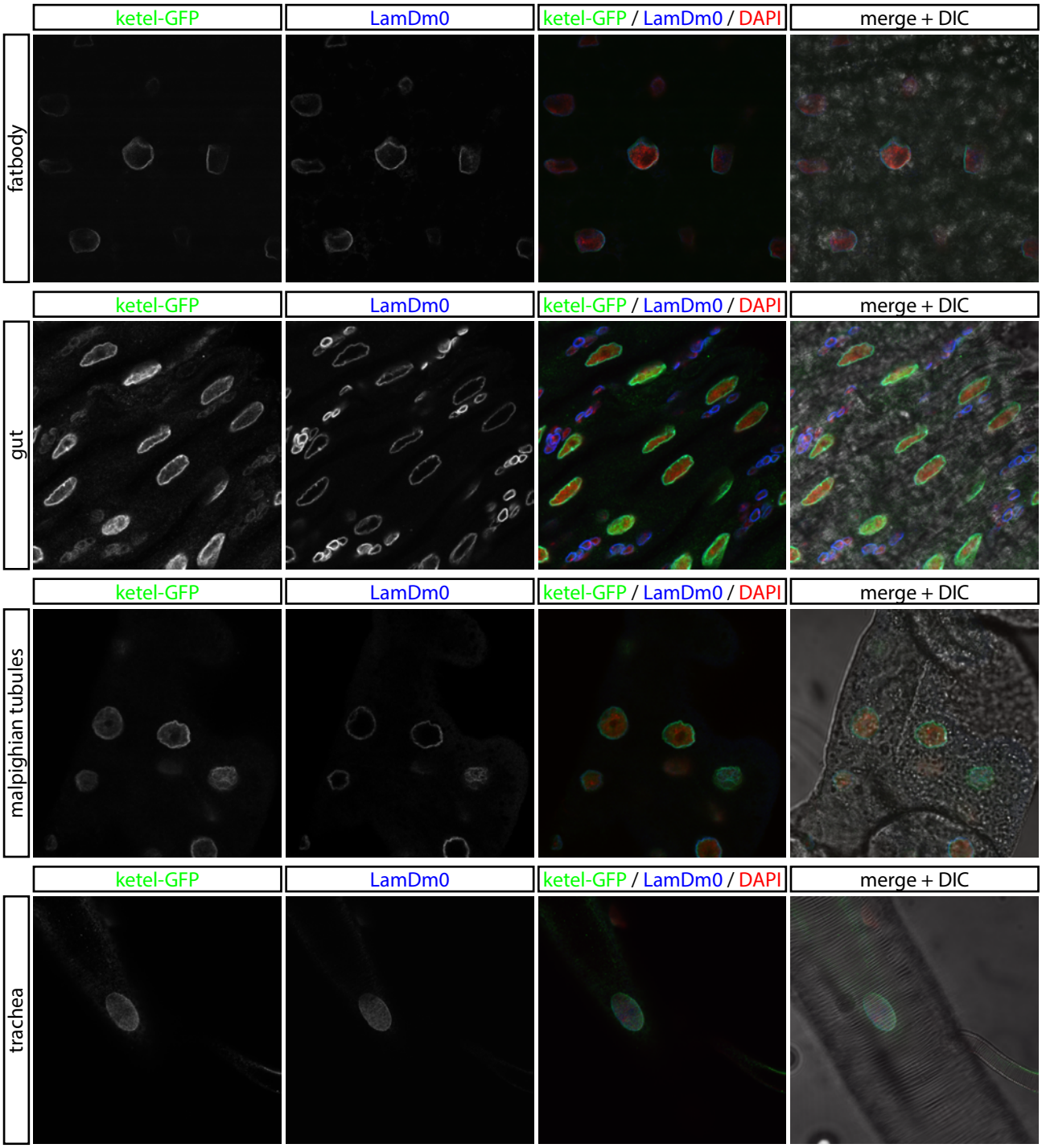

Figure AP 3.8 Ketel-GFP is expressed in most tissues, including fat body, gut, malphigian tubules, and trachea. Ketel-GFP larvae were stained for Lamin Dm0 as marker for the nuclear envelope and DAPI as DNA stain. Ketel-GFP fluorescence was imaged as is without antibody staining. Differential interference contrast (DIC) shows tissue morphology.

AP3.9 Validity of the clonal GAL4-UAS *ketelRNAi* system for subcellular protein localization experiments

Following parameters should be met for the GAL4-UAS *ketelRNAi* system to be valid for the analysis of a change in Schlank subcellular distribution:

(A) Expression of UAS-*ketelRNAi* should knock down *ketel* expression, (B) expression of GAL4 and GFP should not change / induce autofluorescence in fat body cells (except for the GFP-based fluorescence to visualize the clones) and (C) activation of the RNAi response should not change Schank protein distribution. To address those aspects, (1) *ketelRNAi* was expressed via an *actin*-GAL4 driver line. *KetelRNAi*-line 27567 proved to be able to repress *ketel* expression (Fig. AP 3.9 A). (2) Induction of clones via the hsFLP yw; +; actin-promotor FRT CD2stop FRT GAL4, UAS-GFP did not induce fluorescence in the Cy3 channel when fat body cells were incubated with anti-guinea pig-Cy3 antibodies (Fig. AP 3.9 B). (3) Induction of clonal *pex19RNAi*, a protein that is thought not to be directly involved in cellular trafficking, did not change Schlank subcellular distribution – there is no difference between wildtypic and *pex19RNAi* clonal cells (Fig. AP 3.9 B). Thus the heatshock-flippase induced clonal GAL4-UAS-system seems to be suitable to analyze the effect of *ketel* knockdown on Schlank subcellular distribution.

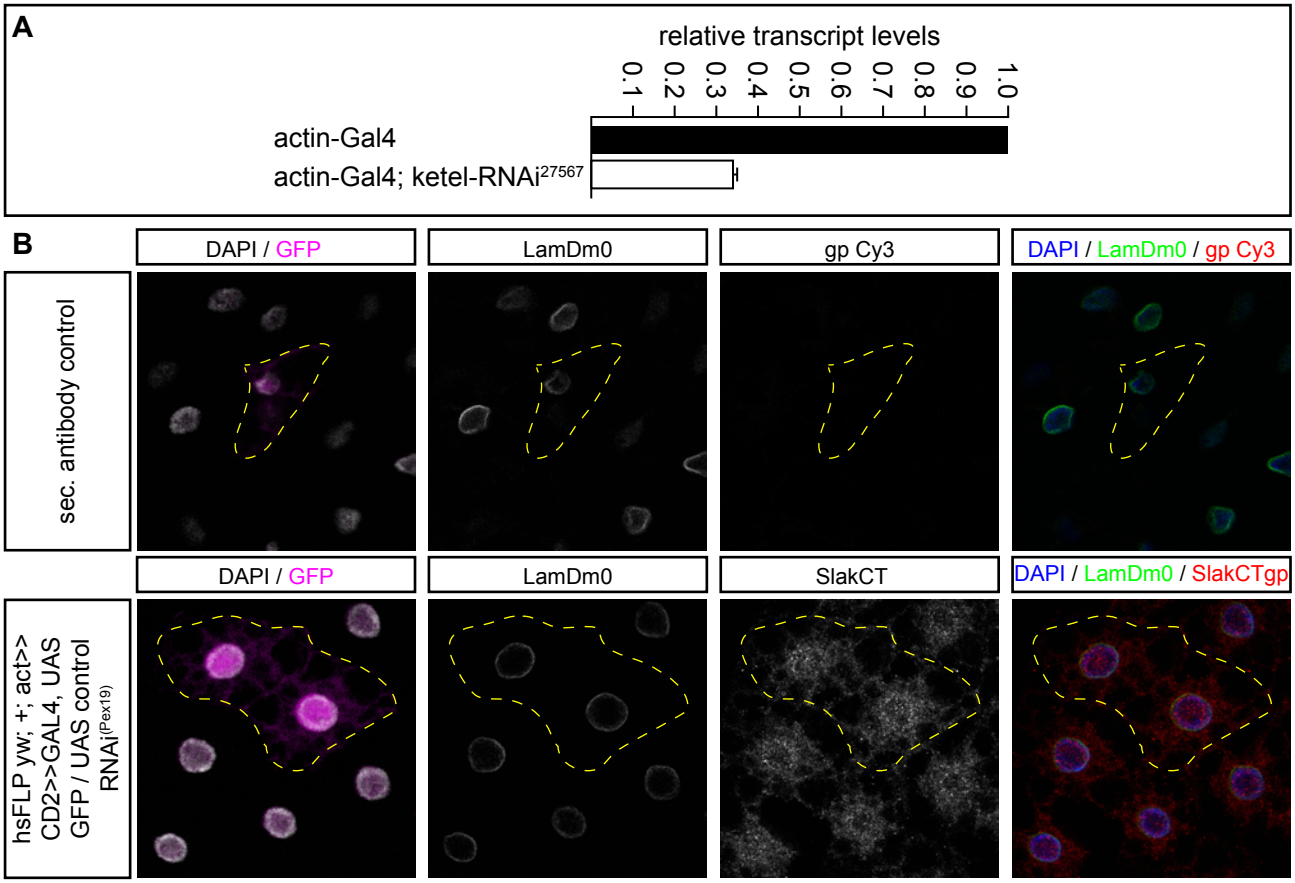

Figure AP 3.9 The clonal GAL4-UAS expression system itself does not change the Schlank staining pattern in fat body cells. **A**, *Ketel-RNAi*^{27567} is able to downregulate *ketel* expression. **B**, As a negative control to account for effects of GFP expression and RNAi response in general, Pex19RNAi was clonally expressed in fat body cells using the hsFLP, UAS-Dcr2 / +, act-[FRT-CD2 stop-FRT]-Gal4, UAS-GFPnls fly line. There are no changes in Schlank (red in merge) expression. Clones are marked by GFP (magenta in column 1, clonal areas are highlighted by yellow dotted lines). Secondary antibody control shows that there is no unspecific staining in the system by the secondary guinea pig antibody itself. Lamin Dm0 (green in merge) was used to visualize the nuclear envelope.

AP4.1 A Schlank is expressed in a subset of central nervous system glia cells

Initial IHC stainings showed that there is substantial Schlank expression in the embryonic nervous. The strongest enrichment is indeed found in glia cells (André Völzmann, 2007, Voelzmann & Bauer, 2011, Fig. AP 4.1.1). There are various types of glia cells that are each characterized by differing expression profiles of various marker genes (Beckervordersandforth et al, 2008 May-Jun). The relative position of glia cells to each other and peripheral nerves becomes fixed from late stage 15 on to stage 16 and can also be used to identify glia subtypes when different co-markers are stained (Fig. AP 4.1.2).

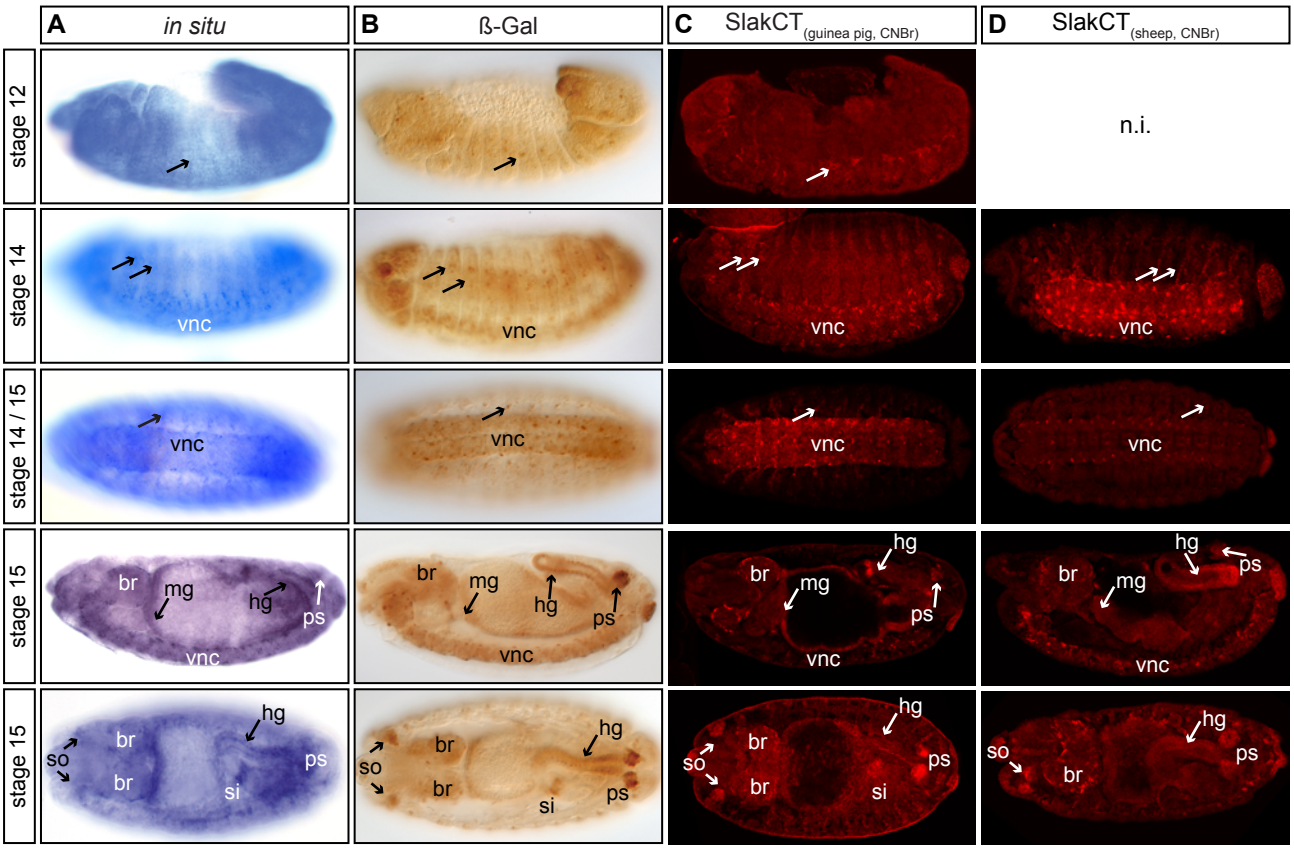

Figure AP 4.1.1 Schlank is enriched in the central and nervous system during embryonic development. A, Schlank in situ staining (B. Bauch). **B**, X-ß-Gal4 staining on schlankG0349 / FM7c embryos (B. Bauch). **C**, Antibody stainings with SchlankCT antibody from guinea pig #1. **D**, SchlankCT staining with antibodies raised in sheep. Schlank is enriched in

central and peripheral nervous system (arrows in rows 1-3) from embryonic stage 12 onwards. In addition, there is staining in hind (hg)- and midgut (mg), small intestine (si), sensory organs (so) and posterior spiracles (ps). *In situ*-, ß-Gal- and antibody patterns correlate. Stainings in **A** and **B** were done by Bianca Bauch (Bauch, 2003) and are shown as a comparison for the expression pattern of transcript with protein. br, brain; vnc, ventral nerve cord. n.i., not imaged

To determine subtype-specificity of Schlank expression, Schlank was stained in combination with several glia subtype markers:

Prospero (Pros) and Nazgul (Naz, von Hilchen et al, 2010) mark longitudinal glia cells (LG), while Neprilysin 4 (Nep4, Meyer et al, 2009; Beckervordersandforth et al, 2008 May-Jun) marks longitudinal as well as cell body glia (CBG). Schlank does not show coexpression in Pros, Naz or Nep4 positive glia cells (Fig. AP 4.1.3 A - B). There is also no co-expression in Wrapper (Wrap, Noordermeer et al, 1998) positive midline glia cells (Fig. AP 4.1.3 C). Nervana2-Gal4 drives expression in MM- and M- CBG as well as M-intersegmental nerve root glia (M-ISNG) in most segments. Only a minority of segments also show Nrv2-expression pattern in L-CBG, LP-LG or L-ISN or dorsal channel glia (D-CG). There is no enrichment of Schlank in Nrv2 positive M-ISNG cells (Fig. AP 4.1.4).

Following markers can be used to identify subperineural glia cells: P101-LacZ marks all reversed polarity (repo)-positive subperineural glia cells except for channel glia; M84-LacZ marks all repo-positive SPGs including the V-CG and Svp-LacZ marks all repo-positive SPGs and the L-ISNG. Schlank is enriched in all SPGs except for ML-SPG but is also enriched in L-ISNG (Fig. AP 4.1.5). Similarly SP2637 that recapitulates the Mz97-pattern marks SPGs except ML-SPG but also marks L-ISNG. Co-staining confirms that Schlank is enriched in SPGs except ML-SPG but is also enriched in L-ISNG (Fig. AP 4.1.6).

Taken together, co-stainings with various markers show that Schlank is strongly enriched in most subperineural glia cells as well as L-ISNG (Fig. AP 4.1.7). There is no expression in LGs, CBGs, M-ISNG or L-SNG.

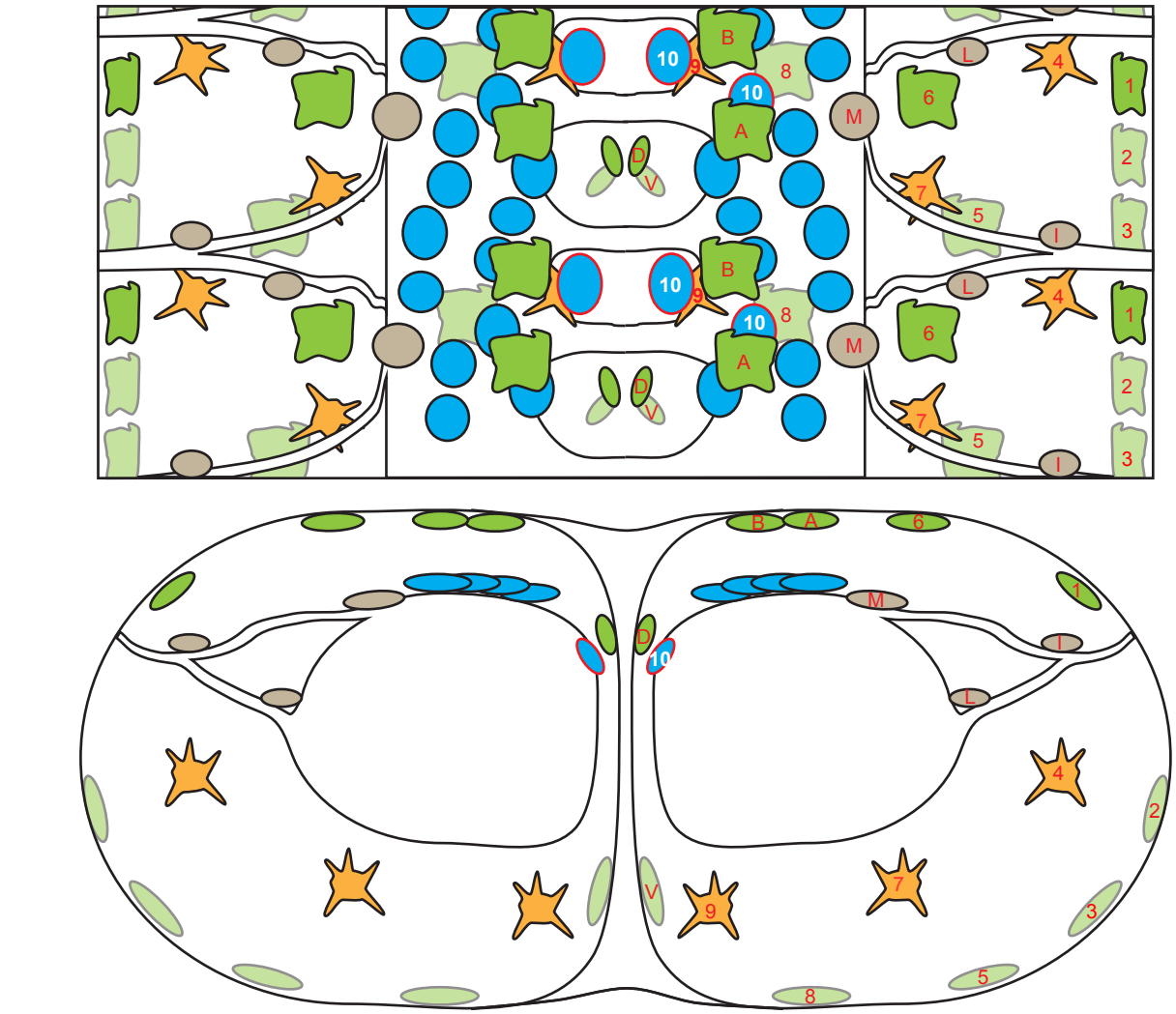

longitudinal glia cells surface glia cells (SPG + CG) cell body glia cells nerve root glia cells

A A-subperineural glia (SPG)
B B-subperineural glia (SPG)
D dorsal channel glia (CG)
V ventral channel glia (CG)
M medial intersegmental nerve root glia (M-ISNG)
L lateral segmental nerve root glia (L-SNG)
I lateral intersegmental nerve root glia (L-ISNG)
1 dorsolateral subperineural glia (DL-SPG)
2 ventrolateral subperineural glia (VL-SPG)
3 mediolateral subperineural glia (ML-SPG)
4 lateral cell body glia (L-CBG)
5 lateroventral subperineural glia (LV-SPG)
6 mediodorsal subperineural glia (MD-SPG)
7 medial cell body glia (M-CBG)
8 medial ventral subperineural glia (MV-SPG)
9 medialmost cell body glia (MM-CBG)
10 medial longitudinal glia cell cluster (M-LG cluster)

Figure AP 4.1.2 Schematic representation of spatial glia cell distribution in abdominal segments of stage 16 embryos. The upper scheme represents a dorsal on top view of the central nervous system, the lower scheme a vertical section. Surface glia are shown in green (ventral SPGs are shown semi-transparent), longitudinal glia in blue, nerve root glia in grey and cell body glia in apricot. The identity of individual glia cells is indicated in the legend. The schemes are modified from (Beckervordersandforth et al, 2008 May-Jun).

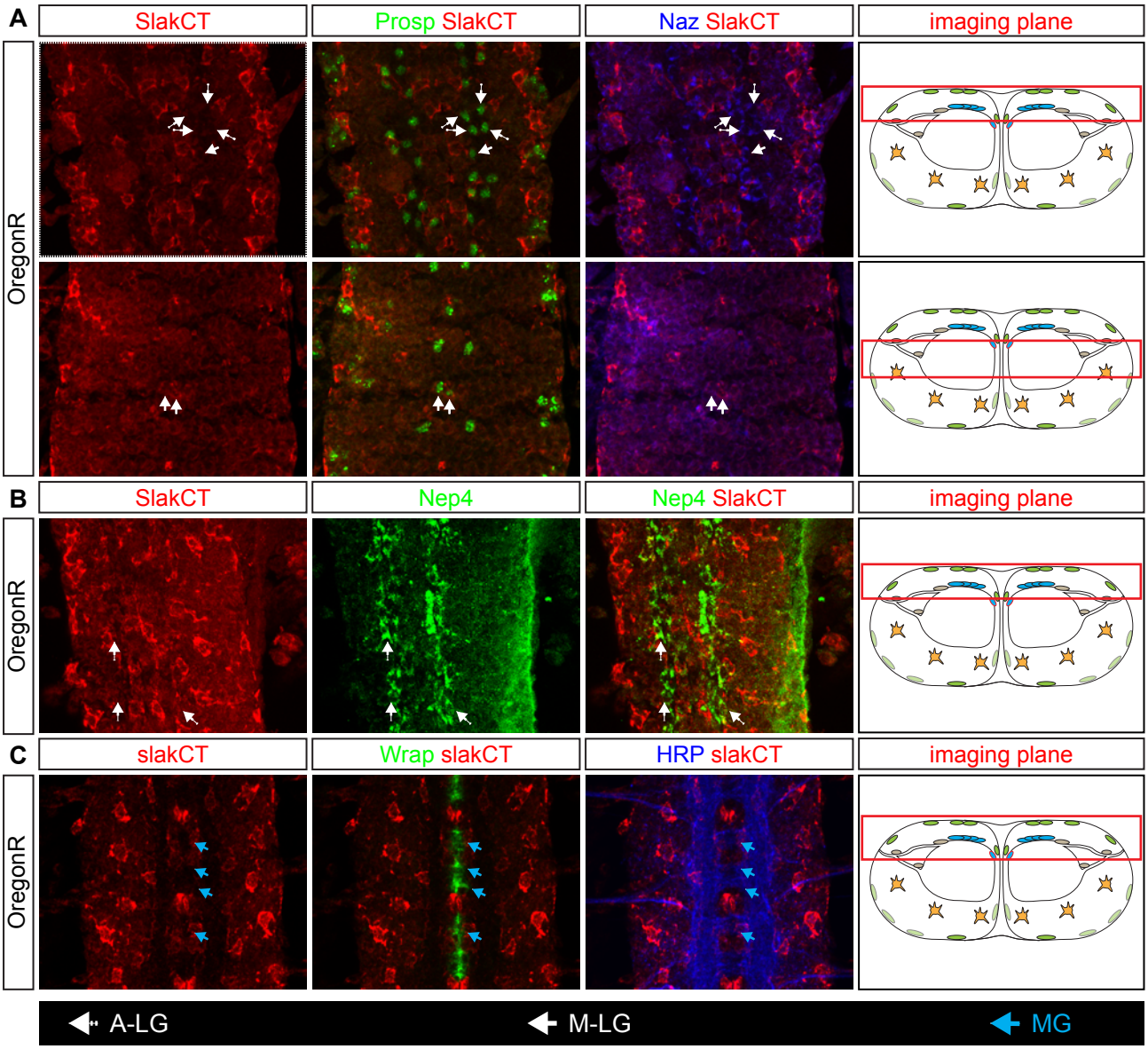

Figure AP 4.1.3 Schlank is not enriched in longitudinal and midline glia cells. Flat preparations of stage 16 embryos. **A**, Posterior (P)- and medial (M)-longitudinal glia cells co-express Prospero (Prosp) and Nazgul (Naz). **B**, Neprilysin-4 marks longitudinal glia cells and cell body glia cells. Schlank (SlakCT, red) is not enriched in longitudinal glia cell populations (white arrows). **C**, Wrapper is widely used as marker for midline glia cells (green). For orientation within the central nervous system, horseradish peroxidase (HRP) antibody was used to mark axonal tracts. There is no enrichments of Schlank in midline glia cells. A-LG, anterior longitudinal glia; M-LG, medial longitudinal glia; MG, midline glia. The imaging plane is indicated by a red rectangle in the cartoon to the right.

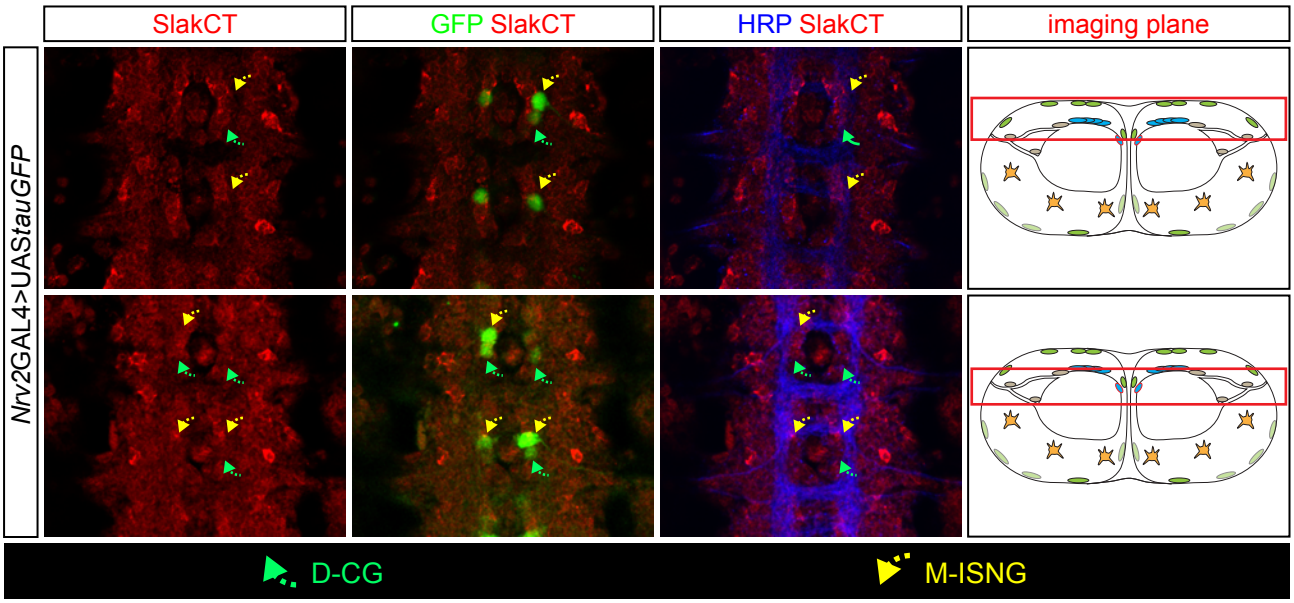

Figure AP 4.1.4 Schlank is not enriched in medial intersegmental nerve root glia cells. Flat preparations of stage 15 embryos. Nervana2-Gal4 drives GFP (green) expression in medial intersegmental nerve root glia (M-ISNG) as well as in dorsal channel glia and lateral cell body glia. HRP antibody (blue) was used to mark axonal tracts. There is no enrichment of Schlank (red) in M-ISNG cells. The imaging plane is indicated by a red rectangle in the cartoon to the right.

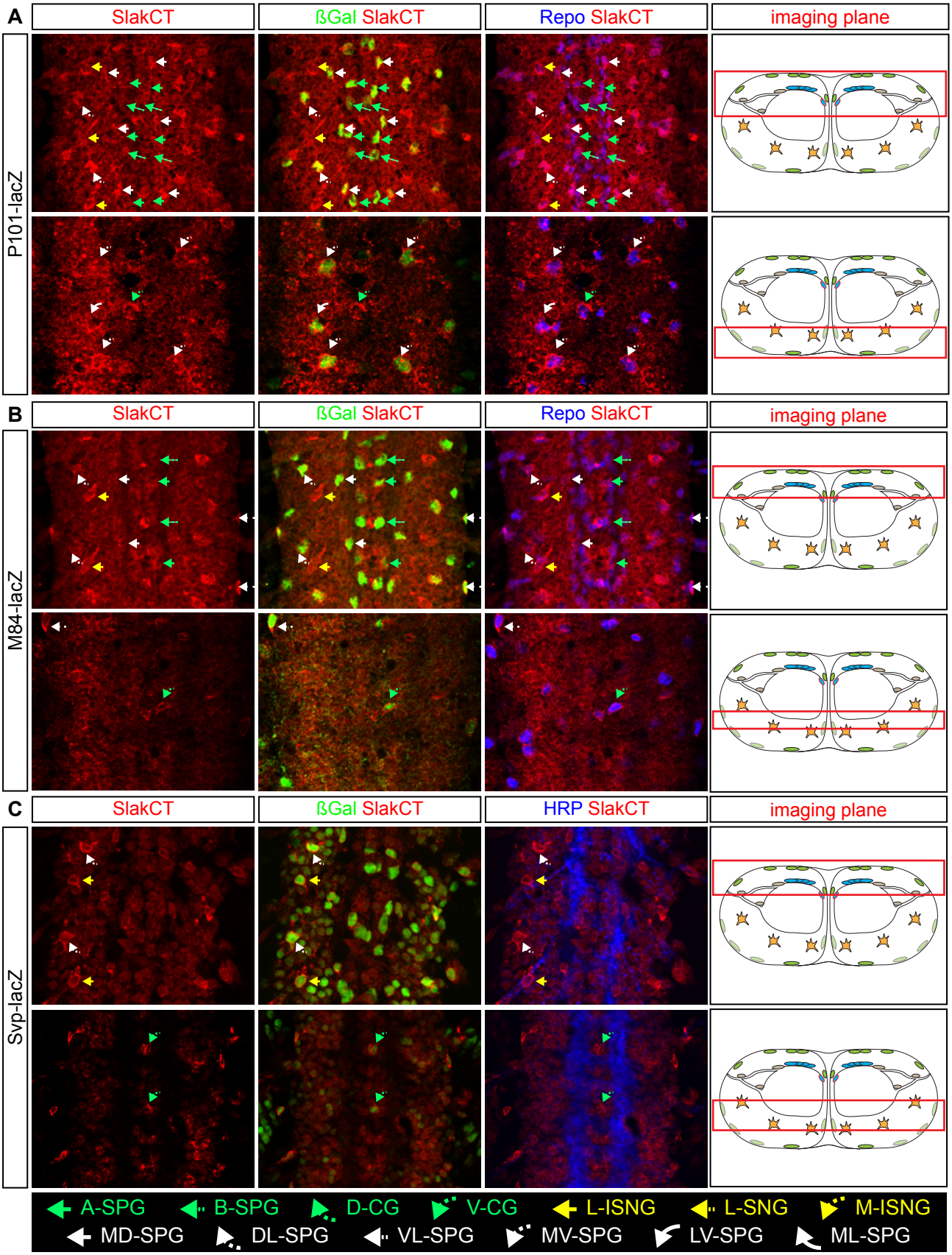

Figure AP 4.1.5 Schlank is enriched in subperineural and channel glia cells. Flat preparations of stage 16 embryos. **A**, P101-LacZ reporter line marks all subperineural glia cells. **B**, M84-LacZ marks subperineural glia cells and ventral glia cell. **C**, Seven-up (Svp)-LacZ marks subperineural glia, dorsal and ventral channel glia as well as lateral intersegmental nerve root glia cells. Schlank is enriched in dorso-lateral (DL)-, medial-lateral (MD)-, ventro-lateral (VL)-subperineural

glia (SPG), lateral intersegmental nerve root glia (L-ISNG), ventral (V)-channel glia (CG) but not A- and B-SPG at stage 15. The imaging plane is indicated by a red rectangle in the cartoon to the right.

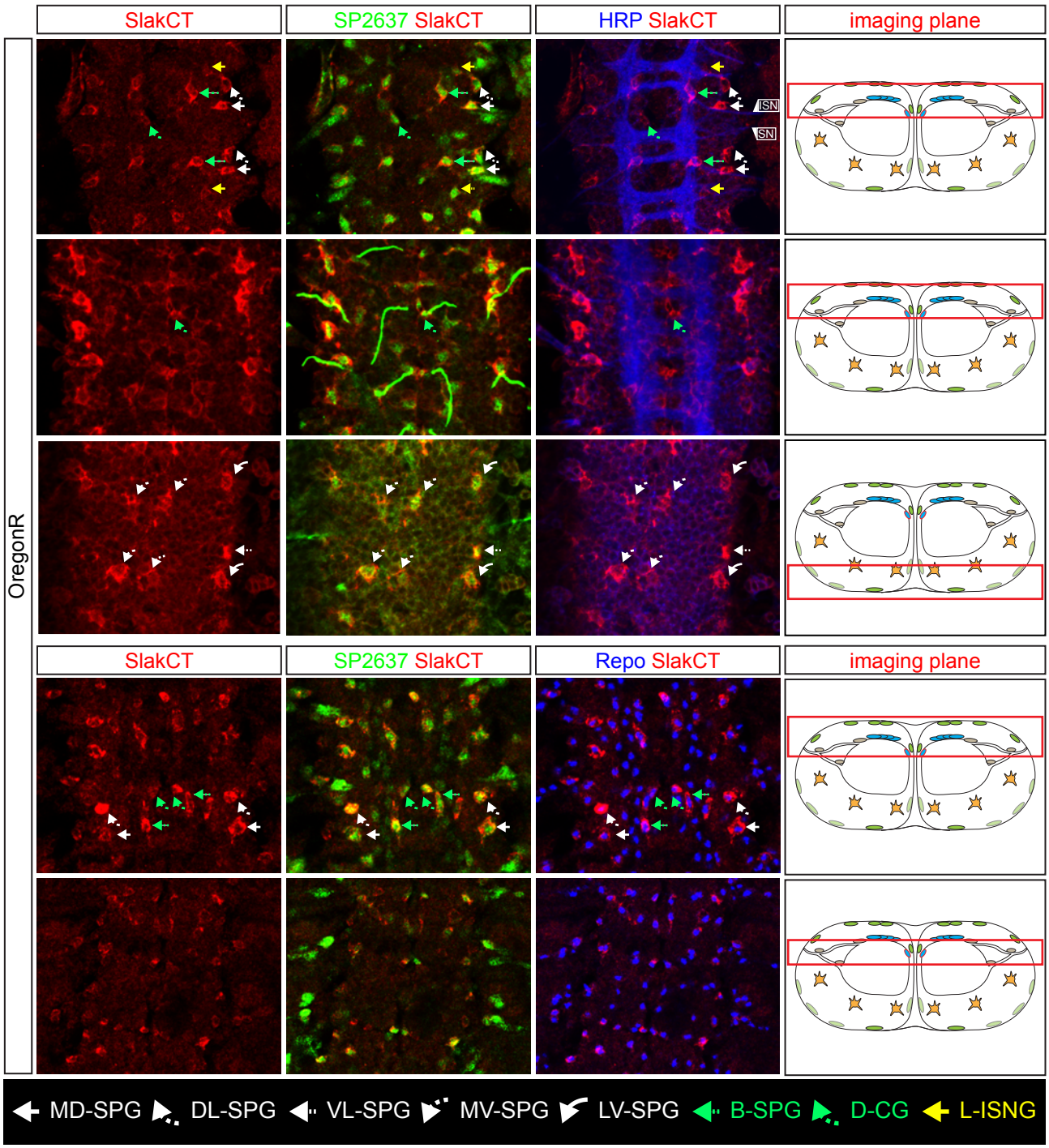

Figure AP 4.1.6 Schlank is enriched in most SP2637 (Mz97-Gal4 equivalent)-positive glia cells. Flat preparations of stage 16 embryos. All glia cells can be marked by reversed polarity (Repo). SP2637 antibody (green) marks all subperineural glia except A-SPG, ML-SPG. It also marks dorsal channel glia and lateral intersegmental nerve root glia. HRP was used as landmark for axonal tracts. Schlank is enriched in dorso-lateral (DL)-, B-, medial-dorsal (MD)-, ventro-lateral (VL)-, medial-ventral (MV)-, and latero-ventral (LV) subperineural glia cells (SPG), dorsal (D)-channel glia (CG) as well as lateral (L)-intersegmenal nerve root glia (ISNG) cells. The imaging plane is indicated by a red rectangle in the cartoon to the right.

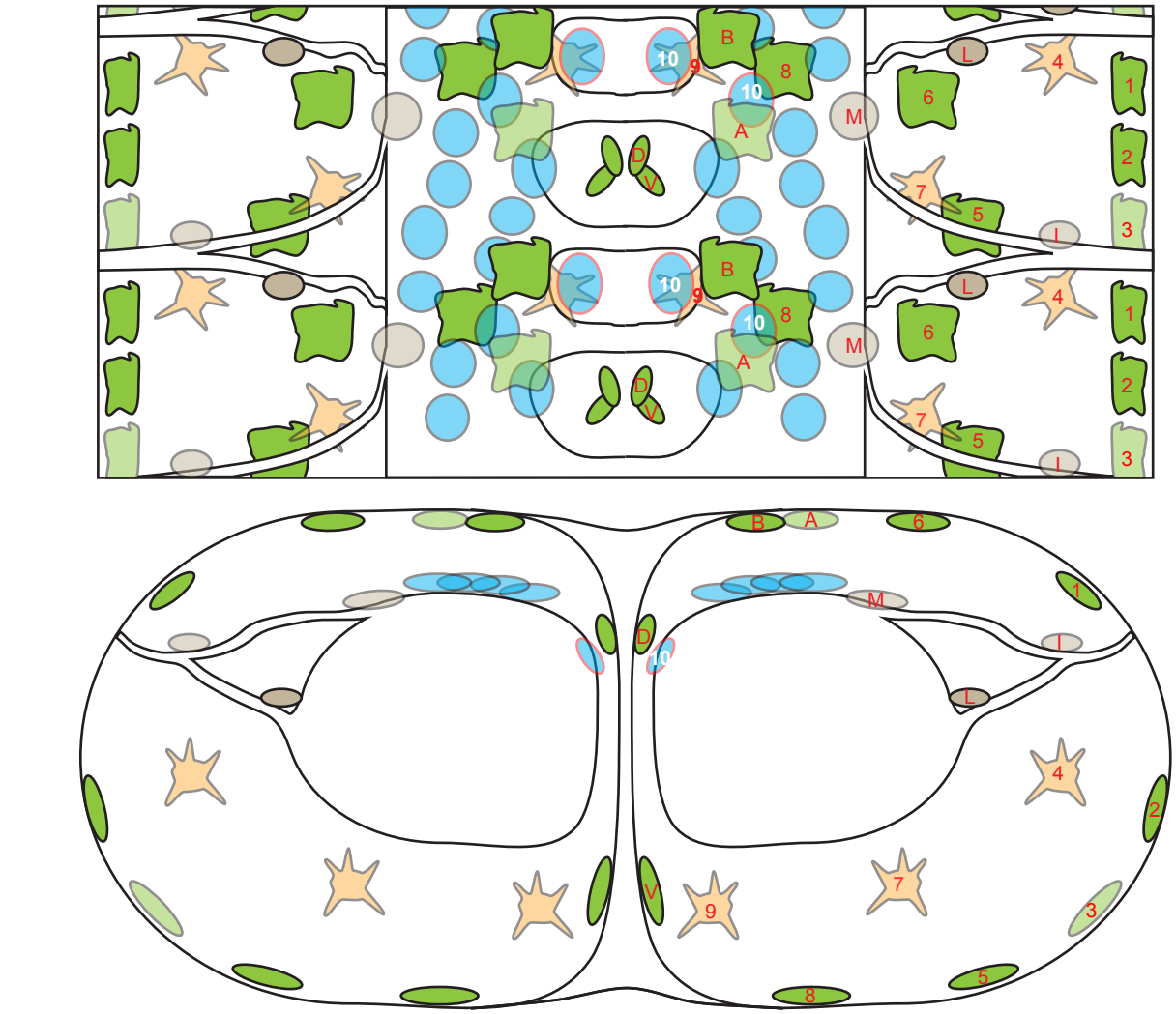

longitudinal glia cells | surface glia cells (SPG + CG) | cell body glia cells | nerve root glia cells

A A-subperineural glia (A-SPG)
B B-subperineural glia (B-SPG)
D dorsal channel glia (D-CG)
V ventral channel glia (V-CG)
M medial intersegmental nerve root glia (M-ISNG)
L lateral segmental nerve root glia (L-SNG)
I lateral intersegmental nerve root glia (L-ISNG)
1 dorsolateral subperineural glia (DL-SPG)
2 ventrolateral subperineural glia (VL-SPG)
3 mediolateral subperineural glia (ML-SPG)
4 lateral cell body glia (L-CBG)
5 lateroventral subperineural glia (LV-SPG)
6 mediodorsal subperineural glia (MD-SPG)
7 medial cell body glia (M-CBG)
8 medial ventral subperineural glia (MV-SPG)
9 medialmost cell body glia (MM-CBG)
10 medial longitudinal glia cell cluster (M-LG cluster)

Figure AP 4.1.7 Scheme summarizing Schlank enrichment. Cells in which Schlank is enriched are shown in 100 % opacity, cells without Schlank enrichment are depicted semi-transparent.

AP4.1 B Schlank is expressed in all sensory neuron clusters of the embryonic peripheral nervous system

To follow up Schlank expression in the peripheral nervous system (Fig. AP 4.1.8), sensory nerves were marked by antibodies against the markers FASII, BP104 and HRP in combination with Repo and or Elav stainings. Schlank is enriched in cell clusters along intersegmental (ISN) and segmental nerves (SN) (Fig. AP4.1.9). Staining of this region with the neuron marker Elav and the glia marker repo confirms that Schlank is only enriched in a few glia cells wrapping ISN/SN but is strongly

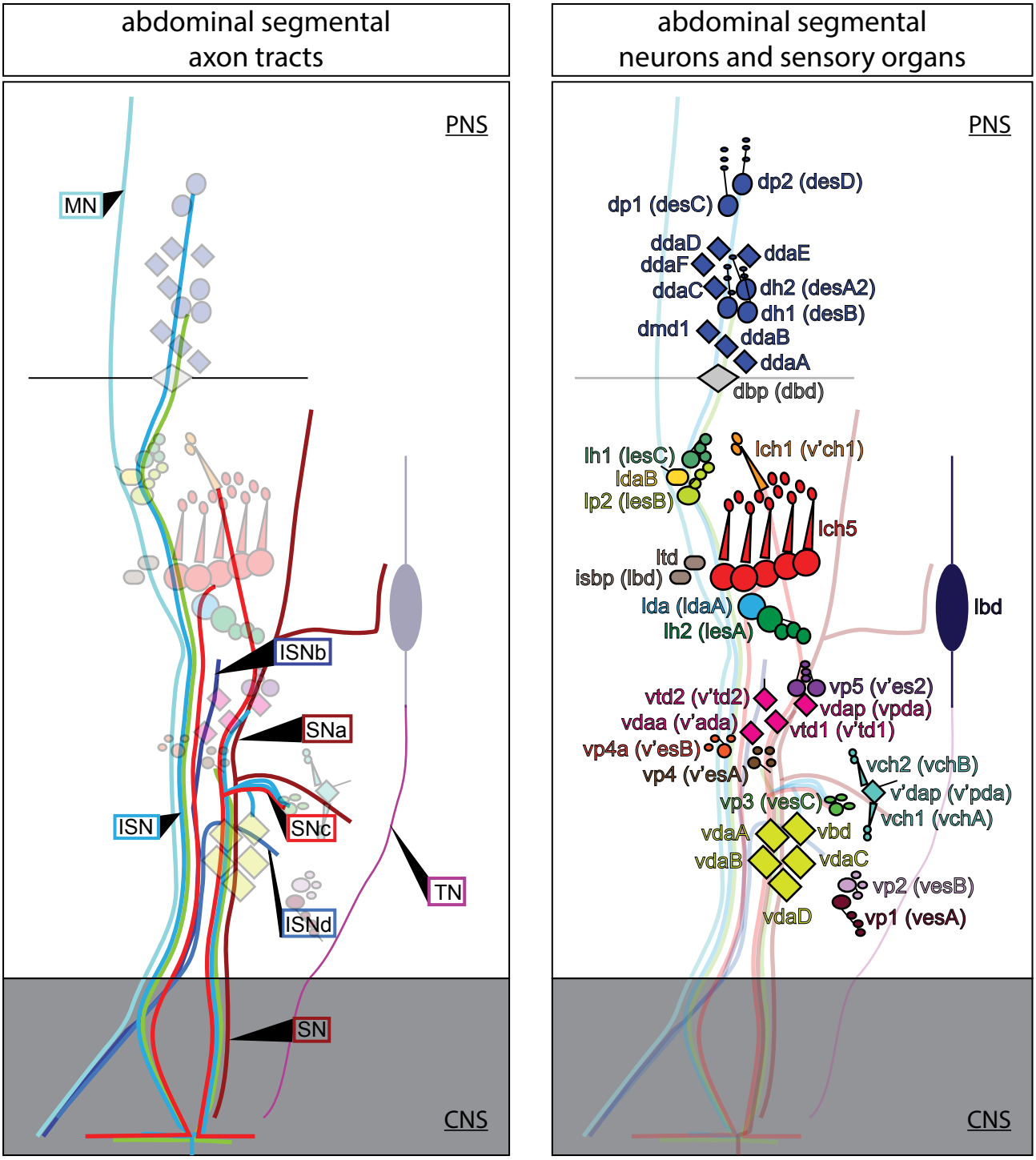

Figure AP 4.1.8 Schematic representation of peripheral nerves and axon tracts. PNS, peripheral nervous system; CNS, central nervous system; MN, motor neuron; ISN, intersegmental nerve; SN, segmental nerve; TN, transverse nerve; a, anterior; bd, bipolar dendritic neuron; ch, chordotonal; d, dorsal; da, dendritic aborisation; es, external sensory; l, lateral; n, neuron; p, posterior; td, tracheal dendritic neuron; v, ventral; v', ventral'. Nomenclature according to Bodmer et al, 1989. Cartoon modified from FlyPNS (Orgogozo & Grueber, 2005) and Campos-Ortega & Hartenstein, 1997.

expressed in basically all Elav-positive neurons of the sensory clusters ranging from vp1 up to lh1 (Fig. AP 4.1.10).

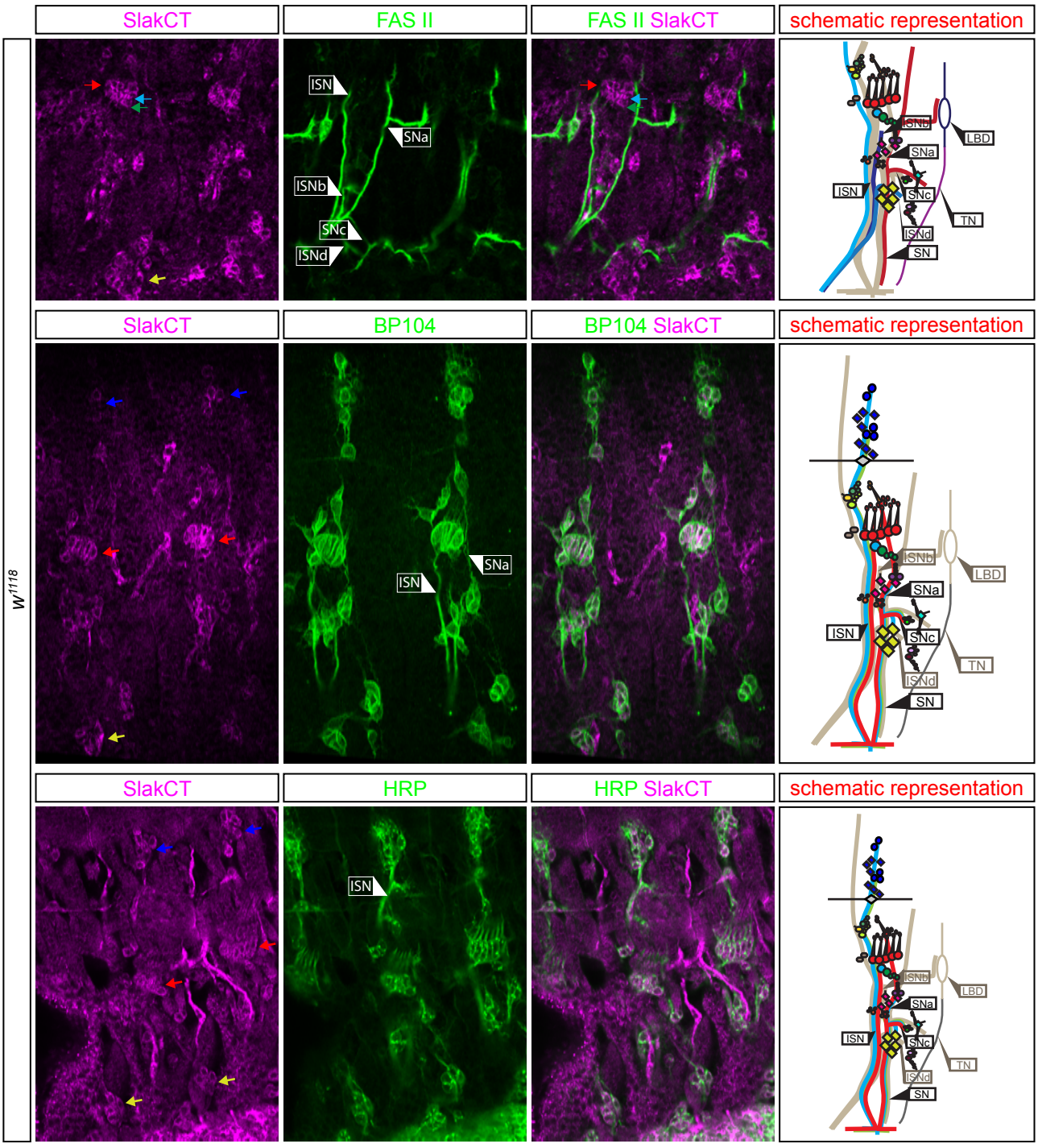

Figure AP 4.1.9 Schlank is enriched in dorsal and lateral sensory neurons. Motoneuron tracts are marked by Fasciclin II (FAS II, green), sensory neurons by BP104 (green) and horseradish peroxidase (HRP, green). Schlank is shown in magenta. Cartoons to the right show segment nerve and neuron patterns. Colored arrows point to the corresponding nerve clusters. Color code for arrows and neurons is identical. SN, segmental nerve; ISN, intersegmental nerve.

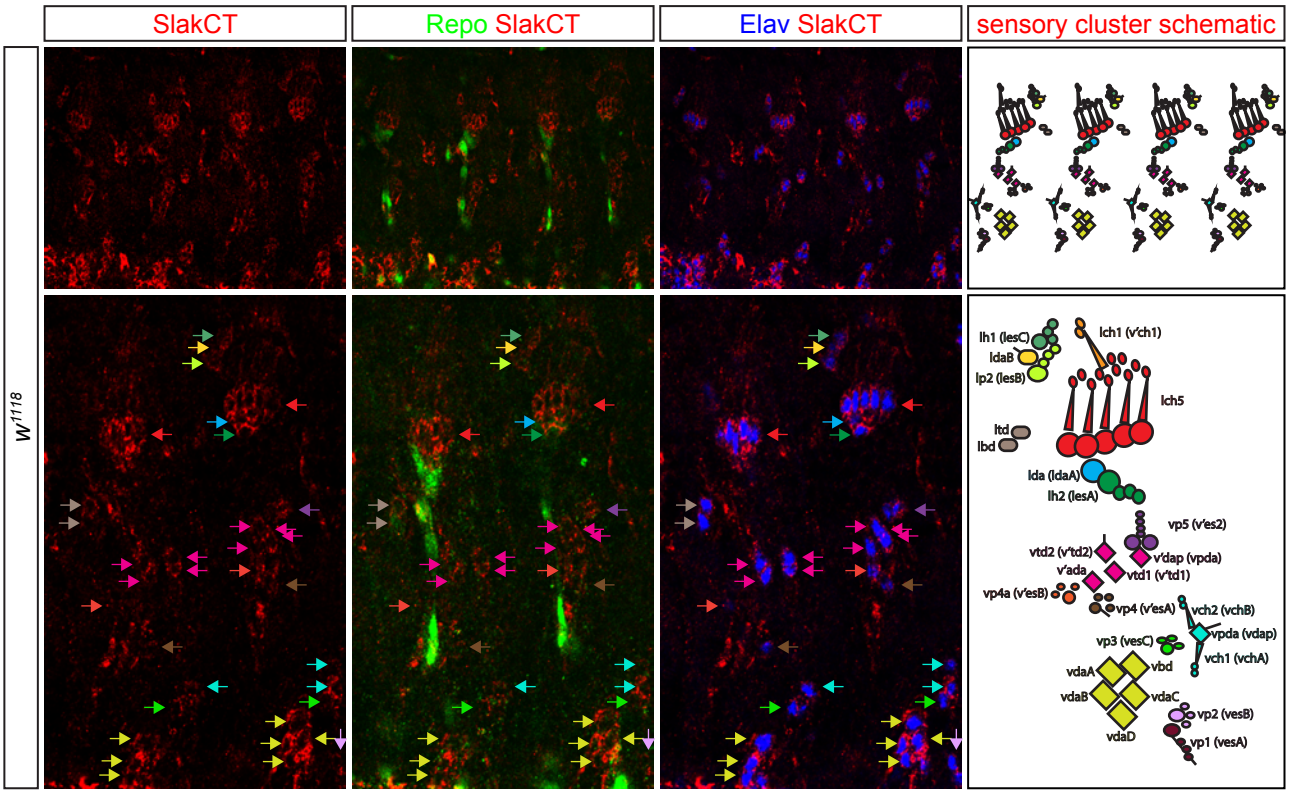

Figure AP 4.1.10 Schlank is enriched in all sensory neuron clusters of the peripheral nervous system. The upper panel shows an overview image of four abdominal segments. Cartoons to the right illustrate the position and identity of sensory neurons (for abbreviations, see Fig AP 4.1.8). Arrows point towards neuronal sensory clusters in the same color code as the cartoon. Neurons are marked by Embryonic lethal abnormal vision (Elav, blue), glia cells by Reverse polarity (Repo, green). Schlank (SlakCT) is marked in red.

AP4.1 C Schlank is enriched in most sensory organs of the embryonic head region

The embryonic head region in later stage embryos is characterized by the developing sensory organs that later are needed for touch, taste and chemical sensory input in larvae as well as light perception (Fig. AP 4.1.11).

There are labral, (hypo)pharyngeal, labial and Bolwig organs clustered anterior or lateral to the brain lobes. Schlank is expressed in do, to, vo, pao, lbso, lrso and pao neurons as marked by BP104, HRP and Elav (Fig. AP 4.1.12).

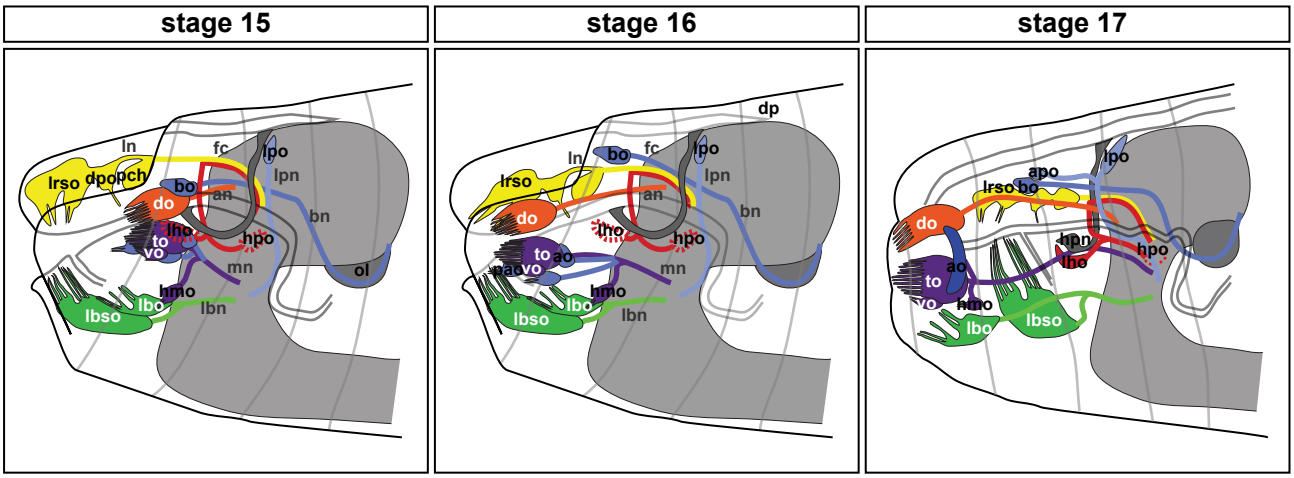

Figure AP 4.1.11 Schematic representation of sensory neurons of the embryonic head region. The cartoon shows sensory organs at stages 15, 16 and 17. an, antennal nerve; ao, antennal organ ; bo, Bolwig's organ; bn, Bolwig nerve; do, dorsal organ; dpo, dorsal pharyngeal organ; fc, frontal comissure; hmo, hypomaxillary organ; hpo, hypopharyngial organ; lbn, labial nerve; lbo, labial organ; lbso, labial sense organ; lho, latero-hypopharyngeal organ; ln, labral nerve; lpo, lateropharyngial organ; lpn, lateropharyngial nerve; lrso, labral sensory organ; mn, maxillary nerve; ol, optic lobe; pch, posterior chiasm; pao, papilla organ; to, terminal organ; vo, ventral organ. Modified from Campos-Ortega & Hartenstein, 1997

Taken together, there is strong expression in embryonic stages in ensheathing and subperineural glia cells as well as sensory neurons in head region and lateral sensory organs (Voelzmann & Bauer, 2011).

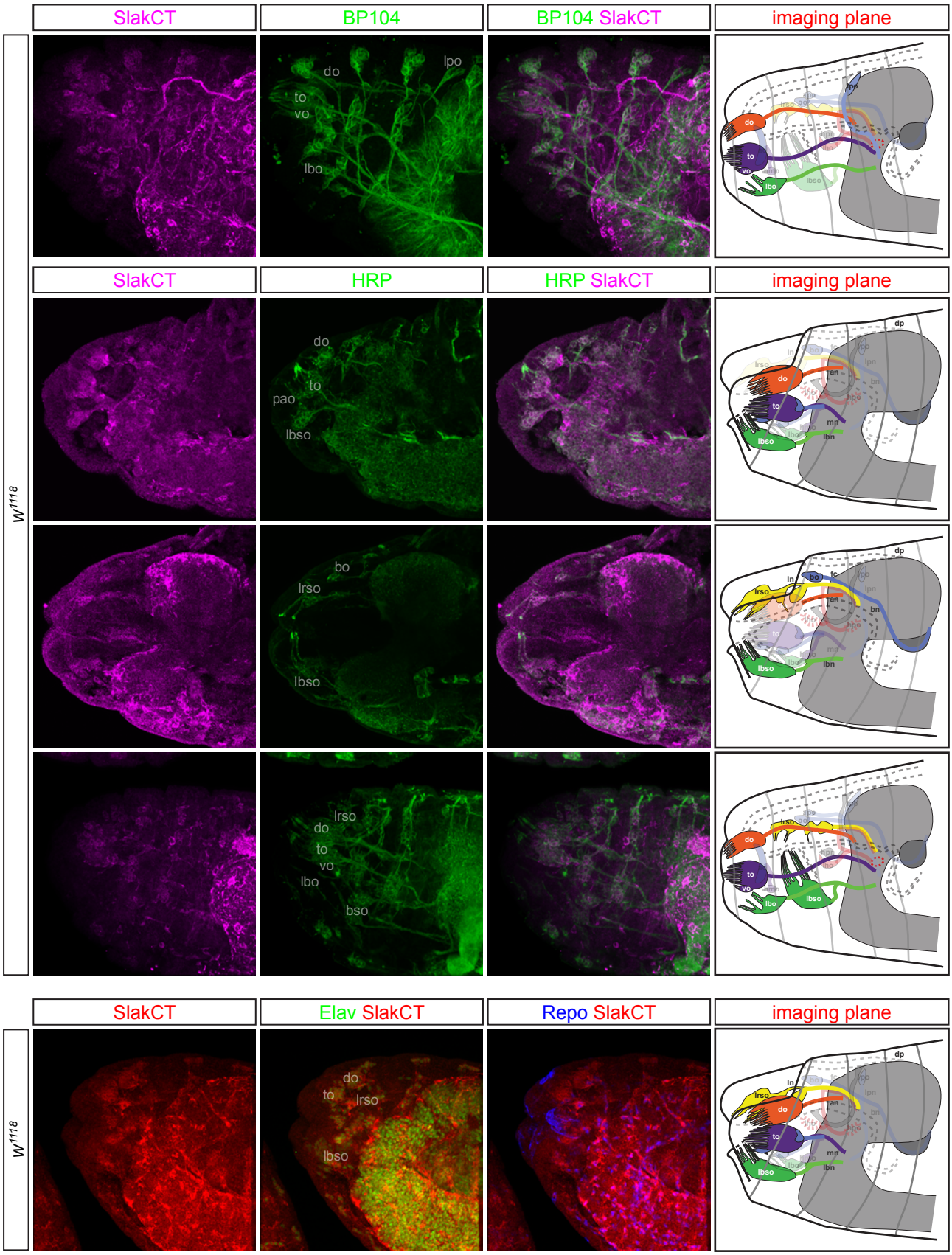

Figure AP 4.1.12 Schlank is enriched in neuronal sensory organs of the head region. Whole-mount embryonic staining. Sensory neurons are marked by BP104 (green) or Elav (green). Schematic representations on the right give an overview of the visible sensory organs and the imaging plane. For abbreviations see Fig. AP 4.1.11.

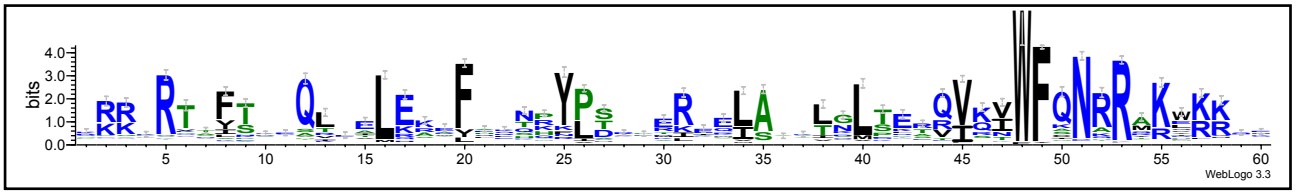

Figure AP 4.2.1 WebLogo of human homeodomains. The WebLogo was generated with homeodomain sequences listed in Holland et al, 2007a excluding CerS homeodomains.

AP4.2 Establishment of a transcription factor chromatin immunoprecipitation (TF-ChIP) protocol

In order to identify Schlank binding sites used under physiological conditions, a transcription factor chromatin immuoprecipitation was established. Hemagglutinin-tagged Schlank full length protein was expressed in larval tissues via the heatshock-inducible GAL4 system (*hs*GAL4). HA-tagged Cycle was expressed as positive control, because Cycle target genes and binding regions have been previously described. To pull down a transcription factor and the bound DNA regions, both are crosslinked by formaldehyde fixation, the plasma and nuclear membrane lysed. To facilitate a pull down, the DNA is sheared by sonication. Subsequently the transcription factor with the crosslinked DNA is immunoprecipitated. For further analysis, after several washing steps, the crosslink is reversed and the pulled DNA fragments have to be amplified. For Schlank, concrete binding sites were not known, thus the DNA had to be amplified blindly. To that end, primer sequence were ligated to the extracted DNA from the pull down experiments and then amplified (ligation mediated PCR, LM-PCR). In the case of Cycle, where some physiological binding sites are known, a subsequent nested PCR should be able to amplify the binding regions from the amplified DNAs. It was possible to immunoprecipitate HA-Schlank (Fig. AP 4.2.2 A) and Cycle-HA (data not shown) as well as bound DNA. Subsequent sonification protocols gave varying DNA size and the DNA could be sheared to suitable ranges in a minority of experiments (Fig. AP 4.2.2 B). When DNA shearing was acceptable, primer sequences were successfully ligated to the precipitated DNA (Fig. 4.2 C). Nested PCR was possible on LM-PCR amplified DNA from input samples but not from TF-ChIP samples (Fig. 4.2 D).

Thus the major steps of the TF-ChIP protocol could be established for Schlank-IPs out of larval extracts: TF-pulldown itself, primer ligation to the precipitated DNA as well as its amplification by LM-PCR. A combination of the TF-ChIP protocol with DNAseq techniques (ChIPseq) should allow the identification of so far unknown Schlank binding sites. However, there

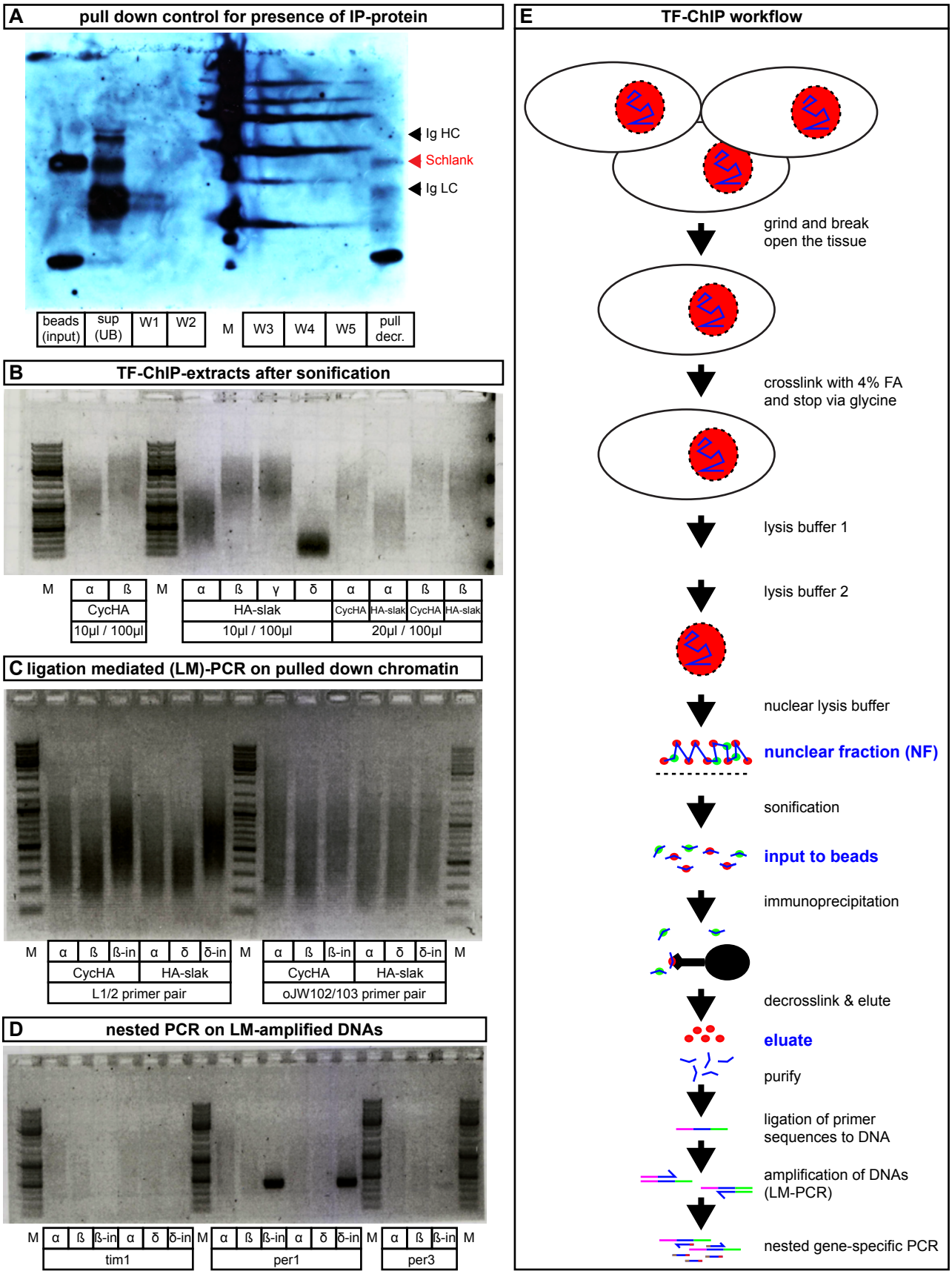

Figure AP 4.2.2 Establishment of a transcription factor chromatin immunoprecipitation protocol. A, Western Blot with anti-hemagglutinin-antibody. A fraction of the Schlank protein is pulled down by the transcription factor chromatin immunoprecipitation (TF-ChIP). Height of Schlank is marked by red arrow. Immunoglobulin (Ig) heavy chain

(HC) and light chain (LC) sizes are indicated (black arrows). **B**, 10 µL -20 µL of 100 µL TF-ChIP pull down extracts were run on a 1 % agarose gel after sonification with different settings (α, ß, γ, δ). CycHA, Cycle-HA (positive control); HA-Slak, Schlank-NTHA. **C**, After decrosslinking, 3/4th of the pulled DNA was precipitated and ligated to primer sequences (L1 / L2 or oJW102 / 103 pairs). After 2 amplification steps (½ pull down, 15 cycles; 2 µL of step 1, 40 cycles) 1 / 5 (10 µL) of the LM-PCR was run on an agarose gel. α, ß, γ, δ, decrosslinked extracts from indicated sonications; in, input extract without IP. **D**, LM-PCR of Cycle-HA extracts was used as input for a nested PCR for Cycle target genes timeless and period. Tim1, *timeless* gene primer pair 1; per1, *period* gene primer pair 1; per3, *period* gene primer pair 3. **E**, Transcription factor immunoprecipitation (TF-ChIP) workflow.

are some pre-requisites to a ChIPseq: Enrichment of specific DNAs and not amplification of unspecifically interacting DNAs has to be ascertained. Although dye-based nano-scale determination of DNA amounts can give some indication to overall DNA-enrichment compared to a negative control, this does not give any indication towards specificity. To that end, at least one target gene sequence has to be known. *Lip3* would be a suitable gene, as Schlank consensus binding sites seem to be present in its promoter region and it is regulated in schlank mutants. Successfully enriched DNA should allow amplification of the target region from the Schlank-pulldown but not by an identical experimental setup from extracts in which Schlank-HA is not expressed. If those criteria are met, ChIPseq should be run comparing the negative control and the Schlank pulldown. As alternative setup, the newly generated SchlankCT antibodies can be used for Schlank pulldown from wildtypic lysates with an immunoglobulin isotype control as well as a pulldown from a lysate of Schlank null alleles generated by genomic engineering.

6 Summary

Ceramide Synthases (CerS) are membrane bound enzymes at the center of the sphingolipid synthesis cascade. A sub-class of CerS also codes for a homeodomain of unknown function.

We previously identified the single *Drosophila* Ceramide Synthase Schlank (type II CerS) as essential regulator of fat stores in the larval fat body by modifying the transcription of two key regulators of lipolysis, *lipase 3* (*lip3*) and *adipokinetic hormone* (*akh*; Bauer, Voelzmann et al 2009). Data on a point mutation that disables CerS enzymatic activity suggested that these transcriptional regulations would be independent of the catalytic activity but rather depend on another activity of the protein.

To assess a potential role of the protein in transcriptional regulation, gene and protein expression patterns (Voelzmann, Bauer 2011) and subcellular localizations were determined. While the majority of the protein is localized in cytoplasmic organelles in neuronal and gut cells, there is strong enrichment of Schlank in fat body cells. In fat body nuclei, Schlank is present at type I indentations of the nuclear envelope, which form tubular structures in the nucleoplasm. As a transmembrane protein, Schlank is thought to remain within the inner nuclear membrane part of those indentations. Protein structure predictions show that the homeodomain would face the cytosol and nucleosol, respectively. Motif recognition algorithms predicted the presence of two nuclear localization sequences (NLS) within the homeodomain. N-terminal eGFP fusion constructs were used to verify the functionality of nuclear targeting sequences in the homeodomain and deletion constructs of the NLS proved them to be essential for nuclear import. NLS sequences are known to be bound by the Importin family of nuclear importers. Most nuclear import mechanisms rely on the ß-Importin variant. Using a clonal UAS-GAL4-based RNAi system it was shown that Schlank is imported to the nucleus via a Importin-ß-dependent mechanism.

To assess a potential nuclear function of Schlank, properties of the homeodomain were studied in great detail – phylogenetic analysis showed that it was taken up early during evolution and remains conserved on the structural level to classical homeodomains. A solid-phase DNA-binding assay with randomized DNA and electromobility shift assays with *lip3* and *akh* promoter fragments containing the previously identified Schlank consensus binding site (Noyes et al 2008a) proved that the Schlank homeodomain is capable of binding DNA.

Thus, the data on the Ceramide Synthase Schlank summarized in this thesis challenge two central dogmas in current Ceramide Synthase research: 1) Ceramide Synthases are not confined to the endoplasmic reticulum, as previously thought. 2) Ceramide Synthase homeodomains are not degenerate in structure and keep their DNA binding potential, a notion that is strongly debated in literature.

In light of these data, it seems necessary for the research field in general to step back from the sphingolipid-centered viewpoint and reach a more balanced standpoint. Functions of Ceramide Synthases themselves independent of the mere enzymatic activity have to be considered. Both aspects and potential links between them should be addressed in the future.

7 References

Acharya U, Patel S, Koundakjian E, Nagashima K, Han X & Acharya JK (2003) Modulating sphingolipid biosynthetic pathway rescues photoreceptor degeneration. *Science* **299:** 1740–1743

Albi E & Magni MV (1999) Sphingomyelin synthase in rat liver nuclear membrane and chromatin. *FEBS Lett* **460:** 369–372

Altekar G, Dwarkadas S, Huelsenbeck JP & Ronquist F (2004) Parallel Metropolis coupled Markov chain Monte Carlo for Bayesian phylogenetic inference. *Bioinformatics* **20:** 407–415

André Völzmann (2007) *Molekulare und funktionelle Analyse des Lag1-Proteins in* Drosophila melanogaster. Diploma, Bonn, Germany

Arboleda G, Morales LC, Benítez B & Arboleda H (2009) Regulation of ceramide-induced neuronal death: Cell metabolism meets neurodegeneration. *Brain Research Reviews* **59:** 333–346

Arnold K, Bordoli L, Kopp J & Schwede T (2006) The SWISS-MODEL workspace: a web-based environment for protein structure homology modelling. *Bioinformatics* **22:** 195–201

Arrese EL, Mirza S, Rivera L, Howard AD, Chetty PS & Soulages JL (2008) Expression of lipid storage droplet protein-1 may define the role of AKH as a lipid mobilizing hormone in Manduca sexta. *Insect Biochem. Mol. Biol* **38:** 993–1000

Arrese EL, Patel RT & Soulages JL (2006) The main triglyceride-lipase from the insect fat body is an active phospholipase A(1): identification and characterization. *J. Lipid Res* **47:** 2656–2667

Bahadorani S, Cho J, Lo T, Contreras H, Lawal HO, Krantz DE, Bradley TJ & Walker DW (2010) Neuronal expression of a single-subunit yeast NADH-ubiquinone oxidoreductase (Ndi1) extends Drosophila lifespan. *Aging Cell* **9:** 191–202

Bauer R, Voelzmann A, Breiden B, Schepers U, Farwanah H, Hahn I, Eckardt F, Sandhoff K & Hoch M (2009) Schlank, a member of the Ceramide Synthase family controls growth and body fat in Drosophila. *EMBO J* **28:** 3706–3716

Beckervordersandforth RM, Rickert C, Altenhein B & Technau GM (2008 May-Jun) Subtypes of glial cells in the Drosophila embryonic ventral nerve cord as related to lineage and gene expression. *Mechanisms of development* **125:** 542–557

Bharucha KN, Tarr P & Zipursky SL (2008) A glucagon-like endocrine pathway in Drosophila modulates both lipid and carbohydrate homeostasis. *J. Exp. Biol* **211:** 3103–3110

Bianca Bauch (2003) *Identifizierung und Charakterisierung von Interaktionspartnern des LAG1-Proteins in* Drosophila melanogaster *(DLAG1).* Diploma, Bonn, Germany

Bieberich E (2011) Ceramide in stem cell differentiation and embryo development: novel functions of a topological cell-signaling lipid and the concept of ceramide compartments. *J Lipids* **2011:** 610306

Bieberich E, MacKinnon S, Silva J & Yu RK (2001) Regulation of apoptosis during neuronal differentiation by ceramide and b-series complex gangliosides. *J. Biol. Chem* **276:** 44396–44404

Billich A & Baumruker T (2008) Sphingolipid metabolizing enzymes as novel therapeutic targets. *Sub-cellular biochemistry* **49:** 487–522

Bodmer R, Carretto R & Jan YN (1989) Neurogenesis of the peripheral nervous system in Drosophila embryos: DNA replication patterns and cell lineages. *Neuron* **3:** 21–32

Bose R, Verheij M, Haimovitz-Friedman A, Scotto K, Fuks Z & Kolesnick R (1995) Ceramide Synthase mediates daunorubicin-induced apoptosis: an alternative mechanism for generating death signals. *Cell* **82:** 405–414

Broers JL, Machiels BM, van Eys GJ, Kuijpers HJ, Manders EM, van Driel R & Ramaekers FC (1999) Dynamics of the nuclear lamina as monitored by GFP-tagged A-type lamins. *J. Cell. Sci* **112 (Pt 20):** 3463–3475

Brondolin M, Berger S, Reinke M, Tanaka H, Ohshima T, Fuβ B, Hoch M (2013) Identification and expression analysis of the zebrafish homologs of the ceramide synthase gene family. *Dev Dyn.* **242**:189-200

Brondolin M, Völzmann, A & Hahn, I (2012) Straight forward approach to sort fish by gender. *LIMES Klaaf* **6**: 42

Bürglin TR (1994) A comprehensive classification of homeobox genes. In *Guidebook to the homeobox genes,* Duboule D (ed) pp. 25–71: Oxford University Press

Campos-Ortega JA & Hartenstein V (1997) *The Embryonic Development of Drosophila melanogaster.* Springer Berlin Heidelberg, Berlin, Heidelberg

Chandrasekaran S, Ament SA, Eddy JA, Rodriguez-Zas SL, Schatz BR, Price ND & Robinson GE (2011) Behavior-specific changes in transcriptional modules lead to distinct and predictable neurogenomic states. *Proc. Natl. Acad. Sci. U.S.A* **108:** 18020–18025

Cheng Z, Singh RD, Marks DL & Pagano RE (2006) Membrane microdomains, caveolae, and caveolar endocytosis of sphingolipids. *Mol. Membr. Biol* **23:** 101–110

Chou Y & Chien C (2002) Scabrous controls ommatidial rotation in the Drosophila compound eye. *Dev. Cell* **3:** 839–850

Collado-Hilly M, Shirvani H, Jaillard D & Mauger J (2010) Differential redistribution of Ca2+-handling proteins during polarisation of MDCK cells: Effects on Ca2+ signalling. *Cell Calcium* **48:** 215–224

Colombini M (2010) Ceramide channels and their role in mitochondria-mediated apoptosis. *Biochim. Biophys. Acta* **1797:** 1239–1244

Delgado A, Fabrias G, Bedia C, Casas J & Abad JL (2012) Sphingolipid modulation: a strategy for cancer therapy. *Anticancer Agents Med Chem* **12:** 285–302

Demmerle J, Koch AJ & Holaska JM (2012) The nuclear envelope protein emerin binds directly to histone deacetylase 3 (HDAC3) and activates HDAC3 activity. *J. Biol. Chem* **287:** 22080–22088

Dos-Santos N, Rubin T, Chalvet F, Gandille P, Cremazy F, Leroy J, Boissonneau E & Théodore L (2008) Drosophila retinal pigment cell death is regulated in a position- dependent manner by a cell memory gene. *The International journal of developmental biology* **52:** 21–31

Drummond AJ, Rambaut A (2007) BEAST: Bayesian evolutionary analysis by sampling trees. *BMC Evol Biol.* **7**: 214

Dubnau J & Struhl G (1996) RNA recognition and translational regulation by a homeodomain protein. *Nature* **379:** 694–699

Eckhardt M (2010) Pathology and current treatment of neurodegenerative sphingolipidoses. *Neuromolecular Med* **12:** 362–382

Ernst AM & Brügger B (2013) Sphingolipids as modulators of membrane proteins. *Biochim. Biophys. Acta*

Farooqui AA, Ong WY & Farooqui T (2010) Lipid mediators in the nucleus: Their potential contribution to Alzheimer's disease. *Biochimica et biophysica acta* **1801:** 906–916

Faustino RS, Cheung P, Richard MN, Dibrov E, Kneesch AL, Deniset JF, Chahine MN, Lee K, Blackwood D & Pierce GN (2008) Ceramide regulation of nuclear protein import. *Journal of Lipid Research* **49:** 654–662

Fox TE, Houck KL, O'Neill SM, Nagarajan M, Stover TC, Pomianowski PT, Unal O, Yun JK, Naides SJ & Kester M (2007) Ceramide recruits and activates protein kinase C zeta (PKC zeta) within structured membrane microdomains. *J. Biol. Chem* **282:** 12450–12457

Fuller M (2010) Sphingolipids: the nexus between Gaucher disease and insulin resistance. *Lipids Health Dis* **9:** 113

Fyrst H & Saba JD (2010) An update on sphingosine-1-phosphate and other sphingolipid mediators. *Nat. Chem. Biol* **6:** 489–497

Ganten D & Ruckpaul K (2006) *Encyclopedic reference of genomics and proteomics in molecular medicine: Nuclear Import and Export.* Springer, Berlin ;, New York

Gehring WJ, Affolter M & Bürglin T (1994) Homeodomain proteins. *Annu. Rev. Biochem* **63:** 487–526

Geilen CC, Wieder T & Orfanos CE (1997) Ceramide signalling: regulatory role in cell proliferation, differentiation and apoptosis in human epidermis. *Arch. Dermatol. Res* **289:** 559–566

German OL, Miranda GE, Abrahan CE & Rotstein NP (2006) Ceramide is a mediator of apoptosis in retina photoreceptors. *Invest. Ophthalmol. Vis. Sci* **47:** 1658–1668

Gibrat JF, Madej T & Bryant SH (1996) Surprising similarities in structure comparison. *Curr. Opin. Struct. Biol* **6:** 377–385

Gillies L, Lee SC, Long JS, Ktistakis N, Pyne NJ & Pyne S (2009) The sphingosine 1-phosphate receptor 5 and sphingosine kinases 1 and 2 are localised in centrosomes: possible role in regulating cell division. *Cell. Signal* **21:** 675–684

Giot L, Bader JS, Brouwer C, Chaudhuri A, Kuang B, Li Y, Hao YL, Ooi CE, Godwin B, Vitols E, Vijayadamodar G, Pochart P, Machineni H, Welsh M, Kong Y, Zerhusen B, Malcolm R, Varrone Z, Collis A & Minto M et al (2003) A protein interaction map of Drosophila melanogaster. *Science* **302:** 1727–1736

Graham TGW, Tabei SMA, Dinner AR & Rebay I (2010) Modeling bistable cell-fate choices in the Drosophila eye: qualitative and quantitative perspectives. *Development* **137:** 2265–2278

Granado MH, Gangoiti P, Ouro A, Arana L, González M, Trueba M & Gómez-Muñoz A (2009) Ceramide 1-phosphate (C1P) promotes cell migration Involvement of a specific C1P receptor. *Cell. Signal* **21:** 405–412

Grönke S, Mildner A, Fellert S, Tennagels N, Petry S, Müller G, Jäckle H & Kühnlein RP (2005) Brummer lipase is an evolutionary conserved fat storage regulator in Drosophila. *Cell Metab* **1:** 323–330

Grönke S, Müller G, Hirsch J, Fellert S, Andreou A, Haase T, Jäckle H & Kühnlein RP (2007) Dual lipolytic control of body fat storage and mobilization in Drosophila. *PLoS Biol* **5:** e137

Guan XL, Souza CM, Pichler H, Dewhurst G, Schaad O, Kajiwara K, Wakabayashi H, Ivanova T, Castillon GA, Piccolis M, Abe F, Loewith R, Funato K, Wenk MR & Riezman H (2009) Functional interactions between sphingolipids and sterols in biological membranes regulating cell physiology. *Mol. Biol. Cell* **20:** 2083–2095

Guillas I, Kirchman PA, Chuard R, Pfefferli M, Jiang JC, Jazwinski SM & Conzelmann A (2001) C26-CoA-dependent ceramide synthesis of Saccharomyces cerevisiae is operated by Lag1p and Lac1p. *EMBO J* **20:** 2655–2665

Gutierrez E, Wiggins D, Fielding B & Gould AP (2007) Specialized hepatocyte-like cells regulate Drosophila lipid metabolism. *Nature* **445:** 275–280

Hait NC, Allegood J, Maceyka M, Strub GM, Harikumar KB, Singh SK, Luo C, Marmorstein R, Kordula T, Milstien S & Spiegel S (2009) Regulation of histone acetylation in the nucleus by sphingosine-1-phosphate. *Science* **325:** 1254–1257

Hanada K, Kumagai K, Yasuda S, Miura Y, Kawano M, Fukasawa M & Nishijima M (2003) Molecular machinery for non-vesicular trafficking of ceramide. *Nature* **426:** 803–809

Hannich JT, Umebayashi K & Riezman H (2011) Distribution and functions of sterols and sphingolipids. *Cold Spring Harb Perspect Biol* **3**

Hays R, Wickline L & Cagan R (2002) Morgue mediates apoptosis in the Drosophila melanogaster retina by promoting degradation of DIAP1. *Nat. Cell Biol* **4:** 425–431

Herget T, Esdar C, Oehrlein SA, Heinrich M, Schütze S, Maelicke A & van Echten-Deckert G (2000) Production of ceramides causes apoptosis during early neural differentiation in vitro. *J. Biol. Chem* **275:** 30344–30354

Hilchen CM von, Hein I, Technau GM & Altenhein B (2010) Netrins guide migration of distinct glial cells in the Drosophila embryo. *Development* **137:** 1251–1262

Holaska JM, Lee KK, Kowalski AK & Wilson KL (2003) Transcriptional repressor germ cell-less (GCL) and barrier to autointegration factor (BAF) compete for binding to emerin in vitro. *J. Biol. Chem* **278:** 6969–6975

Holland PW, Booth HAF & Bruford EA (2007a) Classification and nomenclature of all human homeobox genes. *BMC Biol* **5:** 47

Holland WL & Summers SA (2008) Sphingolipids, Insulin Resistance, and Metabolic Disease: New Insights from in Vivo Manipulation of Sphingolipid Metabolism. *Endocrine Reviews* **29:** 381–402

Holland WL, Brozinick JT, Wang L, Hawkins ED, Sargent KM, Liu Y, Narra K, Hoehn KL, Knotts TA & Siesky A (2007b) Inhibition of Ceramide Synthesis Ameliorates Glucocorticoid-, Saturated-Fat-, and Obesity-Induced Insulin Resistance. *Cell Metabolism* **5:** 167–179

Huang X, Suyama K, Buchanan J, Zhu AJ & Scott MP (2005) A Drosophila model of the Niemann-Pick type C lysosome storage disease: dnpc1a is required for molting and sterol homeostasis. *Development* **132:** 5115–5124

Huelsenbeck JP, Ronquist F, Nielsen R & Bollback JP (2001) Bayesian inference of phylogeny and its impact on evolutionary biology. *Science* **294:** 2310–2314

Ida H, Suzusho N, Suyari O, Yoshida H, Ohno K, Hirose F, Itoh M & Yamaguchi M (2009) Genetic screening for modifiers of the DREF pathway in Drosophila melanogaster: identification and characterization of HP6 as a novel target of DREF. *Nucleic Acids Res* **37:** 1423–1437

Igarashi N, Okada T, Hayashi S, Fujita T, Jahangeer S & Nakamura S (2003) Sphingosine kinase 2 is a nuclear protein and inhibits DNA synthesis. *J. Biol. Chem* **278:** 46832–46839

Imgrund S, Hartmann D, Farwanah H, Eckhardt M, Sandhoff R, Degen J, Gieselmann V, Sandhoff K & Willecke K (2009) Adult Ceramide Synthase 2 (CERS2)-deficient mice exhibit myelin sheath defects, cerebellar degeneration, and hepatocarcinomas. *J Biol Chem* **284:** 33549–33560

Jarman AP, Grell EH, Ackerman L, Jan LY & Jan YN (1994) Atonal is the proneural gene for Drosophila photoreceptors. *Nature* **369:** 398–400

Jennemann R, Rabionet M, Gorgas K, Epstein S, Dalpke A, Rothermel U, Bayerle A, van der Hoeven F, Imgrund S, Kirsch J, Nickel W, Willecke K, Riezman H, Gröne H & Sandhoff R (2012) Loss of Ceramide Synthase 3 causes lethal skin barrier disruption. *Hum. Mol. Genet* **21:** 586–608

Jia Z, Pei Z, Maiguel D, Toomer CJ & Watkins PA (2007) The fatty acid transport protein (FATP) family: very long chain acyl-CoA synthetases or solute carriers? *J. Mol. Neurosci* **33:** 25–31

Käll L, Krogh A & Sonnhammer ELL (2004) A combined transmembrane topology and signal peptide prediction method. *J. Mol. Biol* **338:** 1027–1036

Käll L, Krogh A & Sonnhammer ELL (2007) Advantages of combined transmembrane topology and signal peptide prediction--the Phobius web server. *Nucleic Acids Res* **35:** W429-32

Kirch T, Bitter S, Kisters-Woike B & Werr W (1998) The two homeodomains of the ZmHox2a gene from maize originated as an internal gene duplication and have evolved different target site specificities. *Nucleic Acids Res* **26:** 4714–4720

Kok JW, Babia T, Klappe K, Egea G & Hoekstra D (1998) Ceramide transport from endoplasmic reticulum to Golgi apparatus is not vesicle-mediated. *Biochem. J* **333 (Pt 3):** 779–786

Kosugi S, Hasebe M, Matsumura N, Takashima H, Miyamoto-Sato E, Tomita M & Yanagawa H (2009a) Six classes of nuclear localization signals specific to different binding grooves of importin alpha. *J. Biol. Chem* **284:** 478–485

Kosugi S, Hasebe M, Tomita M & Yanagawa H (2009b) Systematic identification of cell cycle-dependent yeast nucleocytoplasmic shuttling proteins by prediction of composite motifs. *Proc. Natl. Acad. Sci. U.S.A* **106:** 10171–10176

Kraft ML (2013) Plasma membrane organization and function: moving past lipid rafts. *Mol. Biol. Cell* **24:** 2765–2768

Krogh A, Larsson B, Heijne G von & Sonnhammer EL (2001) Predicting transmembrane protein topology with a hidden Markov model: application to complete genomes. *J. Mol. Biol* **305:** 567–580

Krumins AM, Barker SA, Huang C, Sunahara RK, Yu K, Wilkie TM, Gold SJ & Mumby SM (2004) Differentially regulated expression of endogenous RGS4 and RGS7. *J. Biol. Chem* **279:** 2593–2599

Lahiri S & Futerman AH (2007) The metabolism and function of sphingolipids and glycosphingolipids. *Cell. Mol. Life Sci* **64:** 2270–2284

Larkin MA, Blackshields G, Brown NP, Chenna R, McGettigan PA, McWilliam H, Valentin F, Wallace IM, Wilm A, Lopez R, Thompson JD, Gibson TJ & Higgins DG (2007) Clustal W and Clustal X version 2.0. *Bioinformatics* **23:** 2947–2948

Ledeen RW & Wu G (2008) Nuclear sphingolipids: Metabolism and signaling. *Journal of Lipid Research* **49:** 1176–1186

Levy M & Futerman AH (2010) Mammalian Ceramide Synthases. *IUBMB Life* **62:** 347–356

Linde N & Stick R (2010) Intranuclear membranes induced by lipidated proteins are derived from the nuclear envelope. *Nucleus* **1:** 343–353

Liu Y & Lehmann M (2008) A genomic response to the yeast transcription factor GAL4 in Drosophila. *Fly (Austin)* **2:** 92–98

Loewer A, Soba P, Beyreuther K, Paro R & Merdes G (2004) Cell-type-specific processing of the amyloid precursor protein by Presenilin during Drosophila development. *EMBO Rep* **5:** 405–411

Lu B (2009) Recent advances in using Drosophila to model neurodegenerative diseases. *Apoptosis* **14:** 1008–1020

Lucki NC & Sewer MB (2012) Nuclear sphingolipid metabolism. *Annu. Rev. Physiol* **74:** 131–151

Malhas A, Goulbourne C & Vaux DJ (2011) The nucleoplasmic reticulum: form and function. *Trends Cell Biol* **21:** 362–373

Marks DL & Pagano RE (2002) Endocytosis and sorting of glycosphingolipids in sphingolipid storage disease. *Trends Cell Biol* **12:** 605–613

Mathelier A, Zhao X, Zhang AW, Parcy F, Worsley-Hunt R, Arenillas DJ, Buchman S, Chen C, Chou A, Ienasescu H, Lim J, Shyr C, Tan G, Zhou M, Lenhard B, Sandelin A & Wasserman WW (2013) JASPAR 2014: an extensively expanded and updated open-access database of transcription factor binding profiles. *Nucleic Acids Res*

Mattson MP (2003) *Membrane lipid signaling in aging and age-related disease.* Elsevier, Amsterdam ;, Boston

Mesika A, Ben-Dor S, Laviad EL & Futerman AH (2007) A new functional motif in Hox domain-containing Ceramide Synthases: identification of a novel region flanking the Hox and TLC domains essential for activity. *J. Biol. Chem* **282:** 27366–27373

Meyer H, Panz M, Zmojdzian M, Jagla K & Paululat A (2009) Neprilysin 4, a novel endopeptidase from Drosophila melanogaster, displays distinct substrate specificities and exceptional solubility states. *J. Exp. Biol* **212:** 3673–3683

Morante J, Desplan C & Celik A (2007) Generating patterned arrays of photoreceptors. *Curr. Opin. Genet. Dev* **17:** 314–319

Mukherjee K, Brocchieri L & Bürglin TR (2009) A comprehensive classification and evolutionary analysis of plant homeobox genes. *Mol. Biol. Evol* **26:** 2775–2794

Mullen TD, Hannun YA & Obeid LM (2012) Ceramide Synthases at the centre of sphingolipid metabolism and biology. *Biochem. J* **441:** 789–802

Mullen TD, Jenkins RW, Clarke CJ, Bielawski J, Hannun YA & Obeid LM (2011) Ceramide Synthase-dependent ceramide generation and programmed cell death: involvement of salvage pathway in regulating postmitochondrial events. *J. Biol. Chem* **286:** 15929–15942

Myers EW & Miller W (1989) Approximate matching of regular expressions. *Bull. Math. Biol* **51:** 5–37

Nakai K & Horton P (1999) PSORT: a program for detecting sorting signals in proteins and predicting their subcellular localization. *Trends Biochem. Sci* **24:** 34–36

Nakai K & Kanehisa M (1992) A knowledge base for predicting protein localization sites in eukaryotic cells. *Genomics* **14:** 897–911

Noordermeer JN, Kopczynski CC, Fetter RD, Bland KS, Chen WY & Goodman CS (1998) Wrapper, a novel member of the Ig superfamily, is expressed by midline glia and is required for them to ensheath commissural axons in Drosophila. *Neuron* **21:** 991–1001

Novgorodov SA, Chudakova DA, Wheeler BW, Bielawski J, Kindy MS, Obeid LM & Gudz TI (2011) Developmentally regulated Ceramide Synthase 6 increases mitochondrial Ca2+ loading capacity and promotes apoptosis. *J. Biol. Chem* **286:** 4644–4658

Noyes MB, Christensen RG, Wakabayashi A, Stormo GD, Brodsky MH & Wolfe SA (2008a) Analysis of Homeodomain Specificities Allows the Family-wide Prediction of Preferred Recognition Sites. *Cell* **133:** 1277–1289

Noyes MB, Meng X, Wakabayashi A, Sinha S, Brodsky MH & Wolfe SA (2008b) A systematic characterization of factors that regulate Drosophila segmentation via a bacterial one-hybrid system. *Nucleic Acids Res* **36:** 2547–2560

Nylander JAA, Wilgenbusch JC, Warren DL & Swofford DL (2008) AWTY (are we there yet?): a system for graphical exploration of MCMC convergence in Bayesian phylogenetics. *Bioinformatics* **24:** 581–583

Ogretmen B & Hannun YA (2004) Biologically active sphingolipids in cancer pathogenesis and treatment. *Nat. Rev. Cancer* **4:** 604–616

Okajima T, Xu A, Lei L & Irvine KD (2005) Chaperone activity of protein O-fucosyltransferase 1 promotes notch receptor folding. *Science* **307:** 1599–1603

Olivera A & Rivera J (2005) Sphingolipids and the balancing of immune cell function: lessons from the mast cell. *J. Immunol* **174:** 1153–1158

Orgogozo V & Grueber WB (2005) FlyPNS, a database of the Drosophila embryonic and larval peripheral nervous system. *BMC developmental biology* **5:** 4

Oskouian B & Saba JD (2010) Cancer treatment strategies targeting sphingolipid metabolism. *Advances in experimental medicine and biology* **688:** 185–205

Patel RT, Soulages JL & Arrese EL (2006) Adipokinetic hormone-induced mobilization of fat body triglyceride stores in Manduca sexta: role of TG-lipase and lipid droplets. *Arch. Insect Biochem. Physiol* **63:** 73–81

Patel RT, Soulages JL, Hariharasundaram B & Arrese EL (2005) Activation of the lipid droplet controls the rate of lipolysis of triglycerides in the insect fat body. *J. Biol. Chem* **280:** 22624–22631

Pepperl J, Reim G, Lüthi U, Kaech A, Hausmann G & Basler K (2013) Sphingolipid depletion impairs endocytic traffic and inhibits Wingless signaling. *Mech. Dev* **130:** 493–505

Reddy KL, Zullo JM, Bertolino E & Singh H (2008) Transcriptional repression mediated by repositioning of genes to the nuclear lamina. *Nature* **452:** 243–247

Ribbeck K (1998) NTF2 mediates nuclear import of Ran. *The EMBO Journal* **17:** 6587–6598

Riley RT, Enongene E, Voss KA, Norred WP, Meredith FI, Sharma RP, Spitsbergen J, Williams DE, Carlson DB & Merrill AH (2001) Sphingolipid perturbations as mechanisms for fumonisin carcinogenesis. *Environ. Health Perspect* **109 Suppl 2:** 301–308

Roccamo AM, Pediconi MF, Aztiria E, Zanello L, Wolstenholme A & Barrantes FJ (1999) Cells defective in sphingolipids biosynthesis express low amounts of muscle nicotinic acetylcholine receptor. *Eur. J. Neurosci* **11:** 1615–1623

Ronquist F & Huelsenbeck JP (2003) MrBayes 3: Bayesian phylogenetic inference under mixed models. *Bioinformatics* **19:** 1572–1574

Rosen H, Gonzalez-Cabrera PJ, Sanna MG & Brown S (2009) Sphingosine 1-phosphate receptor signaling. *Annu. Rev. Biochem* **78:** 743–768

Rost B, Fariselli P & Casadio R (1996) Topology prediction for helical transmembrane proteins at 86% accuracy. *Protein Sci* **5:** 1704–1718

Rusconi JC, Hays R & Cagan RL (2000) Programmed cell death and patterning in Drosophila. *Cell Death Differ* **7:** 1063–1070

Ryland LK, Fox TE, Liu X, Loughran TP & Kester M (2011) Dysregulation of sphingolipid metabolism in cancer. *Cancer Biol. Ther* **11:** 138–149

Schindelin J, Arganda-Carreras I, Frise E, Kaynig V, Longair M, Pietzsch T, Preibisch S, Rueden C, Saalfeld S, Schmid B, Tinevez J, White DJ, Hartenstein V, Eliceiri K, Tomancak P & Cardona A (2012) Fiji: an open-source platform for biological-image analysis. *Nat. Methods* **9:** 676–682

Schulze H & Sandhoff K (2011) Lysosomal lipid storage diseases. *Cold Spring Harb Perspect Biol* **3**

Schulze H & Sandhoff K (2013) Sphingolipids and lysosomal pathologies. *Biochim. Biophys. Acta*

Schulze SR, Curio-Penny B, Speese S, Dialynas G, CRYDERMAN DE, McDonough CW, Nalbant D, Petersen M, Budnik V, Geyer PK & WALLRATH LL (2009) A comparative study of Drosophila and human A-type lamins. *PLoS ONE* **4:** e7564

Schweitzer JK, Krivda JP & D'Souza-Schorey C (2009) Neurodegeneration in Niemann-Pick Type C disease and Huntington's disease: impact of defects in membrane trafficking. *Curr Drug Targets* **10:** 653–665

Shimeno H, Soeda S, Sakamoto M, Kouchi T, Kowakame T & Kihara T (1998) Partial purification and characterization of sphingosine N-acyltransferase (Ceramide Synthase) from bovine liver mitochondrion-rich fraction. *Lipids* **33:** 601–605

Silva LC, Ben David O, Pewzner-Jung Y, Laviad EL, Stiban J, Bandyopadhyay S, Merrill AH, Prieto M & Futerman AH (2012) Ablation of Ceramide Synthase 2 strongly affects biophysical properties of membranes. *J. Lipid Res* **53:** 430–436

Siskind LJ, Kolesnick RN & Colombini M (2002) Ceramide channels increase the permeability of the mitochondrial outer membrane to small proteins. *J. Biol. Chem* **277:** 26796–26803

Smith AEF & Ford KG (2005) Use of altered-specificity binding Oct-4 suggests an absence of pluripotent cell-specific cofactor usage. *Nucleic Acids Res* **33:** 6011–6023

Song Z, Guan B, Bergman A, Nicholson DW, Thornberry NA, Peterson EP & Steller H (2000) Biochemical and genetic interactions between Drosophila caspases and the proapoptotic genes rpr, hid, and grim. *Mol. Cell. Biol* **20:** 2907–2914

Sonnhammer EL, Heijne G von & Krogh A (1998) A hidden Markov model for predicting transmembrane helices in protein sequences. *Proc Int Conf Intell Syst Mol Biol* **6:** 175–182

Spassieva S, Seo J, Jiang JC, Bielawski J, Alvarez-Vasquez F, Jazwinski SM, Hannun YA & Obeid LM (2006) Necessary role for the Lag1p motif in (dihydro)Ceramide Synthase activity. *J. Biol. Chem* **281:** 33931–33938

Stoffel W & Hofmann K (1993) TMbase - A database of membrane spanning proteins segments. *Biol. Chem. Hoppe-Seyler* **374:** 166

Strutt DI & Mlodzik M (1995) Ommatidial polarity in the Drosophila eye is determined by the direction of furrow progression and local interactions. *Development* **121:** 4247–4256

Strutt H & Strutt D (1999) Polarity determination in the Drosophila eye. *Curr. Opin. Genet. Dev* **9:** 442–446

Suga H, Chen Z, Mendoza A de, Sebé-Pedrós A, Brown MW, Kramer E, Carr M, Kerner P, Vervoort M, Sánchez-Pons N, Torruella G, Derelle R, Manning G, Lang BF, Russ C, Haas BJ, Roger AJ,

Nusbaum C & Ruiz-Trillo I (2013) The Capsaspora genome reveals a complex unicellular prehistory of animals. *Nat Commun* **4:** 2325

Takemura M & Adachi-Yamada T (2011) Cell death and selective adhesion reorganize the dorsoventral boundary for zigzag patterning of Drosophila wing margin hairs. *Dev. Biol* **357:** 336–346

Tedesco P, Jiang J, Wang J, Jazwinski SM & Johnson TE (2008) Genetic analysis of hyl-1, the C. elegans homolog of LAG1/LASS1. *Age (Dordrecht, Netherlands)* **30:** 43–52

Thudichum JWL (1874) Researches on the chemical constitution of the brain. *Reports of the Privy Council and the Local Government Board* Cd. **1021**: 113-247

Tsugane K, Tamiya-Koizumi K, Nagino M, Nimura Y & Yoshida S (1999) A possible role of nuclear ceramide and sphingosine in hepatocyte apoptosis in rat liver. *J. Hepatol* **31:** 8–17

Tusnády GE & Simon I (1998) Principles governing amino acid composition of integral membrane proteins: application to topology prediction. *J. Mol. Biol* **283:** 489–506

Tusnády GE & Simon I (2001) The HMMTOP transmembrane topology prediction server. *Bioinformatics* **17:** 849–850

van Brocklyn JR & Williams JB (2012) The control of the balance between ceramide and sphingosine-1-phosphate by sphingosine kinase: oxidative stress and the seesaw of cell survival and death. *Comp. Biochem. Physiol. B, Biochem. Mol. Biol* **163:** 26–36

van Echten-Deckert G & Walter J (2012) Sphingolipids: critical players in Alzheimer's disease. *Prog. Lipid Res* **51:** 378–393

van Geest M & Lolkema JS (2000) Membrane topology and insertion of membrane proteins: search for topogenic signals. *Microbiol. Mol. Biol. Rev* **64:** 13–33

van Meer G & Lisman Q (2002) Sphingolipid transport: rafts and translocators. *J. Biol. Chem* **277:** 25855–25858

Venkataraman K & Futerman AH (2002) Do longevity assurance genes containing Hox domains regulate cell development via ceramide synthesis? *FEBS Lett* **528:** 3–4

Véret J, Coant N, Berdyshev EV, Skobeleva A, Therville N, Bailbé D, Gorshkova I, Natarajan V, Portha B & Le Stunff H (2011) Ceramide Synthase 4 and de novo production of ceramides with specific N-acyl chain lengths are involved in glucolipotoxicity-induced apoptosis of INS-1 β-cells. *Biochem. J* **438:** 177–189

Vincent I, Bu B & Erickson RP (2003) Understanding Niemann-Pick type C disease: a fat problem. *Curr. Opin. Neurol* **16:** 155–161

Voelzmann A & Bauer R (2010) Ceramide Synthases in mammalians, worms, and insects: emerging schemes. *BioMolecular Concepts* **1**

Voelzmann A & Bauer R (2011) Embryonic expression of Drosophila Ceramide Synthase schlank in developing gut, CNS and PNS. *Gene Expr. Patterns* **11:** 501–510

Wada A & Tanaka A (2002) [RIKEN structural genomics/proteomics initiative (RSGI)]. *Tanpakushitsu Kakusan Koso* **47:** 973–976

Wagner N, Schmitt J & Krohne G (2004) Two novel LEM-domain proteins are splice products of the annotated Drosophila melanogaster gene CG9424 (Bocksbeutel). *Eur. J. Cell Biol* **82:** 605–616

Wang Y, Geer LY, Chappey C, Kans JA & Bryant SH (2000) Cn3D: sequence and structure views for Entrez. *Trends Biochem. Sci* **25:** 300–302

Wang Y, Yamaguchi H, Huo L, Du Y, Lee H, Lee H, Wang H, Hsu J & Hung M (2010) The Translocon Sec61 Localized in the Inner Nuclear Membrane Transports Membrane-embedded EGF Receptor to the Nucleus. *Journal of Biological Chemistry* **285:** 38720–38729

Wilson DS, Sheng G, Jun S & Desplan C (1996) Conservation and diversification in homeodomain-DNA interactions: a comparative genetic analysis. *Proc. Natl. Acad. Sci. U.S.A* **93:** 6886–6891

Wu G, Lu ZH & Ledeen RW (1995) Induced and spontaneous neuritogenesis are associated with enhanced expression of ganglioside GM1 in the nuclear membrane. *J. Neurosci* **15:** 3739–3746

Young MM, Kester M & Wang H (2013) Sphingolipids: regulators of crosstalk between apoptosis and autophagy. *J. Lipid Res* **54:** 5–19

Zinke I, Schütz CS, Katzenberger JD, Bauer M & Pankratz MJ (2002) Nutrient control of gene expression in Drosophila: microarray analysis of starvation and sugar-dependent response. *EMBO J* **21:** 6162–6173

Zullo JM, Demarco IA, Piqué-Regi R, Gaffney DJ, Epstein CB, Spooner CJ, Luperchio TR, Bernstein BE, Pritchard JK, Reddy KL & Singh H (2012) DNA sequence-dependent compartmentalization and silencing of chromatin at the nuclear lamina. *Cell* **149:** 1474–1487

8 Abbreviations

aa	amino acid
bp	base pairs
CAS	cellular apoptosis susceptibility
CerS	Ceramide Synthase
cDNA	complementary DNA
dATP	desoxyadenosinetriphosphate
DNA	desoxyribonucleic acid
dTTP	desoxythymidine triphosphate
EGFR	Epidermal growth factor receptor
ER	endoplasmic reticulum
g	gravitational force
GDP	guanidine diphosphate
GST	Glutathion-S-transferase
GTP	guanosine triphosphate
INM	inner nuclear membrane
kb	kilo bases
µ	micro
m	milli
M	molar
NLS	nuclear localization sequence
Ran	Ras-related nuclear protein
NPC	nuclear pore complex
S1P	Sphingosine-1-phosphate
Sph1K	Sphingosine-1-Kinase
Sph2K	Sphingosine-2-Kinase
ONM	outer nuclear membrane